Formation Control of Autonomous Surface Vehicles for Surveying Purposes

Jeppe Dam and Nick Østergaard

January 8, 2015

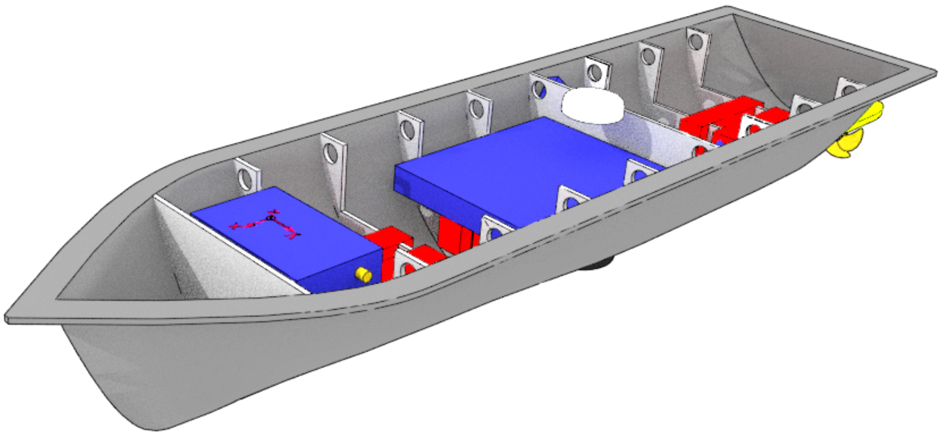

AALBORG UNIVERSITY
DENMARK

Department of Electronic Systems

Department of Electronic Systems
Control Engineering
Fredrik Bajers vej 7
9220 Aalborg Øst
Phone 99 40 86 00
http://es.aau.dk

Title:
Formation Control of Autonomous Surface Vehicles for Surveying Purposes

Theme:
Master's thesis

Project period:
2014

Project group:
1034

Participants:
Nick Østergaard
Jeppe Dam

Supervisor:
Jesper Abildgaard Larsen

Number of printed copies: 4

Number of pages: 159

Appendices: 6 + website [a]

Finished on: January 8, 2015

[a] Website with additional material, `http://kom.aau.dk/group/14gr1034/attached`

Synopsis:

This master's thesis concerns the further work on the platform named AAUSHIP. This is an Autonomous Surface Vessel (ASV) which can have different purposes. Within the scope of this project it will be used for surveying applications, where the AAUSHIP will be expanded to be a fleet of AAUSHIPs to navigate in a formation.
Firstly, the old AAUSHIP is upgraded with respect of hardware and implementation of these have been necessary. The single AAUSHIP have been tested after newly implemented Kalman Filter and a heading controller have been implemented. This is used as a Line-Of-Sight (LOS) guidance to make the AAUSHIP converge onto a predetermined trajectory. Afterwards is the focus to investigate formation strategies to be implemented at the AAUSHIP when more ships are to come. The main investigated strategy is based on a potential field algorithm, which have been simulated with the dynamics of the AAUSHIP. This is the basis of future work to implement this strategy at the coming AAUSHIP fleet for verification of the methods.
Results show that, with the model designed, it is possible to control the AAUSHIP in the area of interest. Further work to the model can improve performance, but this has not been the main focus within the scope of this project, where the surveying purpose have been in focus. Simulation of the formation control strategy with potential field shows the potential to implement this at the coming AAUSHIP fleet, such that these will be able to perform surveying as an entire group of vessels.

Institut for Elektroniske Systemer
Kontrol og Automation
Fredrik Bajers vej 7
9220 Aalborg Øst
Phone 99 40 86 00
http://es.aau.dk

Titel:
Formation Control of Autonomous Surface Vehicles for Surveying Purposes

Tema:
Kandidat speciale

Projektperiode:
2014

Projektgruppe:
1034

Deltagere:
Nick Østergaard
Jeppe Dam

Vejleder:
Jesper Abildgaard Larsen

Antal printede kopier: 4

Antal sider: 159

Appendikser: 6 + hjemmeside [a]

Afsluttet: January 8, 2015

[a] Hjemmeside med mere materiale, http://kom.aau.dk/group/14gr1034/attached

Synopsis:

Dette kandidatspeciale omhandler fortsat arbejde på AAUSHIP platformen. AAUSHIP er en ASV som kan have flere forskellige anvendelsesmuligheder. Fokus i dette projekt er formationskontrol med baggrund i pejlingsopgaver hvortil AAUSHIP skal udvides fra et enkelt skib til en flåde af AAUSHIPs.
Båden er fysisk blevet opgraderet med nyt elektronik som er implementeret. Dertil er den enkelte båd blevet testet med et nyt Kalman Filter (KF) hvortil en retningsregulator også er implementeret. Denne er anvendt som en LOS reference regulator for at få båden til at konvergere til de genererede liniestykker mellem rutepunkter. Efterfølgende har fokus været sat på at identificere og analysere formationsstrategier som skal implementeres på bådene, når disse er produceret. Mest fokus er lagt på en potentialefeltsalgoritme, som er blevet simuleret inklusiv dynamikken fra modellen af AAUSHIP. Dette danner grundlaget for implementering på flåden med opfølgende verifikation.
Resultater viser, at det er muligt at kontrollere AAUSHIP med den designede model, i et område givet af Aalborg Havn. Yderligere arbejde vil ligge i at forbedre modellen af AAUSHIP, men dette har ikke vist sig at være nødvendigt da fokus i dette project har omhandlet pejlingsopgaven. Slutteligt udviser simulering af formationskontrolstrategien potentiale for en mulig implementering af denne på den kommende flåde af AAUSHIPs, så disse kan foretage pejligsopgaver som en dannet formation af skibe.

Preface

This is a master's thesis concerning the platform named AAUSHIP. This platform is an ongoing project at the Department of Automation and Control.

The project have developed into the AAUSHIP platform, which is an ASV in working progress. In this thesis Jeppe Dam and Nick Østergaard has been focusing on upgrading the hardware of the platform to overcome implementation errors, designing an applicable model of the platform and designing formation control strategies for a future fleet of AAUSHIPs for surveying purposes. The idea of surveying have been in focus for some time in the project, from where an initial correspondence between Aalborg University (AAU) and the Port of Aalborg has been created. The Port of Aalborg has the interest in the AAUSHIP project since they have an aim to become an intelligent harbour, and the work of this project is a stepping stone for them. With the Port of Aalborg in focus have the surveying purposes in the Limfjord become the area of interest, which have given rise of directing the AAUSHIP to this surveying purpose.

The work in the project have both given the project group an insight of the hardware issues at the AAUSHIP, but have also given rise to investigate the formation control aspects when dealing with groups of ASV. Since the early work on the AAUSHIP project only have been on a single ship, the need for internal communication have not been crucial. Now, to upgrade the platform, the ROS system have been implemented both for future work but also for testing purposes behind the desk. This have given the group the opportunity to simulate the behaviour of the AAUSHIP in a controlled designed environment, and afterwards implement and realize the design on the actual AAUSHIP.

Thanks to

Karl Damkjær Hansen has been helpful with answering questions related to ROS, which have proven very useful when porting the original AAUSHIP platform operated through ROS.

The Port of Aalborg has been open to share data, information and input in regard of surveying applications, and have shown interest in the project. As the state of the project is not fully working, and the AAUSHIP is a platform in progress, the direct corporation with them has not reached the implementation phase with their system yet.

Nick Østergaard

Jeppe Dam

Reading Guide

The following report is divided into parts, related to different phases of the project. The parts are divided into chapters, the chapters describe different aspects of the project. The chapters are subdivided a number of times to further split up the content into specific topics. The report is ended with an appendix part, that contains all the material that is relevant to the project, but not necessarily interesting to the reader, such as measurement journals and transcripts of meetings.

Citations in the report is done according to the Harvard method, the list of references can be found on page 141. The elements on the list of references are sorted by author.

Acronyms are written to their full extend, the first time they are used, with the acronym in parentheses, thereafter only the acronym is used. The list of acronyms can be found on page xvii.

Notation of vectors are written in bold font with lower case letters ($\mathbf{v}$), matrices are written in bold font with upper case letters ($\mathbf{M}$). Single variables and constants are typeset in normal math (x).

Additional to the report is a website, which contains copies of web references and other digital files (source code, scripts and raw measurement data) that could be of interest to the reader.

Contents

Nomenclature

β	Sideslip angle
$\mathbf{\Phi}$	State transition matrix of a discrete linear dynamic system
$\mathbf{\Theta}_{nb}$	Euler angles between n and b
χ	Course angle
$\hat{\mathbf{x}}$	Estimated state vector
$\mathbf{G}$	Input matrix
$\mathbf{H}$	Measurement sensitivity matrix defining the linear relationship between the state of the dynamic system and the measurements that can be made
$\mathbf{K}$	Kalman gain matrix
$\mathbf{P}$	Covariance matrix of state estimation uncertainty
$\mathbf{Q}$	Covariance matrix of process noise in the system state dynamics
$\mathbf{R}$	Covariance matrix of observational (measurement) uncertainty
$\mathbf{u}$	Input vector
$\mathbf{x}$	State vector of a linear dynamic system
$\mathbf{d}_{i0}$	Desired distance between virtual leader and the i'th agent
$\mathbf{d}_{ij0}$	Desired distance between the i'th and j'th agent
$\mathbf{d}_{ij}$	Distance between the i'th and j'th agent
$\mathbf{d}_{i}$	Distance between virtual leader and the i'th agent
$\mathbf{d}_{ki}$	Distance between objects and the i'th agent
$\mathbf{F}_{i}^{tot}$	Magnitude and direction for the i'th agent
$\mathbf{F}_{ca}^{tot}$	Agent-agent collision avoidance forces

$\mathbf{F}_{ij}^{tot}$	Inter-agent forces
$\mathbf{F}_{oa}^{tot}$	Agent-obstacle collision avoidance forces
$\mathbf{F}_{vl}$	Virtual leader force
$\mathbf{p}_{b/n}^{n}$	Linear position of o_b with respect to n expressed in n
$\mathbf{v}$	Measurement noise vector
$\mathbf{w}$	Process noise vector
$\mathbf{z}$	Measurement vector
$\omega_x, \omega_y, \omega_z$	Angular velocity from rate gyro
ψ	Heading angle (yaw)
a_x, a_y, a_z	Linear accelerations from accelerometer
K_{ca}	Gain of agent-agent forces
K_{ij}	Gain of inter-agent forces
K_{oa}	Gain of agent-object forces
K_{vl}	Gain of virtual leader force
M_A	The added mass matrix
m_x, m_y, m_z	Magnetic field from magnetometer
p_{i0}^{n}	Desired position of the i'th agent in NED
p_{i}^{n}	Position of the i'th agent in NED
p_{j0}^{n}	Desired position of the j'th agent in NED
p_{j}^{n}	Position of the j'th agent in NED
p_{k}^{n}	Position of objects in NED
p_{vl}^{n}	Position of virtual leader
U	Course speed
x_n, y_n	Position in the NED-frame, usually computed from a GPS

Acronyms

AAU	Aalborg University
ASV	Autonomous Surface Vessel
ADC	Analog to Digital Converter
AHRS	Attitude and Heading Reference System
BODY	The body frame
CFD	Computational Fluid Dynamics
DOF	Degrees-Of-Freedom
DP	Dynamic Positioning
EKF	Extended Kalman Filter
FRF	Formation Reference Frame
FRP	Formation Reference Point
GNC	Guidance, Navigation and Control
GNSS	Global Navigation Satellite System
GPS	Global Positioning System
HLI	High Level Interface
IMU	Inertial Measurement Unit
IP	Internet Protocol
IPv4	Internet Protocol version 4
IPv6	Internet Protocol version 6
KF	Kalman Filter
LKF	Linear Kalman Filter

LOS Line-Of-Sight

LLI Low Level Interface

LSB Least Significant Bit

LTI Linear Time Invariant

MMSE Minimum Mean Square Error

MUV Multiple Unmanned Vehicle

MPC Model Predictive Control

NED North-East-Down

PWM Pulse Width Modulation

ROS Robot Operating System

RTK Real Time Kinematic

SOG Speed Over Ground

UKF Unscented Kalman Filter

Part I

Problem Analysis

This part contains an analysis about the project background and its goal, leading to designing a system that can reflect the analysis.

Chapter 1

Introduction

In this chapter is the motivation for the project stated and the link to the Port of Aalborg.

1.1 Motivation and the AAUSHIP Project

The Port of Aalborg would like Aalborg University to help them to expand their options of improving the conditions of the Limfjord. One of their tasks is to map the seabed of the Limfjord to get bathymetry data. This will help them guide larger cargo ships to port while using the autonomous ships as guidance.

Another aspect from The Port of Aalborg is a task to escort larger ships with cargo into The Port of Aalborg. This is done by a pilot whom needs to sail out to incoming larger cargo ships and escort them safely into port. The pilot does this in a pilot boat which is controlled manually by the pilot. The Port of Aalborg would like this process to become autonomous such that an autonomous boat can sail to the cargo ship and to some extend take over the control and guide the cargo ship into port. The system to do this implies that The Port of Aalborg needs an autonomous ship which can perform this task.

The mapping itself can be done by one ship or by more. For the moment one of the ships from The Port of Aalborg, which is manned, covers the mapping of the closer part of the Limfjord ($\approx$ 65 km). This is only done every third year, but mapping around Hals Barre, a sandbar (and not a beach bar) at the end of the Limfjord is a more critical place and is mapped every third month.

If The Port of Aalborg had an autonomous ship fleet at their disposal, which could sail out and do the mapping autonomously, they would get updated bathymetry maps with a higher update frequency than they have currently (Port of Aalborg, 2014). This will result in a digitalizing of the seabed, a digital map, which has different implementation options by The Port of Aalborg.

This thesis will utilise formation control and extensions to manoeuvre agents through a specified area for surveying purposes. The aspect of formation control is chosen due to the rather large areas that The Port of Aalborg needs so cover. When applying formation control it is assumed to be faster to cover a larger area with multiple boats than if one single boat needed to scan the area. The formation that are to be chosen depends on the specific area of interest, which could e.g. be inside the harbour or around the pillars of the bridge. Chapter 2 on page 7 will introduce what kind and scopes of formation control that exists today. These theories makes the basis for the formation control within the scope of this project.

As a future scope this can be used when making a model of the seabed of how this will get sanded. This model can tell The Port of Aalborg when to go clean the seabed. The AAUSHIP project can be used to verify this model, such that The Port of Aalborg do not have to go out with equipment to solve the sanding without the need for it.

1.2 The Mission

Within the scope of this project the ships will be unmanned autonomous ships, ASV. The ship's main purpose will be to map the seabed by using sonars to obtain bathymetry data. When one ship need to do this alone, and due to the range of the sonar, the time spend could be improved by using multiple ships. The sonar scanning would be done as seen on figure 1.1.

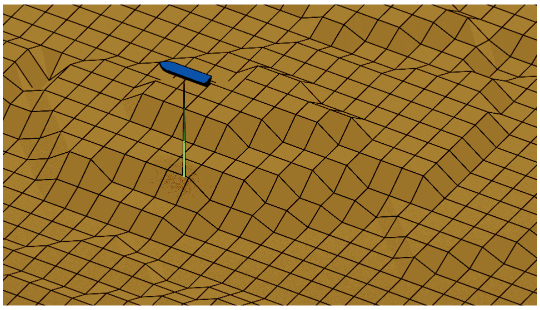

(a) One ship

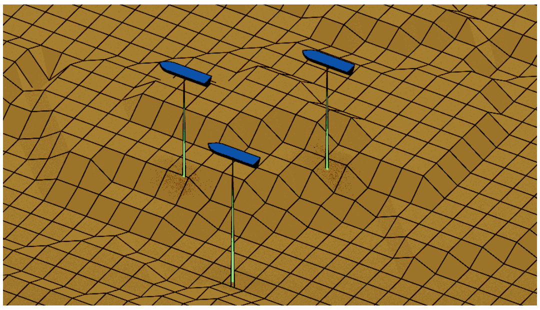

(b) Thee ships

Figure 1.1: Comparison of two ways to cover an area with a lawnmower pattern.

When only one ship (figure 1.1a) need to map a complete seabed this process could take up much time dependent on the area that need to be covered. The time spend could be improved to make this mapping more efficient. One way of optimizing the time used is to add more ships (figure 1.1b) to help map the seabed. To make the process of this as optimal as possible it could be of benefit to implement formation control to the specific assignment.

The implementation of the AAUSHIP as a fleet in formation can have various purposes.

Larger group One advantage is that, instead of being spread out in the fjord at different areas of surveying, they are together and will be seen as a more deterministic group rather than smaller independent vessels, which is less confusing good for other sea fares.

Formation with other vessels When the AAUSHIP project gets implemented with the Port of Aalborg could it be of benefit to have the AAUSHIP as an offset from their own surveying vessel, Alba, such that the AAUSHIP can get into more shallow water than the possibility of Alba.

Scouting If i.e. a larger vessel needs to go into a smaller unexplored fjord the AAUSHIP can be used in front of the larger vessel as a scout to map the seabed in front.

Hardware dependent For future work on the AAUSHIP project it might become available to implement multibeam sonars. If this option becomes available the area that the sonar scans will be dependent of the depth at the current position. This will mean that if more vessels are in a rigid formation, then overlapping of data will happen. This is not in the interest, since the mapping could be done faster. If the formation changes dependent of the overlapping areas from the sonars, this will be a minimization problem to be solved to optimize the survey.

In cooperation with the port of Aalborg, a use case is presented, where it is possible to perform tests of the platform, and use those to compare the performance of the AAUSHIP system with their system.

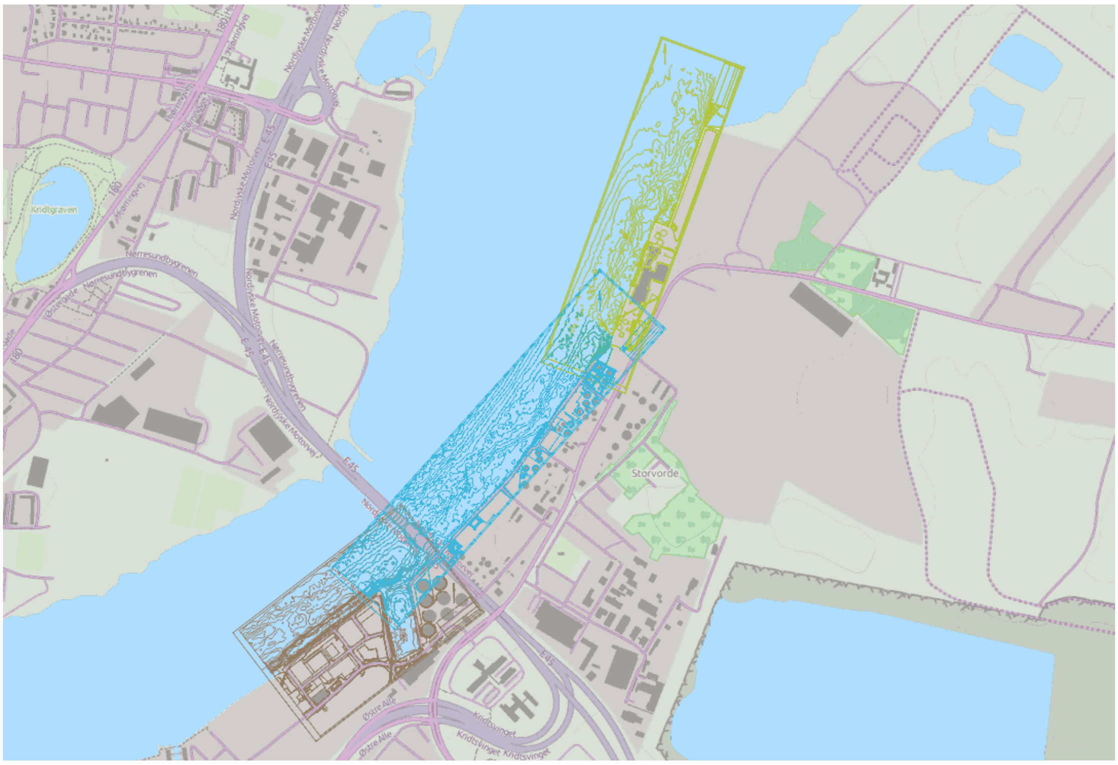

Figure 1.2: Area of the harbour at Aalborg Portland provided as sample data from the Port of Aalborg. Background map data CC BY-SA OpenStreetMap.

When performing this kind of surveying with multiple ships, it is important to take note of the kind of sensor it uses and the coverage that it provides. Initially the Port of Aalborg used

Figure 1.3: The main survey vessel used by the Port of Aalborg named Alba.

single beam echo sounders, but have in recent years turned over to multibeam sonars for their survey boat, which has improved their resolution and time for a survey. But they still wishes to improve the survey update rate, by e.g. using fairly low cost autonomous ships to get better indication of the seabed to identify if an expensive thorough survey is needed. An image of the survey vessel they use now can be seen on figure 1.3. As it can be seen, this survey vessel is relatively large, being over 20 metres long. To comparison is the AAUSHIP only 1.1 metres long. For surveying in smaller areas, like inside the harbour area, the Port of Aalborg uses a smaller scale vessel which is 12 metres long. This vessel is only used at the smaller areas thus not the one being used out in the Limfjord close to Aalborg.

Chapter 2

Formation Control Overview

This section will give a short introduction to formation control in general, by discussing existing formation control paradigms and relating them to the motivation of the AAUSHIP as a survey platform concept. Some of these concepts will be analysed further in chapter 4 on page 23.

The theory of formation control in general is widely applied. It is usually applied in assignments regarding control of robots which needs to be placed relative to each other. Depending on the given task of the robots, and which type of robots are in focus, the formation can be utilized in different ways (Kwang-Kyo Oh and Ahn, 2012).

The robots can also be of various types: Driving vehicles, helicopters, aeroplanes, ships etc. which can be both manned or unmanned. The tasks that these robots needs to fulfil can vary greatly. Robots in groups in general have many purposes such as vacuum cleaning robots, who needs to clean a rather large area or flying swarm robots like quadcoptors who can make different kinds of assignments. When quadcoptors work as a combined group they could lift a certain amount of payload to achieve their goal as a group, or they could work individually in a network to do several smaller tasks. An example of how quadcoptors are working together can be examined at (Augugliaro et al., 2014).

All the robots in the terminology of Zhang and Mehrjerdi (2013) are called *agents*. These agents move either individually or in formation. This formation can be rigid or be flexible. If the agents move in rigid formation they will keep their relative positions to each other and must not diverge from the formation. The formation could also be flexible which sometimes is preferable. If the distances between three agents on line are large, and an obstacle needs to be avoided, only one of the agents needs to move from this obstacle if the formation is flexible (Zhang and Mehrjerdi, 2013). This can be seen on figure 2.1 on the next page.

2.1 State of the Art

When looking into formation control many different types of control can be taken into account. The main types of formation control are separated into six different types, all under the main topic *multiple vehicles coordination strategies*. The overview for this can be found

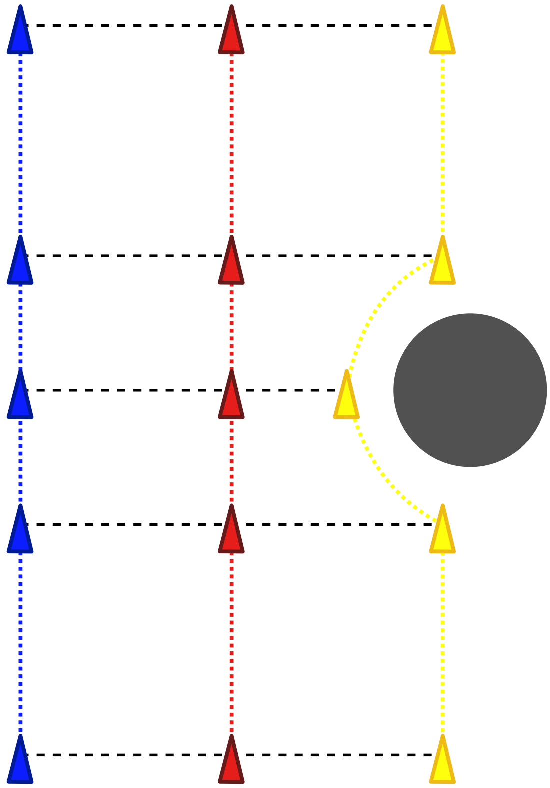

Figure 2.1: A flexible formation where the right agent avoids an obstacle.

in the survey paper (Zhang and Mehrjerdi, 2013) who explains the six main types and a few alternations of these.

The theoretical views on control of Multiple Unmanned Vehicle (MUV)'s behaviour are by (Zhang and Mehrjerdi, 2013) divided into two classes; centralized and decentralized systems. If the system is centralized this means that all control of the formation is done on one agent, and the others receive information from the core agent. This form of system has the advantage that the core agent can optimize vehicle coordination, accommodate individual agent faults and monitor the accomplishment of the mission. The main disadvantage of this system is that if a fault should occur in the core agent this will affect and facilitate a failure of the whole system.

The opposite way of controlling the system would be in a decentralized way. This way of controlling the formation is inspired by the aggregation of birds and fish. This makes each agent able to communicate and share information in between. This means that each agent is given its own part of the complete objective and thus can only complete a part of it, like moving around an object to get to end point of a trajectory. The advantage is that faults in a single agent can be overlooked, thus more robust to faults, but can result in a less efficient objective outcome. A decentralized system may be more appropriate to scale up such that more agents can be included and the computational load can, in difference from the centralized system, be split up onto more agents.

The different types of coordination and control algorithms within centralized and decentralized systems include: *behavioural-based*, *virtual structure*, *leader-follower*, *graph-based* and *potential field approaches*. Within these structures are the terms *cooperation control* and *formation control* used. Cooperative control focuses on the global task that the group of agents needs to fulfil, and the formation control is the actions performed by each agent which is shared with the other agents in the group.

Virtual structure
In a virtual structure is the entire formation treated as a single entity. The behaviour coordination for a group of agents in a virtual structure is uncomplicated compared to the coordination of many agents, due to the making of one structure e.g. based on fixed distances between the agents. The disadvantage falls on the centralization due to the structure treated as a single entity. If a failure in this structure happen results in a failure in the entire structure.

Behaviour Based Methods
The behavioural based method employs several behaviours for each of the agents and the final control used to control the formation is derived from a weighting of the relative importance of each of the behaviours. This could for instance be navigational behaviours to enable a navigation to be the main goal while avoiding hazards and stay in formation. If one agent needs to avoid a collision with an obstacle the rest of the group should not take this into account. Only that single ship needs to leave the formation and get back into formation again.

Leader-Follower Approaches
Applying leader-follower methods designates one agent as being the leader and the rest of the agents as followers. The following agents need to position themselves relative to the leader and maintain a desired relative position to the leader. This makes the simplicity to this method, but there is no feedback from the followers to the leader and thus makes that a disadvantage. Separation-separation and separation-bearing are two popular leader-follower formation controls, where the followers stay at specified separation and bearing from their designated leader. Within this method it is possible to split the group up into several smaller groups with their individual designated leaders.

Potential Field Approach
Potential field approaches assigns potentials to agents to make a weighting between them. This weighting could for instance determine the relative distances between the agents. This is usually used when following a virtual leader, such that this process is only made relative to the agents within the structure. This method can ensure a collision free formation when every agent has been assigned their potential weighting respectively. In this method can obstacles be included and have assigned potentials as well. This potential will become an avoidance parameter from the specific object.

Graph Theory Approaches

When applying the graph theory method one assign every agent as a node and assign connections between the nodes. In graph theory this is denoted vertices and edges. The study with graph theory is mainly concentrated of the formation itself and related to changes within the structure. This can be related to the structure within a tree-structure which is used when assigning the formations in graph theory manor. This can be applied as communication analysis for the agents and consensus analysis can be of benefit. The edges between the nodes symbolizes the possible connections thus communication between them. The nodes that are connected are denoted as neighbours and are capable of communicating through the edges.

2.1.1 Approaches on Formation Control

Different formations of ships can be seen on figure 2.2.

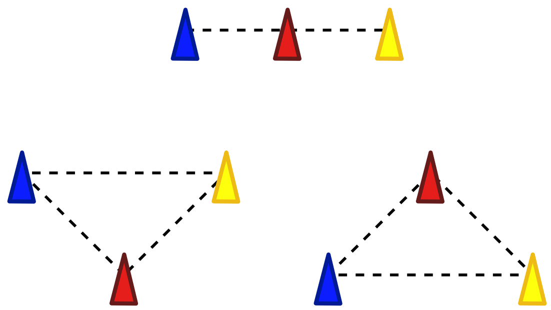

Figure 2.2: Different formations which the ASVs can make.

The formation of the ships may not need to be strictly rigid. Situations could appear where it would be of benefit to change the ship's formation. If the formation need to avoid an obstacle and one or more ships needs to go faster or slower, which leads to a change in the formation, it might be of benefit to regroup the formation which is faster to reach. An example can be seen on figure 2.3 on the next page.

When doing the formation control it is important to figure out what one want to achieve, and depending on the strategy and the formation type some things are to be considered as requirements regarding how the formation should work. In this discussion lawnmower patterns are considered. In this work up to four ships are considered for simplicity, but it should be extensible to n-number of ships. The lawnmower patterns will suit well for the mapping of a seabed where one or more ships are to sail from shore to shore in a fjord.

2.1.2 Initialisation

When looking at the specific task several things needs to be taken into account. When starting the mission, the ships may start at positions that is not in the desired formation. It might be of importance that the ships are in formation when they start tracking the desired path. Therefore some attention must be given on how to make the ships initialize this formation.

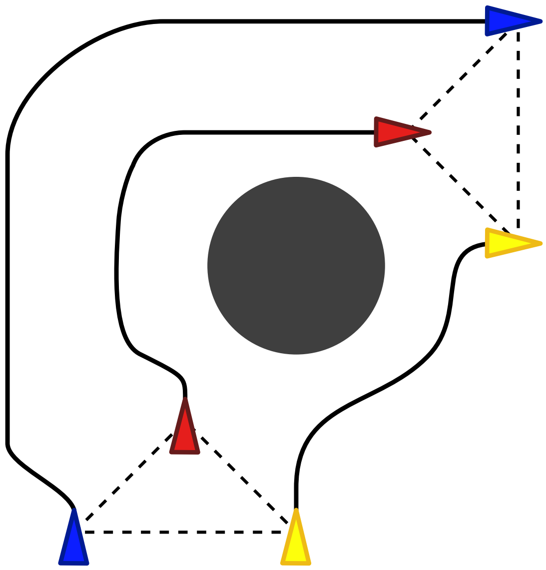

Figure 2.3: A formation needs to go around an obstacle where the inner most ship chooses the shortest path and the formation regroups to a new formation.

This is referred to as the group coordination task. An approach is to make the ships sail individually to the starting positions with a speed that makes them hit their respectively starting points at the same time. If one reaches its start point much earlier than the others it must stop, which is not wanted because it then has the risk to drift out of position again. This basically means that there exists an initialization phase and a tracking phase. The start heading should of course align with the path at the start point such that the path following can begin with zero error. The ships could also target their group formation before starting at time zero at the path. This will eventually make the initialization take longer time but ensure that the ships have made the group coordination task and are ready to start at the path.

Another issue to be considered is to ensure that no ship at any point in time reaches a minimum speed that is necessary for the ship to not drift out of formation. This could be a problem in corners of the formation if a stiff construction, where the inner most ship has to move slower, to accommodate the shorter distance on an inner circle arc.

Faults like blackout on a ship could also be considered in the control design. I.e. what happens with the formation when one ship fails into a blackout. Should the rest of the formation stop, should the formation still follow this drifting ship or should the mission simply terminate when it is discovered that a ship has blackout. This is under the assumption that the formation is decentralized and every ship has its own control and is not controlled from a mother ship.

In the initialization phase it is also relevant to consider how the ships should avoid each other if they are on the wrong side of each other. If it is of benefit that a specific ship is at the most inner route, and is located at an outer position before the group coordination, this ship needs to cross the formation to get to the desired starting position. This initialization needs to be adjusted in the initialization phase to ensure that no ships collide.

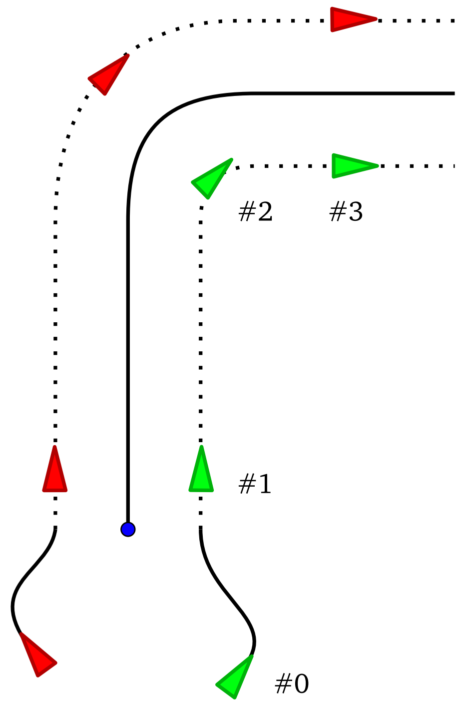

Figure 2.4: Two ships initializing and following the path offset equally on each side, ships are constrained to sailing parallel and heading the same as path when projected onto the path. Blue dot is start of path. Fully drawn splines is initializing phase.

On figure 2.4 is a simple path following performed with two ships in a stiff formation with an equal distance from the path. It illustrates four steps. In step #0 the ships initializes a random position near the start of the path being the group coordination task. At #1 it is tracking the path in formation, whilst still in formation. This is referred to as a formation coordination task. At #2, the green (right) ship is in a tight inner curve where it is important to consider design of the path such that the capabilities of the ship is not exceeded to stay in formation. At #3 it is back to straight line path following in formation.

When the ships needs to make a turn about something they can do it in many ways. On figure 2.5 on the next page the ships keep their formation whilst turning about the object. When they reach the other side and have finished their turn, the ships have kept formation but the outer most ship has now become the inner most ship. The reason to turn like this could be that the inner most ship, the yellow ship, cannot turn as sharp as demanded to stay the inner most ship. Therefore, instead of turning the formation, they stay geometrically rigid.

As seen on figure 2.5 on the facing page the ships could have benefit of turning like this. This way of turning could cause trouble in the top of the turn, where the ships eventually will collide due to errors and the relative close distance to each other. This way could be

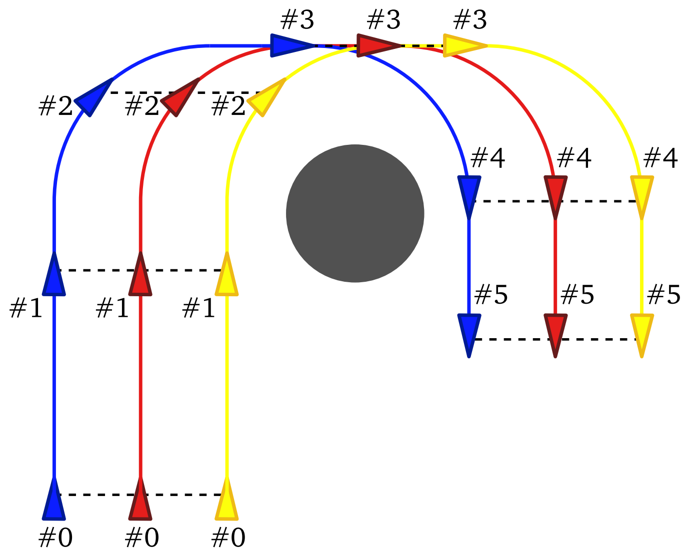

Figure 2.5: Three ships in formation needs to make a 90°turn and stays in their relative positions and keeps the rigid formation.

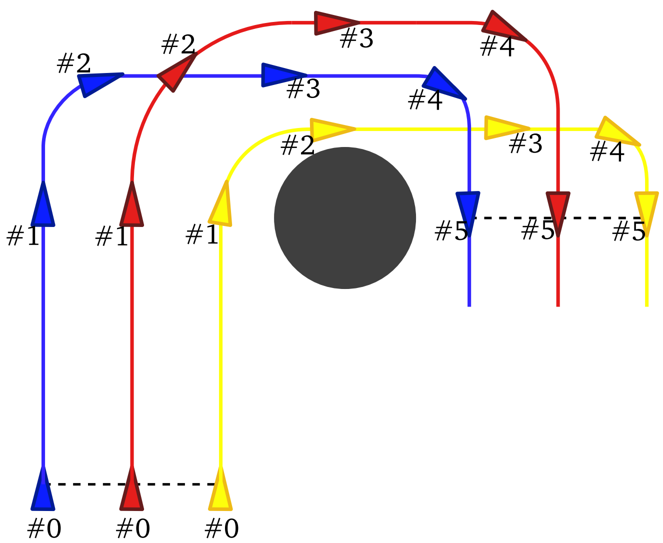

Figure 2.6: Three ships in formation needs to make a 90°turn and changes their relative positions.

altered a little such that the ships will turn like on figure 2.6 on the previous page. There the ships adjust their positions and velocities to ensure that they will not collide, but they will therefore leave their formation shortly to return back into position again (Thorvaldsen, 2011).

2.1.2.1 Degree of Actuation

The degree of actuation is a matter that sets some limitations on how the path following can be made, and thus the methods available to control the ships. Generally speaking when talking marine craft the movements that one is interested in controlling is usually their planar position in the North-East-Down (NED) frame. Exceptions for this is when one needs to perform dynamic positioning operations where one needs the vessel to have a controlled heave.

For controlling of ships there are different configurations which is described by (Fossen, 2011) as the following.

Three or more Controls
: When having three or more control parameters it is said that the vessel is fully actuated. This way of controlling is usually used in low-speed manoeuvring and station keeping mostly by offshore Dynamic Positioning (DP) vessels.

Two Controls and Trajectory-Tracking Control
: Trajectory-Tracking is done in a three Degrees-Of-Freedom (DOF) system, $e(t) \in \mathbb{R}^2$ on the sphere. It is done with two control inputs, $u(t) \in \mathbb{R}^2$. This means that the control problem is under actuated which cannot be solved by linear control theory. A vessel under these terms is able to manoeuvre along a path with constant sideslip angle using only surge and yaw. This is the classic approach for path following.

Two Controls and Weather-Optimal Heading
: When the goal is station keeping with minimal fuel consumption and the heading is not important one could consider the weather conditions and in general the environmental disturbances to perform stable control in disturbing weather. A method of doing this is described by (I. Fossen and Strand, 2001) and (Fossen, 2011, sec. 13.3.10). It is done by making the heading depend of the change in the mean of the environmental disturbances.

Two Controls and Path-Following Control
: The standard way by having two controls, being surge and yaw, and achieving path-following, is to define a 2D workspace. This workspace is placed along the trajectory with along-track and cross-track vectors that are to represent the error to minimize. This is usually done by applying the LOS path following controller that makes use of surge and yaw to accomplish the path following. This implies that a six DOF system model needs to be internally stable such that only the two control inputs are used.

One Control

This is the simplest control for ships, where the yaw is controlled with some form of heading autopilot and is the only thing that is controlled.

For the AAUSHIP this means that it is not a fully actuated ship in the whole 3D space, but this is not needed since it is moving on a surface. To be fully actuated it must be able to have controls for surge, sway and yaw. AAUSHIP is only equipped with two main propellers and one or two bow thrusters, which can only be used for slow speed manoeuvring. The bow thrusters can not be used in normal path following operations since the actuation of these are too low to make the vessel move.

2.1.3 Delimitations

Within the scope of the AAUSHIP project will the focus be to apply and extend a leader-follower approach at the ships. This will include several tasks. The two main tasks will be to make a group coordination task and a formation coordination task. The group coordination task will be, as described earlier, an objective to get the ships into the desired formation before or exactly at the starting point of the path following. The formation coordination task will be to make a leader, virtual or not, follow a predetermined path set by waypoints. The path should be generated from waypoints placed on a map due to that the ship needs to travel over larger distances. This will make a waypoint based follower where the path will be generated between the placed waypoints.

The placement of the waypoints will be placed such that the ships need to surge along a lawnmower pattern, where the turns have a lower requirement of turn radius dependent on the surge velocity of the most inner ship. This is due to the drift if the inner ship looses too much velocity.

When applying the leader-follower approach it needs to be determined how the formation precisely should be set up. In this project is only one leader considered at a time. The rest of the ships will act as followers to the leader. The idea can be seen on figure 2.7 where only one leader is represented with one single or more followers. When the followers are

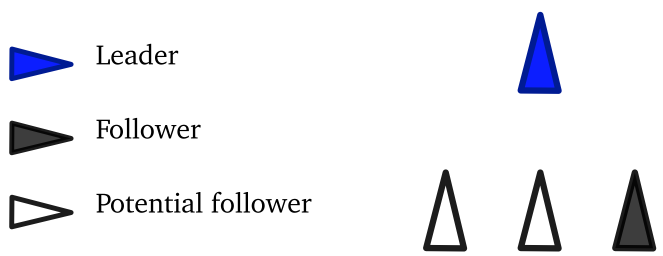

Figure 2.7: A leader is always assigned and potential followers are following.

in formation with the leader it is only the leader who is following a specified trajectory. The other ships, the followers, only keeps their position relative to the leader. This makes the predetermined formation moving along the path relative to how the leader is following the path. The leader is autonomous as well as the followers, but the path following is only done at the leader and the followers maintains their relative positions to the leader.

If the leader diverges from the path, drifting to the left, this will result in the whole formation drifting to the left. This problem can be dealt with in different ways, e.g. the control could react fast enough to make the formation get back on track within a specified time, or some fault tolerance could be done from the whole system. If the leader diverges from the path it could make the formation stay at their respective headings within a time slot before actuating towards the leader.

The formation can take into account if it is of benefit to change leader. If some kind of obstacle makes the formation turn about it, it might come to benefit to change the leader which needs to be done on the fly. This entails a change in the group coordination and the ships needs to set their relative position and heading from another ship.

The configuration of the formation will be set up, as a start, with one leader and a single follower. The follower can be offset from the leader with a distance of five metres. This can be seen on figure 2.8. This will be a rigid formation that the ships needs to keep at all times.

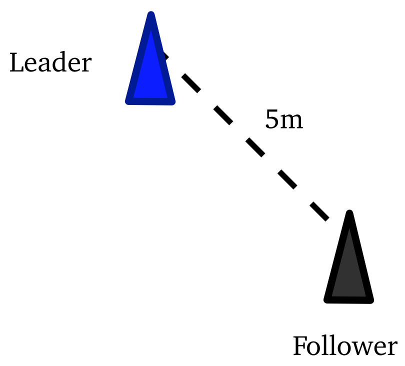

Figure 2.8: The leader with a follower offset by 5 metres radius.

The change of leader will eventually be taken into account when the ships needs to turn. If the formation needs to turn clockwise about it might be of benefit to change the leader.

The location to test the implementation of the AAUSHIPs will be in the Limfjord. The optimum will be to make the formation go across the Limfjord and back in lawnmower pattern and make measurements of the seabed. Due to the location where it is presumed to have enough space, the formation is not of bigger importance to the mapping. The only important thing to include regarding the formation is that the ships needs to be able to turn around without loosing so much velocity such that they start drifting and offset the formation.

Chapter 3

Path Generation

A guidance system usually consist of a subsystem to generate paths for the trajectory which is desired to have the object follow. There exists multiple methodologies for this, also depending on the mission purpose. A description of these methods are described in this chapter with focus on pre-mission defined paths.

For these kinds of guidance systems, they are usually generated via some form of human interface – some more intelligent than others. For the purpose of this thesis, the interest lies in the use of surveying purposes, such that a path should be generated from some waypoints that are generated from some polygonal areas of interest.

The concept of this is to make run lines (lawnmover or plough fure pattern) with straight line segments, and the corners can be handled in a specific way such that the physical constraints of the ship manoeuvring ability is considered to generate feasible paths.

There are basically two ways to consider a lawnmover pattern. The one is to have the area of interest to be covered only by straight line segments and then end the run lines connected with a turning manoeuvre outside the area of interest as show on figure 3.1a. The other way is to cover the area with all manoeuvres constrained inside the area of interest, where the turns are also included in the area of interest, as illustrated on figure 3.1b.

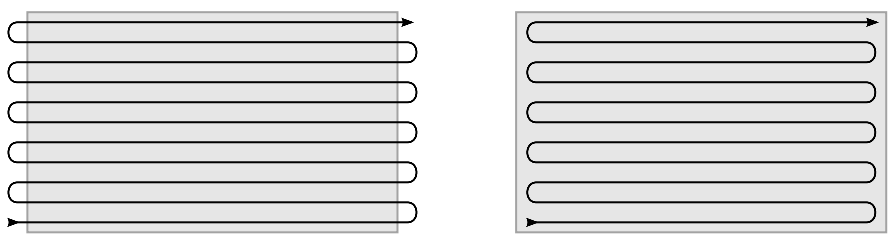

(a) Only straight lines **(b)** All paths constrained

Figure 3.1: Comparison of two ways to cover an area with a lawn mower pattern.

3.1 Dubins Path

Dubins path is one way to define paths which can be used in the context of the AAUSHIP project. The Dubins paths are created by line segments and circle arcs. These arcs can be created in different ways, and the usage of this can be applied when generating lawnmover patterns. The circle arcs can be created from points (waypoints) with line segments between, like it is intended to do within the AAUSHIP lawnmover patterns. Different discrete ways to handle Dubin paths can be found in a summary and discussion with (Eriksson-Bique et al., 2012). The way the Dubins path are used in the AAUSHIP is based on the waypoint terminology, where the vessel needs to go from waypoint to waypoint connected with a line segment to track onto. This is also one of the ways that the Dubin paths can be utilized. In the AAUSHIP is the circle arc defined From a determined distance from between the longer line segments in the lawnmover patterns. This radius cannot be too small such that the dynamics of the AAUSHIP does not allow it to go all around the circle arc without diverge from the determined waypoints in the arc.

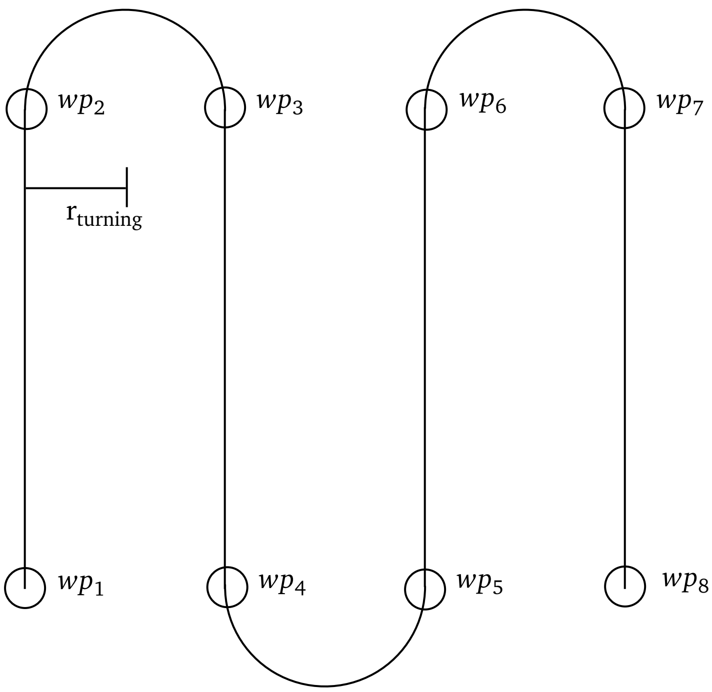

Figure 3.2: The figure shows that the spacing between the lines sets the turning radius for the AAUSHIP. This is constrained by the dynamics of the AAUSHIP.

3.2 Guidance System

The guidance system is a system that takes the wishes from the operator and converts those to some trajectory via a path generating algorithm. This path generating algorithm will be used

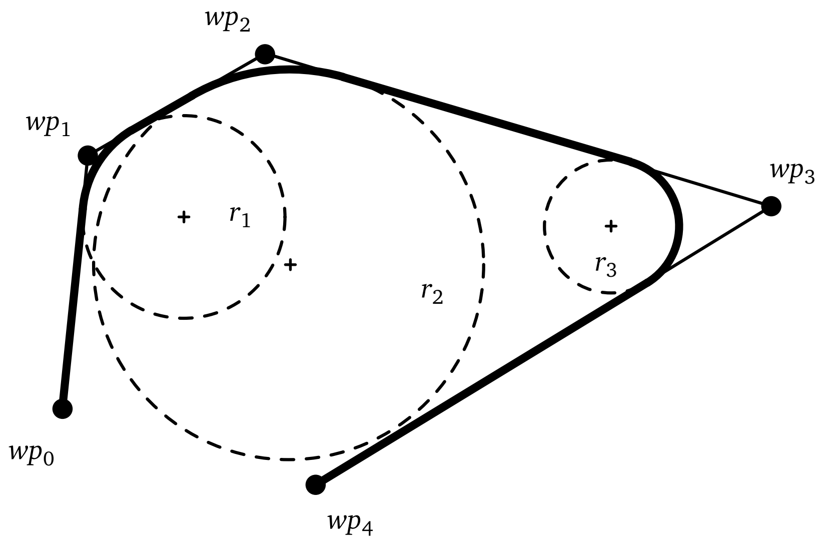

Figure 3.3: An example of a Dubin path generated with straight lines and inscribed circles, where the path corner arc radius is determined with a minimum radius and dependent on the angle between the two segments connecting one waypoint to others.

to generate the lawnmover patterns for the AAUSHIP to follow. These patterns have been discussed within this chapter. After the waypoints from the operator have been translated into a lawnmover pattern it is up for a tracking algorithm to keep the AAUSHIP at the correct course for the next coming waypoint.

This algorithm can have various purposes and in this project it will be a LOS guidance algorithm. This will control the heading of the AAUSHIP such that the vessel will converge to the line segments between the waypoints and afterwards keep the heading at the straight line segment. The guidance system can be one block that keeps the generated track from the waypoints updated, to have the references that the AAUSHIP needs to converge after. This reference is passed on to the control system, which can be seen on figure 3.4.

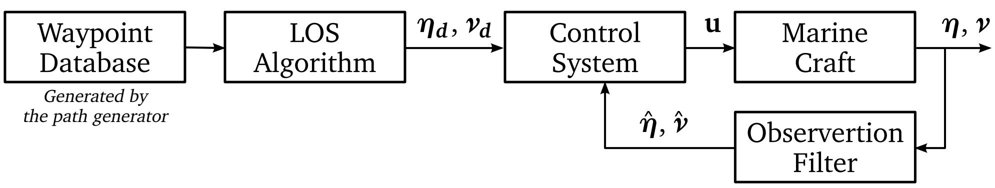

Figure 3.4: Overview of guidance system where a mission static waypoint database is used as the input to a LOS algorithm, which sets the reference for the ships control system, which is usually implemented as some form of heading autopilot.

Tesselation with quadrilaterals (polygons with four edges and four vertices) is a way to help divide a given polygonal shape into some shape where it is useful to apply a plough fure motion. The shapes of these are equal to how the AAUSHIP needs to move when navigating in a specific area to map the seabed.

Part II

System Design

This part includes the design and testing of the different subsystems used at the AAUSHIP.

Chapter 4

Selection of Formation Control Strategy

This chapter firstly introduces the understanding of trajectory tracking and how the a LOS algorithm can be used for this purpose. Next in this chapter will the previously mentioned formation control aspects from section 2 be investigated with overview of three different types of formation control. These three types are shortly analysed with focus on the specific task applied at the Port of Aalborg, afterwards one is chosen and simulated to be able to conclude how beneficial it is to implement in the AAUSHIP fleet.

"A control system that forces the system output $y(t)$ to track a desired output $y_d(t)$ solves a trajectory tracking problem" (Fossen, 2011).

4.1 Trajectory Tracking Control

When applying control to a vessel that needs to track a specified trajectory, then the type of control will be classified according to the number of available actuators. This is usually split between surge, sway and yaw, which corresponds to forward motion, sideslip and turning.

A time varying reference trajectory for a vessel to track can be given as:

$$\eta_d = \begin{bmatrix} N_d(t) \\ E_d(t) \\ \psi_d(t) \end{bmatrix} \tag{4.1}$$

To achieve tracking and convergence to such a trajectory is minimization of the error the main objective, $e(t) := \eta(t) - \eta_d(t)$. Or given by the previous notation:

$$e(t) := \begin{bmatrix} N(t) - N_d(t) \\ E(t) - E_d(t) \\ \psi(t) - \psi_d(t) \end{bmatrix} \tag{4.2}$$

When designing a motion control system with this type of objective it is important to distinguish between the following three important control objectives:

Setpoint Regulation
This is the most basic way of regulating. In this method it is usually a human operator that controls the setpoint or reference to the vessel. The controller will then be a regulator that usually brings the error of the control signal and the real value to zero.

Path-Following Control
The path-following control makes the vessel follow a path independent of time with no temporal constraints. The method is usually used on underwater vessels or vessels in transit between continents.

Trajectory-Tracking Control
When applying trajectory-tracking control, position and velocity of vessels should track the position and velocity of some time varying path reference signal. The feedback is a trajectory tracking controller to make the vessel converge to the trajectory. This is used when having course changing manoeuvres and speed changing along the trajectory. This could for instance be a change of speed in a turn of the vessel.

4.1.1 Manoeuvring the Vessel Using the LOS Method

Path-following problems for vessels are often solved by implementing LOS guidance algorithms. Opposite to other position control algorithms, where the vessel may be driven both in longitudinal and transversal directions to converge to a path, the LOS guidance algorithm gives a more natural motion towards the desired path. This is done by giving a more natural reference to the heading of the vessel. One of the advantages of this is that it can be applied both to fully actuated and under actuated vessels.

Since it is only the leader, and not any of the followers, who need to follow the path, this is only applied on one vessel. This can also be extended to a leader in a virtual structure. To apply the LOS guidance algorithm a setup is needed. To get an overview of the functionality of the LOS guidance algorithm see figure 4.1 on the facing page. On the figure is a green vessel that needs to get onto the blue path. The red points at the path is waypoint positions θ, $\mathbf{p}_d(\theta)$. From this point a tangent to the path is made, which crosses the vessels heading and is along the path. The angle from north to the tangents slope (the path) is the *desired heading*, ψ_d, for the vessel. This will make it converge to the reference path over time. s along the tangent is the *along track error*(tangential to path) and e from the vessel to the path is the *cross track error*(normal to path), which are two distances that needs to be minimized to make the vessel converge to the path. The along track error is not of great interest when applying a *lookahead-based steering* where only the cross track error is of importance. The lookahead distance along the track is denoted Δ and is the distance from the normal at the path to the point of LOS at the path.

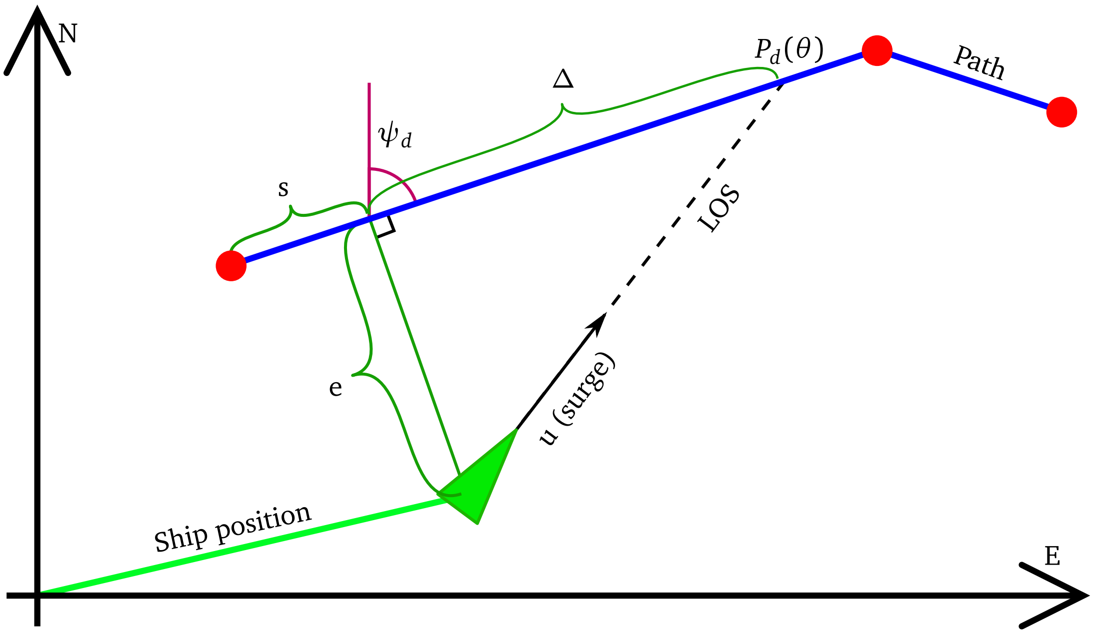

Figure 4.1: A vessel placed beside the path and uses the LOS guidance algorithm to get back on track.

4.1.1.1 The LOS Algorithm

The vessel has a generalized position in the n-frame given as

$$\eta = (\mathbf{p}, \psi)^\top \quad , \quad \mathbf{p} = (x, y)^\top \tag{4.3}$$

with dynamics given by

$$\dot{\eta} = \mathbf{R}(\psi)\boldsymbol{\nu} \tag{4.4}$$

where $\boldsymbol{\nu} = (u, v, r)^\top$.
The path can be parametrized by a set of points with

$$\mathscr{P} = \mathbf{x} \in \mathbb{R}^2 : \quad \exists \theta \in \mathbb{R} \quad s.t. \quad \mathbf{x} = \mathbf{p}_d(\theta) \tag{4.5}$$

where $\mathbf{p}_d(\theta) := (x_d(\theta), y_d(\theta))^\top$ is a smooth function. The path needs to be smooth such that the LOS algorithm makes the vessel converge to the path. When applying the LOS algorithm it makes the setup immune to sideslip error. This is due to the minimization of e when the vessel approaches towards the path.

For a given value of θ, being a specific point on the path, is the tangent to the path introduced with origin located in $\mathbf{p}_d(\theta)$. The orientation of the reference frame, being the desired heading, is given by

$$\psi_d(\theta) = \arctan 2\left(\frac{y_d^\theta(\theta)}{x_d^\theta(\theta)}\right) \tag{4.6}$$

which then will be

$$\psi_d = \arctan 2\left(\frac{E}{N}\right) \tag{4.7}$$

The position of the vessel from the orthogonal position on the path is given in path-tangential coordinates according to

$$\varepsilon(\mathbf{p},\theta) = (s(\mathbf{p},\theta), e(\mathbf{p},\theta))^\top \tag{4.8}$$

where $s(\mathbf{p},\theta)$ is the along track error and $e(\mathbf{p},\theta)$ is the cross track error. These are given on figure 4.1 on the previous page, and is the errors from the vessel to the desired point on the path. This position can also be expressed using the rotation of the ε-vector by

$$\varepsilon(\mathbf{p},\theta) = \mathbf{R}_{2D}(\psi_d(\theta))^T(\mathbf{p}-\mathbf{p}_d(\theta)) \tag{4.9}$$

where

$$\mathbf{R}_{2D}(\psi_d(\theta)) = \begin{bmatrix} \cos(\psi_d(\theta) & -\sin(\psi_d(\theta) \\ \sin(\psi_d(\theta) & \cos(\psi_d(\theta) \end{bmatrix} \tag{4.10}$$

4.2 Relevant Characteristics for the Strategy

To have a tool to determine what strategy is the best suited for the problem described in 1.2 on page 4, some parameters that describes different characteristics of a strategy is needed. Listed here is a description of each key parameter, also mentioning what is desired for the mission at hand. The characteristics are weighted on a scale from −3 to 3 to be able to pick out the relevant formation as a conclusion.

Communication The communication requirements should be a measure of how much bandwidth is used. If the communication bandwidth usage is low it should be rated as a good thing, since the low bandwidth implies that the communication can be performed more easy and the scalability will become less complicated. It is not of importance if the communication breaks a link of the agents, this will be discussed in the individual formation control categories. If the communication has a score of 3, this implies that the bandwidth usage is low and if the score is −3 means that the bandwidth usage is high. If only one way communication exists this will probably also lead to lower communication, thus also making a higher score.

Control Architecture The control architecture is a weighting of the complexity of the control structure. A high weighting will mean that the complexity is low and thus less complicated to implement. It will also be combined with a relation to the type of controller, where a more simple controller can be better if the overall objective can be accomplished. If the control can be done with a less complicated controller, i.e. a LOS controller instead of some a more complex controller like Model Predictive Control (MPC), this can be preferred. The amount of needed inputs to the controller will also be a weighting, thus if the numbers of inputs are high this will be weighted low. The weighting of the control structure is a combination of the above mentioned, where a complex controller with high number of inputs will be weighted as -3 and a simple controller with low input will be weighted 3.

Obstacle Avoidance The obstacle avoidance does not have a specific rating in the use case of the AAUSHIP due to the assumption of a open water manoeuvring. This means that the weighting of this should be taken as neutral and the implementation will be further work. Yet it is described in the specific control strategies because the implementation of this can be useful in the further work of the AAUSHIP projects. The obstacles can be known pre mission or they can be detected during mission and avoided and the task of the avoidance will take different shapes dependent of the specific task. The weighting will be made such that if the obstacle avoidance is easy to implement, it will be weighted 3, and if it is not present it will be weighted 0. The reason why no obstacle avoidance is weighted as 0 is because the criteria does not include obstacle avoidance, but the further work has a weighting to implement it.

Transients The transients will be a weighting of how well the formation can make a turn and meanwhile keep the formation relative to the path. If the formation are unable to track the path during a turn it will be weighted low (-3) and will be the primary weighting. If the formation are able to track the path, but the formation will deviate a little, this will also be a down rating but not as much as if it is unable to track the path. This will i.e. get a weighting of 1. If the formation tracks the path perfectly and the formation is kept rigid through the transient the weighting will be 3. Some formation problems during transients can be solved by the generation of the path but this will result as a limitation to the path generation.

Scalability The weighting of the scaling is done on two criteria. It is a combination of the structure of the complete formation and the control architecture and an estimate of the bandwidth usage from the higher need of communication. This weighting will be a summed weighting, thus both bandwidth and formation complexity is weighted equally. A rather simple expansion of the formation structure will be preferable, and a relative low bandwidth usage is good. If only communication from a single leader to one respective follower is required, this will be a good thing because it leads to half the bandwidth usage. If the bandwidth usage is high and the control architecture is complex this will lead to harder scalability, which in that case will be weighted -3. If the control architecture is low and the input to the controller is low, the bandwidth is low and the communication layer is simple this leads to simple scalability which will be weighted 3.

Failure The failure criteria in these topics are only related to the outcome of the failure. It is not of relevance if the failure arises in sensors, in actuators or in the control structure, but only what will happen to the mission if one agents fails out. The degree of what will happen will choose the weighting such that if one agent fails and every other agent also fails the mission, this will be weighted as -3. If a single agent fails and nothing else happens will lead to a weighting as 3, because if an agent will fail and the mission still can be completed it is preferable.

There are some parameters that are hard to differentiate by the principle of the method, which are listed below. These can be used to compare the strategies after implementation.

Preparation Time This is related to the mission setup time. How much manual labour is needed to prepare the agents for a mission? This could for instance be trajectory generation and how the specific pattern needs to be generated. If the formation control strategy is chosen such that the agents needs to be close to the specific formation this will also take preparation time to place them relative to the desired formation.

Time The mission time for covering the area in a boustrophedon pattern. This will be from the start of the mission to a complete mission.

Energy Efficiency This is a theoretical measure of the formation efficiency. The energy efficiency of any autonomous systems is relevant because it limits how long the autonomous system can operate autonomously, given that it cannot easily recharge or is fatal for the mission. This means that optimising the energy efficiency is desirable.

Wear and Tear Is the controller aggressive? Aggressive controllers is known to make more wear and tear on the actuators. So if the strategy can be chosen to minimize the wear and tear this could be of benefit to the hardware.

4.3 Methods

4.3.1 Direct LOS Guidance

The LOS guidance makes the basis for a formation where one leader has a follower connected and this follower has another follower connected and so on. By having this form of guidance the leader will always control the formation and how the development of the formation should be. The leader does not need to be a specific agent but can be a virtual leader, a point which is seen as leader to all the respective followers. The reference is to the leader can be a guidance reference where the leader needs to track a determined path. The reference to the followers can then either be given as a position offset, a distance and angle offset or only a distance to maintain and then make a direct pursuit of the leader.

4.3.1.1 Duckling Formation

This strategy takes the rise in a duckling or snake formation. In principle is this a leader that has a follower that has a follower and so on. Thereby will the formation take shape as a snake, when the leader takes off and the followers keep the line of sight to their respective leaders. The communication needed in the case of followers only follow one leader, and the communication only works in one direction, then the bandwidth usage is minimal. This implies that the communication it low and simple which is preferable. Similar to the communication will the control architecture become of the simple type where each agent only need to have a LOS controller, such that they track their respective leaders. As such is obstacle avoidance not a native implementation of the formation, but can be implemented for the main leader of the formation. By doing this arises a problem of transients where the followers will 'cut corners'. They will directly pursuit their respective leaders, such that the formation will take sharper corners than the main leader. Adding to that if one agent fails during mission every agent after this in the chain fails. Although the formation does not perform well it has the advantage that the scalability is simple. When linking the formation in the duckling formation a new follower can be attached at the last agent and a new follower to this agent and so on. This implies that, in theory, an infinite tail of followers can be attached.

4.3.1.2 Echelon Formation

The echelon formation is a branch from the duckling formation. In this formation the followers to the leader is not in a tail of the leader, but is offset into a echelon formation. The principle being the simple LOS controller and the communication as followers to their respective leaders still apply in this branch, but the reference is given to the followers as a offset with an angle and a degree. This implies that the problem statements from section 4.3.1.1 also applies to the echelon formation, and the main difference is the shape of the formation and how the reference is passed on.

4.3.1.3 Formation Reference Point (FRP) with Path

This method only makes use of one path for the whole formation. The agents in the setup will be defined with relative positions to a FRP at each time step, such that the formation stays rigid and the arms from the FRP to the agents are constants. This setup will in principle work as the followers working in a rigid formation where only the point on the path (the FRP) determines where the agents need to go. The reference given to the agents will be a position in the Formation Reference Frame (FRF), and the formation will have the origo (turning point) in the FRP. The individual agents will not be able to communicate, due to the rigid formation, but only keep the position relative to the FRP. If the formation stays rigid during transients there will be no problem with collision. If one single agent in the FRF fails it will just fall out of the formation and the rest will continue the mission.

4.3.2 Precomputed Individual Paths

4.3.2.1 Full Communication

The implementation of this strategy needs to know for each time step for each agent when the goal at the trajectory is. By doing this it is possible to make the agents be in formation at all times because they have individual positions at their respective paths to specific times. If one of the agents does not reach its position in time, the rest of the agents should stop, or slow down, such that the missing agent has the possibility to catch up. This will change the 'time goals' for the rest of the agents, but the agents will keep the formation. The other option is that the slower agent speeds up, if the agents are not already working at full speed. In this formation principle every agent needs formation about where the others are, which might not be preferable when looking at the bandwidth usage and the scalability of this principle. The same problem will arise when looking at the control architecture, which will only expand more and more when adding more agents. If every agent needs to know information for the others, and act dependent on every single other agent, then the decision and the task allocation will become more complex. When looking into the problem of transients and 'cutting corners', the strategies with individual paths does not have any problems with this. If the formation does cut corners and fail in transients, it is mainly a design error of the path, such that the paths intersect each other. If one of the agents fail during mission then rest will keep close to that agent, unless some kind of exception handling has been made, such that the rest can continue the mission.

4.3.2.2 Limited Communication

The overall principle of this implementation is the same as when full communication, the one mentioned above. The difference is that the communication will be greatly decreased when looking at the bandwidth usage and how many agents that needs to know of each other. In this formation strategy agent i only knows information about the neighbour agents, i_{-1} and i_1. By doing this the information about a slower, or even failed, agent needs to propagate through the formation. If the formation is relatively small, it will not make any remarkable change in the formation structure. If the formation is of a larger size, then the formation will not be as rigid as the one with full communication. If the outer most agent for some reason slows down, then the neighbour needs to act according to that, and the the neighbour of the neighbour needs to act according to that and so on. This will make the formation, in this situation, become skewed, but will go into formation again over time. This is a downside when looking at the transients of the formation and how rigid it is. If the given agent completely fails the mission and breaks down, then the same applies as if there were full communication. An exception needs to be programmed such that the formation will leave the failed agent. The advantage of this strategy is that the control architecture and the communication level will become less complicated, and the scalability to in theory infinitely many agents becomes possible.

4.3.2.3 No Communication

Again is the main principle the same for this strategy, only that no information is shared between the agents. If no information is shared between the agents it is assumed that they do not experience any faults. If one of the agents has a fault, that it changes course, slows down or fails in the mission, it will make the formation to fail. The individual agents will still follow their respective paths, and therefore reach their end goals, but not at the same time. If the agent has failed the mission the others does not take this into account, but instead continues their individual mission. The communication in this strategy is very low, since the agents does not exchange information at all. The control architecture also becomes less complex while this strategy only controls the individual agents i.e. with a simple LOS controller to track their individual paths. If the individual paths have been generated properly there should not be any problems relating the transients, if assumed that every agent follows its path with acceptance. If it does not, and deviate a little, the formation is not rigid. If one agent fails in the mission, it will also lead to formation deviation, but the rest of the agents will keep their respective goals. Though when working as individual agents, this also implies that the scalability becomes less complex because the control is applied at the individual agent that follows its own path.

4.3.3 Potential Field

4.3.3.1 Full Communication

In the strategy with potential fields the level of communication can also vary. If the communication can be shared by all the agents within the potential field, the communication is said to be full. When this is the case, every agent has the information about every other agents position and potential field. This makes the formation, made by the potential field, able to correct if any agent starts to fall behind. This concept is the same as with the precomputed paths, where the communication also could be full. In this case the bandwidth usage is also larger when having full communication than with lower communication. Therefore is the communication level also more complex then every agent needs to exchange information with each other. When every single agent need to be dependent on all the other agents, the constraint level gets higher and the complexity of the needed control architecture also becomes higher. When every agent knows the potential fields of the others there should not become any collision problems in transients. But the formation in general is not as rigid when working with potential fields, because of the principle of attraction and repelling. If one single agent fails, breaks down, the others should still know of its appearance such that they can use the potential field to manoeuvre away from the agent. This is mainly to avoid collision. When the communication and the control architecture becomes more complex under full communication, the scalability also becomes more complex. It is not impossible to scale, but a scaling in theory to infinity will become very complex.

4.3.3.2 Limited Communication

When the communication is said to be limited it means that not all agents can communicate with each other. The communication range of the agents are reduced, such that i.e. agent i only can communicate with agent i_{-1} and i_1, but the range can also be large, i_{-r} and i_r, where r is the communication radius. When doing this the same thing will happen as in the case of limited communication with the individual paths. If one agent starts falling behind then the nearby agents starts to reach first, which then leads to that all agents will reach on the slower agent. Dependent on the formation this will make different hurdles. The formation can try to manoeuvre dependent on the slower agent, but they meanwhile have to follow the potential field map, the given trajectory. In the case of limited communication the same things apply to transients as when full communication, but the formation might diverge more from the determined due to the passing of information between the agents. If one agent breaks down the same goes as with full information, because only the closest agents needs the information about the breakdown to avoid collision. The rest can still continue the mission afterwards. The scaling of the formation becomes a little less complicated than if the agents needed to know information from every agent. Though the potential field mapping will still be complex, and the trajectory generation can be hard.

4.3.3.3 No Communication

In the case where no communication are to find in the system the agents will act like no potential field exists from the other agents, and try to follow the potential field trajectory. This will make every agent, independent of the others, try to follow the trajectory and thereby be in the same point. This will over time make the agents collide, if not on the way to the mission goal then at the mission goal. This means that in this case they need a individual potential field trajectory. When making individual potential field trajectories will the scenario be as in the case of individual paths, where the agents will be controlled individually but with respect of a potential field trajectory. This may also lead to colliding agents but it is not necessary as it will be if they followed the same trajectory. If they follow the same reference trajectory a failed agent will result in all the others following behind that will collide resulting in a complete mission failure. Though if the agents instead have their own respective reference trajectory one failing will not fail the mission. If the formation are unlucky, they can collide, but not necessarily.

4.3.3.4 Summation

The sum is based on the above mentioned categories and is a weighting from -3 to 3 including 0. The focus will be placed on the three strategies that scores the highest rating. These can be seen in table 4.1 to be **Duckling formation**, **Echelon formation** and **Potential field formation**. The duckling- and echelon formations have achieved the high rating due to their simplicity and their relatively easy implementation possibilities, while the potential field formation is of higher complexity but still fulfils the criteria from the analysis. When analysing these three strategies it becomes clear that the difference between duckling formation and echelon formation regarding implementation is not very different. The duckling formation will become a direct intercept from follower to leader, where in theory an infinite number of agents can be attached. These all need to fulfil a distance reference in between to avoid colliding, and a trajectory will need to take wide turns to ensure that the absolute speed of every agent stays above a threshold. If the speed decreases it will lead to the agent over steering thus needs to over actuate in the opposite direction. This will lead to oscillations in the trajectory tracking and a risk of colliding becomes relevant. The echelon formation is an offset between a follower to the leader, where the same applies as for the duckling formation. It is also possible to expand this to an infinite number of agents that couples

Approach	Communication	Control architecture	Obstacle avoidance	—
Leader follower:				
Duckling	Simple, 3	Simple LOS, 3	None, 0	
Echelon	Simple, 3	Simple LOS, 3	None, 0	
FRP with path	Low communication, 0	Simple, 2	None, 0	
Precomputed individual paths:				
Full communication	High bw, 0	Multi agent info, 0	None, 0	
Limited communication	Middle bw, 1	Local agent info, 1	None, 0	
No communication	Low bw, 2	Single agent info, 2	None, 0	
Potential field:				
Full communication	High bw, 0	Multi agent info, 0	Natural, 3	
Limited communication	Middle bw, 1	Local agent info, 1	Natural, 3	
No communication	Low bw, 2	Single agent info, 2	Natural, 2	
	Transients	**Scalability**	**Failure**	**Sum**
Leader follower:				
Duckling	improper path, -1	Easy duplicate, 3	Formation continue, 2	10
Echelon	Improper path, 0	Easy duplicate, 3	Formation continue, 2	11
FRP with path	Improper path, 0	Duplicable, 2	Collapse, -2	2
Precomputed individual paths:				
Full communication	No risk, 3	More bandwidth, -1	Low failure, 2	4
Limited communication	Risk, 2	Possible, 1	Can occur, 0	5
No communication	Risk, 1	Individual paths, 3	High risk, -2	6
Potential field:				
Full communication	No risk, 3	More bandwidth, 0	Low failure, 2	8
Limited communication	Risk, 1	Possible, 1	Low failure, 2	9
No communication	High risk, -2	Single fields, 3	Risk, -1	6

Table 4.1: Decision matrix for the formation strategies. The strategy row from the upper half of the table continues on the lower half, with the points summed in the last column in the lower half.

the formation together. There the agents also need to fulfil a distance reference to withhold the determined distances in between and thus also a speed reference. The last formation is the potential field, which becomes more abstract to interpret. The theory of setting control structures for the potential field is designed of attracting and repulsing forces and be using those also implements obstacle avoidance. The formation strategies are explained in more detain in the following.

4.4 Strategy 1: Potential Field Formation

4.4.1 Potentialfield

In potential fields it is commonly used that a multi-robot group should move in an environment, either with or without obstacles. Papers related to this i.e. are (Song and Kumar, 2002), (Pereira et al., 2003) and (Paul et al., 2008). Within the environment there need to be specified some relative measurements, or states, such that the robots are capable to manoeuvre relative to something. This reference, that the robots should manoeuvre with, is in this case the potential fields. When looking at robots that should keep distance from each other (in a formation), or should move to a desired position (trajectory tracking), the implementation of potential fields come in handy.

The potential field approach can be utilised or implemented in different ways when taking about formation control. Potential fields is often used for cooperative control where the formation between agents is not as important, but rather have the goal of moving agents into formation and then make groups of agents move from one point to another (Goncalves et al., 2010). Therefore to use the potential field mindset it is important to define how these fields works together to achieve some form of formation that can be moved after a predefined path.

Some ideas are to use an individual potential field seen from each agent and combine this with the other agent's local potential field. Here the potential field has local minima defining the desired formation. In addition to this there is also a need to define how this formation can be moved in a predefined path.

Another idea is to use the same potential field, that is a global and common time varying potential field, to define the formation, but this will require that the agents are already near their formation, such that every agent will approach their separate local minimum. This can be used as a leader follower concept where the leader is defining this global potential field.

The potential fields can be defined from attraction- and repulsion forces, dependent on if the robots need to move toward or away from a target, described in (Song and Kumar, 2002), where potential fields are utilized with a virtual structure. When applying a virtual structure the group of robots follow a virtual leader and not another robot relative to the formation. The potential functions can now be used as forces between the agents to repel them, such that they do not collide, which can be called inter-vehicle forces. The potential functions are also used as forces around the virtual leader such that the agents gets as close as possible to the virtual leader without ever reaching it, which can be called virtual leader forces. This will make a defined formation around the virtual leader (Elkaim and Kelbley, 2006). The repelling forces can be utilized in different ways and with advantage used with obstacle avoidance, where these need to contribute with a repelling force to the potential field, making agents diverge from these objects. A great advantage to the virtual leader is that the potential forces can be used to keep the formation and then only generate the trajectory for the virtual leader and not for every individual agent (Elkaim and Kelbley, 2006). The virtual leader can also be an agent as the reference point in the formation but is mostly thought of as the reference point for all agents in the formation.

4.5 Strategy 2: Leader-Follower

The leader-follower principle is used as a higher order principle of how to navigate a group of robots. The principle is that a leader is defined to lead the group of robots in an environment relative to a trajectory. Instead of all the individual robots tracking their respective trajectories, only the leader follows a trajectory and the following robots keep their position relative to the leader position.

The way that the followers maintain their position can be done in different ways e.g. potential fields (Song and Kumar, 2002), behavioural methods as Null Space Based behavioural methods (Arrichiello et al., 2006) or versions of a direct LOS algorithm. With the focus in here the formation should be defined as a ’rigid’ formation, where the follower’s positions are defined as fixed distances from the leader. The term rigid is not a strict description in this case because the formation can vary a little all the time, but it is not flexible either (Egerstedt and Hu, 2001).

The positions should be defined individually for each of the followers to the position of the leader. This can be done through a formation constraint function, $F(\eta)$, which should be a strict convex function to ensure the formation constraint (the actual formation). This formation constraint function can be expressed in different ways, with the actual positions of the agents and the virtual leader or positions of the agents relative to the virtual leaders starting position.

From the decision table 4.1 it can be seen that duckling formation and echelon formation have got a high rating. These are both branches of the leader-follower principle which often shows to be applicable in formation issues (Tanner et al., 2004), (Carpin and Parker, 2002), (Egerstedt and Hu, 2001).

The duckling formation is a direct intercept algorithm, where the followers intercept their respective leaders and withholding a desired safety distance to their leaders. They will form a chain of leader-follower-follower-follower continuing with followers until the desired amount of robots are in the formation. This formation is named duckling since this will be as a family of ducks where the children follow directly after their parents and does not care about anything on their way.

The echelon formation is a branch from the duckling formation where, instead of a direct pursuit, the followers are given a offset from the leader thus spanning the formation. This offset can be given in different ways i.e. with a desired difference in distance in a fixed angle from the leader. In the same way as the duckling formation this also has the opportunity to expand with a desired amount of robots in the formation that follows their respective leaders.

4.6 Strategy 3: Multi Path Following

Multi paths, or individual paths, for the vessels is where the agents follow their respective paths with respect to time along the path. This needs to make a formation for the vessels. They might only need to know from each other how far they are on their respective paths, such that every agent has a time depending factor on the path. If every agent fulfils its time dependency, this ensures, also by design of the path, that no collision will occur. The paths for the individual agents can be designed from the trajectory of the leader with an offset both in distance in a direction and a time. The time dependencies can make the following agents lack in time thus make this formation as a echelon formation, and the distance with a direction spans the formation itself. The different positions for the ith agent will then need to fulfil that the position is the desired position at a specific time

$$\eta_d(t) = \eta(t) \tag{4.11}$$

where the error in position needs to be zero, $e_\eta(t) = \eta_d(t) - \eta(t) = 0$. The same needs to be fulfilled for the heading of the agents

$$\psi_d(t) = \psi(t) \tag{4.12}$$

where the error in heading needs to be zero, $e_\psi(t) = \psi_d(t) - \psi(t) = 0$. When these two parameters given at the path are fulfilled the group of agents are said to be in formation. This formation strategy will not be tested as it did not get the highest rating from the analysis in the decision table 4.1. Though it can be a preferable way of designing the formation if the path can be generated to the specific case.

Chapter 5

Modelling

This chapter describes the modelling of AAUSHIP. This is necessary to be able to use model based control algorithms and estimators.

5.1 Hydrodynamic Modelling

Hydrodynamic added mass is defined as the mass added to a system due to an accelerating or decelerating body that needs to move a volume of the surrounding fluid as it moves through it. To this is said that the object and fluid is not able to occupy the same physical space simultaneously. An overall model can be given as:

$$M_A \dot{\nu}_r + C_A(\nu_r)\nu_r + D(\nu_r)\nu_r + g(\eta_r) = \tau \tag{5.1}$$

where

$$\begin{aligned}
&M_A \text{ is the added mass matrix from the system}\\
&C_A \text{ is the added mass matrix due to the Coriolis force}\\
&D(\nu) \text{ is a combination of the potential and viscous damping matrices}\\
&g(\eta) \text{ is the restoring forces, which is dependent on the position of the vessel}\\
&\tau \text{ is control and propulsion forces}\\
&\nu \text{ is the velocities of the vessel in all directions and moments}
\end{aligned} \tag{5.2}$$

5.2 Rigid Body Modelling

The rigid body is used to model the physics of the vessel. It is an idealisation of the solid body from where the physical motions of the vessel are to be derived. Translational motion and rotational motion can be derived by analysis of this, and by (SNAME, 1950) and (Fossen, 2011, sec. (3.3.1)) written in component form as:

$$f_b^b = [X,Y,Z]^T \quad - \text{force through } o_b \text{ expressed in } \{b\} \tag{5.3}$$
$$m_b^b = [K,M,N]^T \quad - \text{moment about } o_b \text{ expressed in } \{b\} \tag{5.4}$$
$$v_{b/n}^b = [u,v,w]^T \quad - \text{linear velocity of } o_b \text{ relative } o_n \text{ expressed in } \{b\} \tag{5.5}$$
$$\omega_{b/n}^b = [p,q,r]^T \quad - \text{angular velocity of } b \text{ relative to } \{n\} \text{ expressed in } \{b\} \tag{5.6}$$
$$r_g^b = [x_g,y_g,z_g]^T \quad - \text{vector from } o_b \text{ to CG expressed in } \{b\} \tag{5.7}$$

The rigid body forces are written as:

$$M_{RB}\dot{\nu}_r + C_{RB}(\nu_r)\nu_r = \tau_{RB} \tag{5.8}$$

where

M_{RB} is the system inertia matrix
C_{RB} is coriolis-centriopedal matrix
τ_{RB} is a lumped force combined of $\tau_{\text{hyd}} + \tau_{\text{hs}} + \tau_{\text{wind}} + \tau_{\text{wave}}$

where in τ_{RB}

τ_{hyd} is the hydrodynamic force
τ_{hs} is the hydrostatic force
τ_{wind} is the wind force
τ_{wave} is the wave force

5.3 Total Model of Vessel

$$\underbrace{M_{RB}\dot{\nu}_r + C_{RB}(\nu_r)\nu_r}_{\text{rigid-body forces}} + \underbrace{M_A\dot{\nu}_r + C_A(\nu_r)\nu_r + D(\nu_r)\nu_r + g(\eta_r)}_{\text{hydrodynamic forces}} = \tau + \tau_{RB} \tag{5.9}$$

Since the vessel within this project is of smaller scale, the C_A and C_{RB} from (5.1) and (5.8) are neglected (Wondergem, 2005, eq. (2.23)). The model also builds on the assumption that the vessel will manoeuvre at lower speed, being $|u| < 2.0$. By assuming this the terms of low speed can be applied, which implies that some of the forces and moments can be linearized about $\nu = 0$ and that the pitch and roll angles can be linearized about the zero angle, their steady state (Fossen, 2011, p.174-175). M_A is the added mass and is as a start omitted due to the tests needs to be made as an object moving through the water with some drag, mass damper test. If the model needs to be further improved in the process this is a place to start modelling. The coefficients of M_A are rather inconvenient to determine without advanced equipment like a towing tank, where constant velocity can be applied and measure drag and more in all directions and moments. C_A and C_{RB} represents forces due to a rotation of the body frame, $\{b\}$, about the inertial frame, the NED frame. These are omitted as well due to the small vessel where the body frame is placed in a predefined local frame which acts as the NED frame. This reduces equation (5.9) down to the following:

$$M_{RB}\dot{\nu}_r + D(\nu_r)\nu_r + g(\eta_r) = \tau_{RB} + \tau \tag{5.10}$$

The damping matrix which contains the coefficients of the drag is denoted the hydrodynamic damping matrix. This consists both of D which is the linear damping matrix due to potential damping and possible skin friction with the water and $D_n(\nu_r)$ which is the nonlinear damping matrix due to quadratic damping and higher order terms. This can be expressed as $D(\nu_r) = D + D_n(\nu_r)$. This will, as a start, be modelled as the linear part, being potential and viscous damping. At higher velocities will the nonlinear part become more dominant due to the quadratic terms of the velocity, thus is mostly used with faster vessels. The linear damping matrix D contributes more at lower speed manoeuvrings and stationkeeping, $|u| < 2$ ${}^{\mathrm{m}}/_{\mathrm{s}}$ (Fossen, 2011, fig. (7.2)). Therefore is the damping matrix D used, and is expressed by (Fossen, 2011, eq. (6.62)) for a 6 DOF system to be:

$$D = -\begin{bmatrix} X_u & 0 & 0 & 0 & 0 & 0 \\ 0 & Y_v & 0 & Y_p & 0 & Y_r \\ 0 & 0 & Z_w & 0 & Z_q & 0 \\ 0 & K_v & 0 & K_p & 0 & K_r \\ 0 & 0 & M_w & 0 & M_q & 0 \\ 0 & N_v & 0 & N_p & 0 & N_r \end{bmatrix} \tag{5.11}$$

The rigid-body system matrix of the vessel is given for a 6 DOF system by (Fossen, 2011, eq. (3.44)) as:

$$\begin{aligned} M_{RB} &= \begin{bmatrix} m\boldsymbol{I}_{3x3} & -m\boldsymbol{S}(r_g^b) \\ -m\boldsymbol{S}(r_g^b) & \boldsymbol{I}_b \end{bmatrix} \\ &= \begin{bmatrix} m & 0 & 0 & 0 & mz_g & -my_g \\ 0 & m & 0 & -mz_g & 0 & mx_g \\ 0 & 0 & m & my_g & -mx_g & 0 \\ 0 & -mz_g & my_g & I_x & -I_{xy} & -I_{xz} \\ mz_g & 0 & -mx_g & -I_{yx} & I_y & -I_{yz} \\ -my_g & mx_g & 0 & -I_{zx} & -I_{zy} & I_z \end{bmatrix} \end{aligned} \tag{5.12}$$

The restoring forces acting on the vessel, while not in zero angle position in pitch and roll, is given by the coefficients of the g matrix. The restoring forces acts on the vessel when it is perturbed away from the steady state angle in both pitch and roll. Then vessel will, due to Archimedes law, move back into steady state. The change in mass under waterline will rotate back to steady state and the change in angle will become zero. The coefficients in g is the nonlinear terms contributing to the restoring force. Though it can be convenient to use the linear approximation, defined for a 6 DOF system by (Fossen, 2011, eq. (4.22)(4.26)), as:

$$g(\eta) \approx G\eta \tag{5.13}$$

where G, for an asymmetric vessel, is defined as:

$$G = -\begin{bmatrix} 0 & 0 & 0 & 0 & 0 & 0 \\ 0 & 0 & 0 & 0 & 0 & 0 \\ 0 & 0 & -Z_z & 0 & -Z_\theta & 0 \\ 0 & 0 & 0 & K_\phi & 0 & 0 \\ 0 & 0 & -M_z & 0 & M_\theta & 0 \\ 0 & 0 & 0 & 0 & 0 & 0 \end{bmatrix} \tag{5.14}$$

This reduction is done under the assumption of small angles. Therefore is the water plane area approximately the same, which makes the of this a constant. By doing this it is only relevant to look at the heave, roll and pitch restoring forces, which can be used in a linearised model.

5.3.1 Model reduction

The model will be reduced to a 5 DOF system due to the fact that the vessel's buoyancy cannot be controlled as such. The vessel will always be on the water surface and this removes the degree a freedom which is the heave, the change of z position of the vessel. A 5 DOF system will be modelled as:

$$M_{RB} = \begin{bmatrix} m & 0 & 0 & mz_g & -my_g \\ 0 & m & -mz_g & 0 & mx_g \\ 0 & -mz_g & I_x & -I_{xy} & -I_{xz} \\ mz_g & 0 & -I_{yx} & I_y & -I_{yz} \\ -my_g & mx_g & -I_{zx} & -I_{zy} & I_z \end{bmatrix} \tag{5.15}$$

and

$$D = -\begin{bmatrix} X_u & 0 & 0 & 0 & 0 \\ 0 & Y_v & Y_p & 0 & Y_r \\ 0 & K_v & K_p & 0 & K_r \\ 0 & 0 & 0 & M_q & 0 \\ 0 & N_v & N_p & 0 & N_r \end{bmatrix} \tag{5.16}$$

and

$$G = -\begin{bmatrix} 0 & 0 & 0 & 0 & 0 \\ 0 & 0 & 0 & 0 & 0 \\ 0 & 0 & K_\phi & 0 & 0 \\ 0 & 0 & 0 & M_\theta & 0 \\ 0 & 0 & 0 & 0 & 0 \end{bmatrix} \tag{5.17}$$

where the heave are neglected from the 6 DOF system. In the principle could a 3 DOF system be enough to make the control to the vessel and make it manoeuvre in the water, but as the scope is to exploit the sonar to map the seabed it would be beneficial to implement the roll and pitch as well and make the system as a 5 DOF. The G matrix has been reduced under the assumption that there exists yz-symmetry, which is a good assumption based on the design of the vessel.

5.4 Identification of Hydrodynamic Derivatives

The linear model ((5.18)), which is used to model AAUSHIP, consists of the mass matrix M_{RB}, the damping matrix D and the restoring force matrix G. This makes the system as:

$$M_{RB}\dot{\nu}_r + D\nu_r + G\eta = \tau_{RB} + \tau \tag{5.18}$$

The coefficients of the model needs to be determined before the model can be simulated and implemented. These coefficients can be determined in multiple ways. Often ship design companies are able to use Computational Fluid Dynamics (CFD) to determine the coefficients, or make use of a towing tank to determine the coefficients. These applications are often expensive and proprietary. So a third method to do this is to perform tests to do approximations of the coefficients. To do so some assumptions needs to be made. The model is defined as:

$$M_{RB}\dot{\nu}_r + D\nu_r + G\eta = \tau_{hyd} + \tau_{hs} + \tau_{wind} + \tau_{wave} + \tau \tag{5.19}$$

Since the tests will be performed in still water some of the forces can be neglected. This makes τ, τ_{hyd} and τ_{hs} the only forces to be taken into account to perform the tests. This is the input to the vessel and the forces acting on the vessel while moving, and after reduction make the system as (5.20), which is assumed while tests are performed:

$$M_{RB}\dot{\nu}_r + D\nu_r + G\eta = \tau_{hyd} + \tau_{hs} + \tau \tag{5.20}$$

The system is modelled as a 5 DOF system and the necessary coefficients are found in appendix A. In the appendix are some tests described and performed to be able to determine the coefficients for the model. This includes both the rigid body mass, the damping matrix and the restoring force matrix.

The final system ends up being as follows.

The rigid body mass matrix have been weighted and measured, and is estimated to be as in equation (5.21).

$$M_{RB} = \begin{bmatrix} 13 & 0 & 0 & -0.39 & 0 \\ 0 & 13 & 0.39 & 0 & -0.39 \\ 0 & 0.39 & 0.06541 & -0.01260 & -0.05359 \\ -0.39 & 0 & -0.01260 & 1.08921 & -0.00108 \\ 0 & -0.39 & -0.05359 & -0.00108 & 1.10675 \end{bmatrix} \tag{5.21}$$

The linear damping matrix, which holds the translational damping and cross terms, have been estimated to be as in equation (5.22).

$$D = \begin{bmatrix} 2.86 & 0 & 0 & 0 & 0 \\ 0 & 32.5 & -0.00503 & 0 & 0.09263 \\ 0 & -0.975 & 0.1094 & 0 & 0.01273 \\ 0 & 0 & 0 & 7.2030 & 0 \\ 0 & 0.975 & -0.00069 & 0 & 0.26285 \end{bmatrix} \tag{5.22}$$

Lastly is the restoring force matrix, which is the one bringing the vessel back to steady state in pitch and roll. This has been estimated to be as in equation (5.23).

$$G = \begin{bmatrix} 0 & 0 & 0 & 0 & 0 \\ 0 & 0 & 0 & 0 & 0 \\ 0 & 0 & 6.9736 & 0 & 0 \\ 0 & 0 & 0 & 131.8316 & 0 \\ 0 & 0 & 0 & 0 & 0 \end{bmatrix} \tag{5.23}$$

Chapter 6

Simulation Model

This chapter will describe the model that is used for simulation of the system, as a replacement for testing on the real ship.

To make a model as simulation model, it is needed to emulate the real sensor outputs with noise imposed onto the signals. Using a Linear Time Invariant (LTI) state space model based on the unified model (5.9) on page 38 is constructed as (6.1) as defined by (Fossen, 2011, p. 175).

$$\dot{x} = Ax + Bu + Ew \tag{6.1a}$$

$$y = Hx + v \tag{6.1b}$$

$$A = \begin{bmatrix} 0 & I \\ -M^{-1}G & -M^{-1}D \end{bmatrix}, \quad B = \begin{bmatrix} 0 \\ M^{-1} \end{bmatrix}, \quad E = \begin{bmatrix} 0 \\ M^{-1} \end{bmatrix} \tag{6.1c}$$

The matrix E describes the sea state and vector w the process noise, and vector v the sensor (measurement) noise. Both noise vectors are assumed zero-mean Gaussian white noise processes.

6.1 Position Trajectory in NED

The position trajectory (6.2b) in NED is calculated with numerical euler integration of the velocities (6.2a).

$$\dot{\mathbf{p}}^n_{b/n} = \mathbf{R}^n_b(\mathbf{\Theta}_{nb})\boldsymbol{\nu}^b_{b/n} \tag{6.2a}$$

$$\mathbf{p}^n_{b/n}(k+1) = \mathbf{p}^n_{b/n}(k) + h\dot{\mathbf{p}}^n_{b/n} \tag{6.2b}$$

$$= \mathbf{p}^n_{b/n}(k) + h\mathbf{R}^n_b(\mathbf{\Theta}_{nb}(k+1))\boldsymbol{\nu}^b_{b/n}(k+1) \tag{6.2c}$$

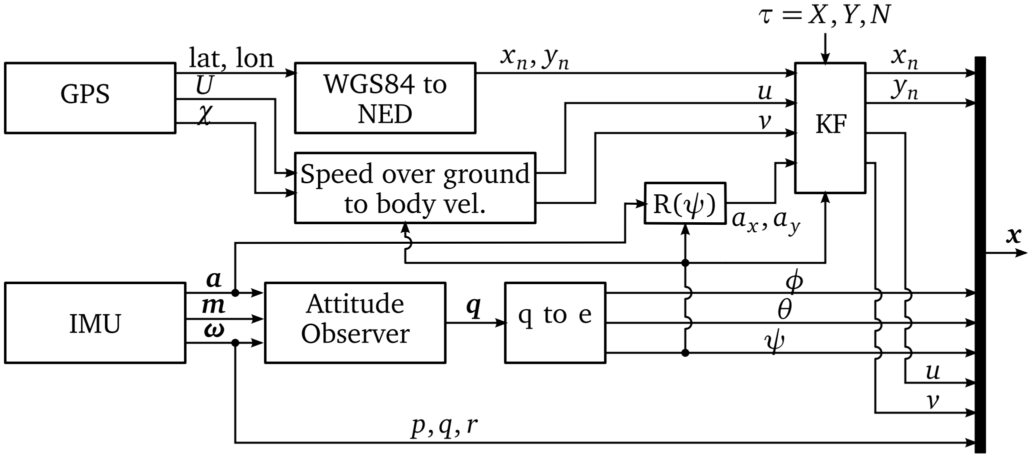

Figure 6.1: Block diagram over the computation of system states from raw sensor measurements.

The generalised position, velocity, acceleration and force vectors, in that order, is:

$$\boldsymbol{\eta}^n = \begin{bmatrix} \mathbf{p}^n_{b/n} \\ \boldsymbol{\Theta}_{nb} \end{bmatrix}, \qquad \boldsymbol{\nu}^b = \begin{bmatrix} \boldsymbol{\nu}^b_{b/n} \\ \boldsymbol{\omega}^b_{nb} \end{bmatrix}, \qquad \dot{\boldsymbol{\nu}}^b = \begin{bmatrix} \dot{\boldsymbol{\nu}}^b_{b/n} \\ \dot{\boldsymbol{\omega}}^b_{n/b} \end{bmatrix}, \qquad \boldsymbol{\tau}^b = \begin{bmatrix} \mathbf{f}^b_b \\ \mathbf{m}^b_b \end{bmatrix} \tag{6.3}$$

From this it can be seen that the velocities, the derivative of η, can be given as:

$$\dot{\eta} = J_{\Theta}(\eta)\nu \tag{6.4}$$

$$\begin{bmatrix} \dot{\mathbf{p}}^n_{b/n} \\ \dot{\boldsymbol{\Theta}}_{nb} \end{bmatrix} = \begin{bmatrix} \boldsymbol{R}^n_b(\boldsymbol{\Theta}_{nb}) & 0_{3x3} \\ 0_{3x3} & \boldsymbol{T}_{\Theta}(\boldsymbol{\Theta}_{nb}) \end{bmatrix} \begin{bmatrix} \boldsymbol{\nu}^b_{b/n} \\ \boldsymbol{\omega}^b_{b/n} \end{bmatrix} \tag{6.5}$$

These are the basis of the model that are to be developed and used within the AAUSHIP project.

6.2 Sensor Measurements to State Vector

For the control system it is needed to convert the sensor measurements to the system state vector, such that the control system can be designed. Figure 6.1 shows the computation flow to determine this. It shall be noted that the Global Positioning System (GPS) and Inertial Measurement Unit (IMU) blocks has the sensor noise integrated in them.

Now that the state vector is present, a state observer can be used in i.e. a KF to filter and reduce the noise.

Since the simulation is performed by iterating over the state space model, it is somehow needed to get the variances from the sensors modelled in the state space model. Because of the intermediate computations described in the figure 6.1 it is not straight forward to add the sensor noise to the model, because this noise is specified at the raw sensor measurements. So some way has to be made to calculate the noise.

A method is to set the sensor measurements to no movement values, and only add the noise on the measurements. If all sensors were zero in stagnation, then it would be enough to simulate this with only noise and get the corresponding variance out. This is not the case, as the magnetometer has a bias, just because it is situated in a constant magnetic field and this is dependent on the attitude of the ship. So to compute the variances on the state vector it is needed to make multiple simulations where this bias is different also. A normalized normal distribution of this should suffice.

6.3 SOG to Body Frame Velocities

The Speed Over Ground block on the figure 6.1 on the preceding page is used to calculate the body frame velocities in surge u and sway v, which in turn is filtered by the Kalman filter described in section 6.9 on page 54. The block on the diagram uses the Speed Over Ground (SOG) from the GPS, denoted as the magnitude U and the course angle relative to true north, denoted the course angle χ, which is the sum of the heading ψ and sideslip β angles:

$$\chi = \psi + \beta \quad \Rightarrow \quad \beta = \chi - \psi \tag{6.6}$$

To calculate the body frame velocities the rotation matrix around z is used. It is enough to use this one basic rotation, because this is on the 2D system (x, y) in the NED frame.

$$R_z(\psi) = \begin{bmatrix} \cos(\psi) & -\sin(\psi) \\ \sin(\psi) & \cos(\psi) \end{bmatrix} \tag{6.7}$$

First the course speed magnitude U can be calculated in NED by the following computation, where we describe the course speed as a vector $[U \quad 0]^\top$, such that the

$$U_n = R_z(\chi) \begin{bmatrix} U \\ 0 \end{bmatrix} = \begin{bmatrix} \cos(\chi) \\ \sin(\chi) \end{bmatrix} U \tag{6.8}$$

Now this can be rotated into The body frame (BODY), using the same rotation matrix (6.7), but with the sideslip angle instead of the course angle. Such that:

$$U_b = \begin{bmatrix} u \\ v \end{bmatrix} = R_z(\beta) U_n \tag{6.9}$$

Assuming the course speed vector in relation to the BODY (as opposed to NED initially suggested) it is enough to use the sideslip for rotation directly.

$$U_b = R_z(\beta) \begin{bmatrix} U \\ 0 \end{bmatrix} = \begin{bmatrix} \cos(\beta) \\ \sin(\beta) \end{bmatrix} U \tag{6.10}$$

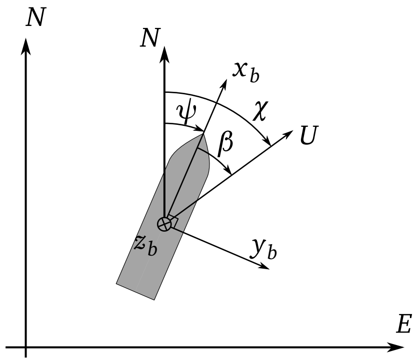

Figure 6.2: Plot showing the different angles used. The in equation (6.6) on the previous page. χ is the course angle, ψ is the heading angle, β is the sideslip angle, U is the velocity vector, and N and E is the northing and easting in NED, respectively.

6.4 Magnetic and Acceleration Vectors from State Attitude

The simulation model state vector do not contain magnetic field strength directly. Therefore it has to be calculated from the attitude, which is the pitch, roll and yaw values.

First the magnetic field direction has to be known for the area where the system operates. There exists models of the magnetic field on the earth, accessible from (National Oceanic and Atmospheric Administration , NOAA). Using the "WMM 2010" model, the declination and inclination has been determined to be 2.167° (east), and 70.883° (down) respectively. Additionally the field strength is about 50432 nT.

This defines the magnetic field in the earth frame as:

$$m_n = \begin{bmatrix} 0 & \text{inclination} & \text{declination} \end{bmatrix}^\top \tag{6.11}$$

The magnetic field in the body frame m_b is:

$$m_b = R_b^n(\Theta_{nb}) m_n \tag{6.12}$$

where the rotation matrix $R_b^n(\Theta_{nb})$ (6.14).

$$R_b^n(\Theta_{nb}) = \begin{bmatrix} c\psi c\theta & -s\psi c\theta + c\psi s\theta s\phi & s\psi s\phi + c\psi c\phi s\theta \\ s\psi c\theta & c\psi c\phi + s\phi s\theta s\psi & -c\psi s\phi + s\theta s\psi c\phi \\ -s\theta & c\theta s\phi & c\theta s\phi \end{bmatrix} \tag{6.13}$$

$$R_n^b(\Theta_{nb}) = R_b^n(\Theta_{nb})^{-1} \tag{6.14}$$

where $s\cdot = \sin(\cdot)$ and $c\cdot = \cos(\cdot)$. Θ_{nb} is the Euler angles of the b in n.

The acceleration is made in a similar way as the magnetic body vector is made, except it adds the bodyframe accelerations caused by the ship itself.

$$a_{\text{IMU}} = [a_{bx}, a_{by}, 0]^T + R_n^b(\Theta_{nb})[0, 0, g]^\top \tag{6.15}$$

where g is the gravity, defined as 9.82 m/s^2

6.5 Reconstruction of Body Accelerations

The ship is equipped with an accelerometer, but this does not mean that the accelerations measured is in the body frame, a_b, because it also measure the the added gravity vector. This gravity vector has to be subtracted before the body acceleration is know. This is calculated by defining the gravity vector in the NED frame a_g, then rotate that to the body frame and subtract it from the IMU measurement a_{IMU}.

$$a_g = [0, 0, g]^\top \quad , \quad a_{\text{IMU}} = [a_x, a_y, a_z]^\top \quad , \quad a_b = [a_{bx}, a_{by}, a_{bz}]^\top \tag{6.16}$$

Where g is the gravitational acceleration, and the computation is (6.17), which is basically the opposite of (6.15) on the facing page.

$$a_b = a_{\text{IMU}} - R_n^b(\Theta_{nb})a_g \tag{6.17}$$

6.6 Attitude and Heading Reference System

On figure 6.1 on page 44 a block is representing an attitude observer. This part of the system is an observer that is used together with the on-board IMU. Its input is raw linear acceleration, gyration rate and magnetic field strength to determine the attitude and heading of the ship.

As described on figure 6.9 on page 55 and attitude observer is needed, this is realised by implementing the Attitude and Heading Reference System (AHRS) described here.

6.6.1 Mahony Filter

An AHRS filter described in the (Mahony et al., 2008a) is widely used on mini aerial vehicles worldwide according to the conclusion of the paper. Other papers of the same authors discuss different aspects of this filter in (Mahony et al., 2008b) and (Euston et al., 2008).

The paper demonstrates two filter approaches, termed the *direct complementary filter* and the *explicit complementary filter*, where the first needs all outputs typically found in IMU's measurements (accelerometer, gyrometer and magnetometer) whilst the second does not need the magnetometer measurements.

In its simplest form a complementary filter is a filter, which takes advantage of the difference between two types of measurements, in this case the gyrations and accelerations. In a stationary case the accelerations are enough to determine the attitude when exposed to the gravitational field, which should point "down". For the case of a actuated body, not only the gravitation is affecting the measured accelerations, but also the forces from the actuators (or disturbances for that matter) is imposed on the measurements.

This means that it is not enough to use only the accelerometer to calculate the attitude, so an option is to use the gyrometer, which measures the angular rate, which again can be integrated to give an angular position. This position from the gyrometer, will drift over time, but will be fairly accurate in a short lookahead time.

The complementary filter uses these properties and fuses the measurements to an estimate of the attitude. This can be done by interpreting the accelerations over longer time and add those to the attitude from the gyrometer, hence the result is an estimate that is composed of the most recent gyrations and the average acceleration.

6.7 Thrust Allocation

Thrust allocation is a way to relate the desired actuation forces to multiple inputs. In the simplest case it is a scaling factor on the inputs. On real ship one also include the power management system in the thrust allocation system, such that the system knows if it can deliver the power needed or reconfigure the allocation such the need can be met.

For AAUSHIP there is no power management, hence a simple case of the thrust allocation can be used.

$$f = Ku \tag{6.18}$$

$$\begin{aligned} \tau &= T(\alpha)f && \text{(6.19a)} \\ &= T(\alpha)Ku && \text{(6.19b)} \end{aligned}$$

For thrusters where the thrust characteristics do not map proportionally to forces, the computed u values must be mapped to the relevant actuator commands. This is done through a thrust allocation matrix, which are to be determined.

Symbol	Value	Unit
l_{x1}	0.41	m
l_{x2}	0.18	m
l_{x3}	0.48	m
l_{x4}	0.48	m
l_{y3}	0.05	m
l_{y4}	0.05	m

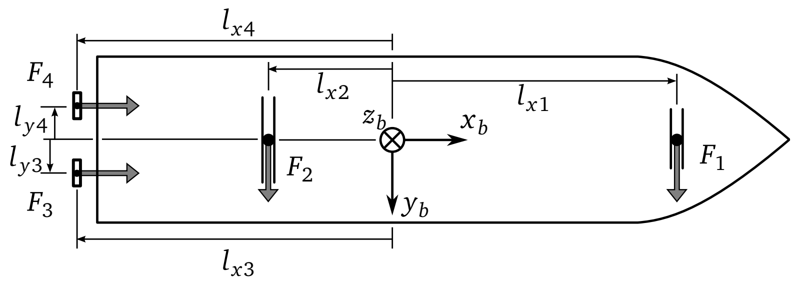

Figure 6.3: Thrust configuration for AAUSHIP. F_1 and F_2 are the bow thrusters and F_3 and F_4 the main propellers. Grey fat arrows indicate positive thrust vector given positive input.

As seen on figure 6.7 there are forces applied in determined directions. These have been set to calculate how the forces acts on the vessel. The distances from the centre of the vessel to the actuators determine with what angle the actuators act on the AAUSHIP and thus how the resulting thrust allocation will be.

The arms from the centre to the actuators is given by the respective lengths, such that these will be given as, in $[x, y, z]$ distances:

$$l_1 = [0.41, 0, 0.05] \tag{6.20}$$
$$l_2 = [-0.18, 0, 0.05] \tag{6.21}$$
$$l_3 = [-0.48, 0.05, 0.05] \tag{6.22}$$
$$l_4 = [-0.48, -0.05, 0.05] \tag{6.23}$$

After determine the arms to the actuators it can be specified how the angles will be to afterwards determine the individual components of the forces. This will, with the arms to the thrusters, give the rotational forces acting on the AAUSHIP.

The only angles that are needed are the angles to the two main thrusters from the centre, since they are the only ones that gives a rotational force to the vessel. This angle is the same to both thrusters, and are given from the arms by:

$$\alpha = \arctan\left(\frac{l_z}{l_x}\right) = \arctan\left(\frac{0.05}{0.48}\right) \tag{6.24}$$

The top of the thrust allocation matrix will be given by the X and Y forces, which are purely translational forces. These can be given by the forces from each of the thrusters in x, y and z directions, named by every thruster as F_1, F_2, F_3 and F_4:

$$F_1 = [0, 1, 0] \tag{6.25}$$
$$F_2 = [0, 1, 0] \tag{6.26}$$
$$F_3 = [\cos(\alpha), 0, -\sin(\alpha)] \tag{6.27}$$
$$F_4 = [\cos(\alpha), 0, -\sin(\alpha)] \tag{6.28}$$

The forces of F_3 and F_4 can be split as seen on figure 6.4, which shows why the z part is of negative sign. Though only the two top rows are the ones contributing in the X and Y

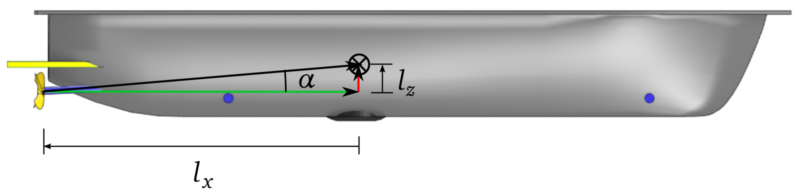

Figure 6.4: Split up of the components of F_3 to see the translational forces.

forces, thus those being in the final thrust allocation matrix.

The contribution of forces in roll, pitch and yaw, K, M and N, will be determined by the cross product of the translational forces and the arms, which will give the rotational moments and their contributions. These will be calculated as:

$$\tau_{1r} = F_1 \times \mathrm{l}_1 \tag{6.29}$$
$$\tau_{2r} = F_2 \times \mathrm{l}_2 \tag{6.30}$$
$$\tau_{3r} = F_3 \times \mathrm{l}_3 \tag{6.31}$$
$$\tau_{4r} = F_4 \times \mathrm{l}_4 \tag{6.32}$$

By doing this will the thrust allocation matrix be given as the top two rows of the translational forces and the bottom three rows of the rotational moments:

$$\mathbf{T} = \begin{bmatrix} F_1(1:2) & F_2(1:2) & F_3(1:2) & F_4(1:2) \\ \tau_{1r} & \tau_{2r} & \tau_{3r} & \tau_{4r} \end{bmatrix} \tag{6.33}$$

$$= \begin{bmatrix} 0 & 0 & 0.9946 & 0.9946 \\ 1 & 1 & 0 & 0 \\ -0.05 & -0.05 & 0.0052 & -0.0052 \\ 0 & 0 & 0.0995 & 0.0995 \\ 0.41 & -0.1800 & -0.0497 & 0.0497 \end{bmatrix} \tag{6.34}$$

The two bow thrusters are not at the moment used to control the AAUSHIP because their individual forces that they can apply at the vessel are relatively low. This means that the final thrust allocation matrix should neglect these two actuators, which is done by removing the two first columns of the thrust allocation from before. Thereby will the final thrust allocation matrix be defined as in equation (6.35).

$$\mathbf{T} = \begin{bmatrix} 0.9946 & 0.9946 \\ 0 & 0 \\ 0.0052 & -0.0052 \\ 0.0995 & 0.0995 \\ -0.0497 & 0.0497 \end{bmatrix} \tag{6.35}$$

On figure 6.5 can be seen in principle how this thrust allocation will be implemented. It takes in the desired control forces to the AAUSHIP and converts these to actuator inputs that are needed to make the AAUSHIP move with the desired forces.

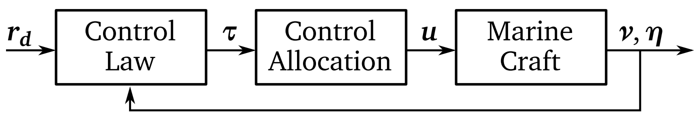

Figure 6.5: Block diagram showing the thrust allocation block in a feedback control system (Fossen, 2011, fig.12.25). The thrust allocation converts the computed control forces to actuator inputs.

6.8 Model Verification

In order to confidently use the model developed in the modelling chapter 5 on page 37, it is important to verify that it actually reflect the real behaviour of the AAUSHIP. This section will be used as a sanity check for the model and give indication of how well the model fits with the real ship.

As the hydrodynamic model parameters has been determined in the appendix A on page 95, using the state space representation presented in (6.1) on page 43, it can be used to verify the complete simulation model.

6.8.1 Step Response

A step response of the model can be used to verify the steady state input-output relations. This can both give the steady state but also the time constant to verify the system. This can be done by accelerating the vessel from steady state and measure the velocity curve of the ship. The vessel will reach zero acceleration which implies constant velocity, from where the time constant can be measured. This time constant needs to be approximately the same for the vessel and the model of the vessel. All the steady state input-output relations will be approximately the same, i.e. like the time constant in surge. The same kind of test may be performed from all steady state scenarios, but the critical is the surge velocity, that ensures that the vessel reaches the correct velocity and decelerates again. The model have been tested in surge, which can be seen on figure 6.6. On the figure can be seen that the vessel accelerates to a constant surge velocity, which is also assumed to happen. Afterwards, when then input it set to zero, the velocity will go toward zero and the vessel will be still in position. On the lower half of the figure is the pitch angle represented. This pitch does not apply the assumptions and observations from the real AAUSHIP. It can be noted that the pitch angle is very small, being $\theta = 6 \cdot 10^{-3}$ rad. This corresponds to a pitch angle of $\theta = 0.34°$. This is not a correct value of the pitching angle, but the work with the model does not seem to uncover why this angle is not correct. It is expected by observation that the pitch angle should be around $\approx 4°$ which is far from what the model predicts. Though after trying to locate the error, it is assessed that this is not that critical an error. This is due to the fact it does not have an influence of how the model will perform while surging. The correct pitch angle can be read from the sensors and used to make the post processing of the seabed data from the surveying.

6.8.2 Stability

A stability analysis can be conducted by examining the eigenvalues of the system. To ensure stability it is a criteria that the eigenvalues should all be stable for this system. This is fulfilled if the real part of all the eigenvalues of the system are negative, which implies a stable fixed point.

Stability of the discretised version also has to be checked by ensuring that the pole-zero map is within the unit circle. The eigenvalues of the Jacobian also needs to have absolute value less than one, which implies placement within the unit circle. If these are placed within the unit circle it is also a fixed point. If just one eigenvalue is greater than one it implies instability. If the eigenvalue is exactly equal to one it needs further investigation by looking more into the Jacobian.

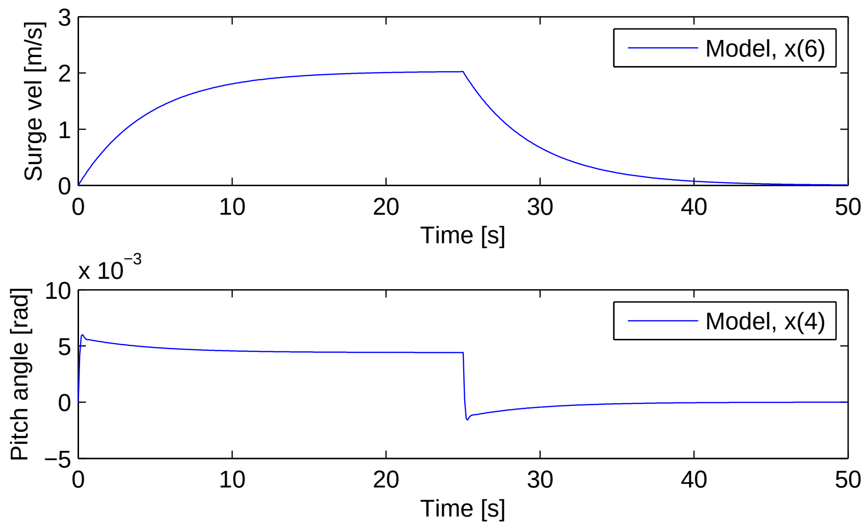

Figure 6.6: The output of the model in surge, where constant input is applied and after some time set to zero.

6.8.3 Simulation of the Model

A final verification is to compare the correlation between a sea trail operated by human operator. It is desired to make manoeuvres similar to what the system is supposed to perform with focus on the surge velocity. That is i.e. making a test with the same input as given to the model in figure 6.6. The velocities should map approximately with each other within an acceptable level. Four tests with the same input as in figure 6.6 have been showed on figure 6.7.

The comparison between those shows that the constant surge velocity is approximately the same. The measurements is a little lower in the velocity but not at a critical level. The damping of the system has been determined from appendix A, thus is the damping also a relatively good match. In both cases, the model and the measurements, it takes about 20s for the vessel to reach almost zero velocity. Though since the model is linear it does not cover the extreme input to the system, thus is the measurement at the accelerating ramp much faster than the model predicts it to be. Since the vessel is assumed to reach and sail with constant velocity is this problem not as critical as it seems. The pitch angle are as concluded above not correct. To verify that the form of the pitch angle are correct has the measurements from the surge tests been compared with the pitch angles. The results of the pitch angle for a surge test can be seen on figure 6.8.

The pitch angle is rising above the steady state of the constant velocity, since the forward thrust is as high as it is. Then the vessel tilts a little down and reaches a steady angle at $\approx 4°$, which is also as observed during testing. When the input is set to zero the vessel will decelerate and the pitch will become a little negative around zero due to the high damping factor, and then settle at new steady state, determined by the physics of the vessel and the restoring forces. The value of the pitching angles are as expected from the observations,

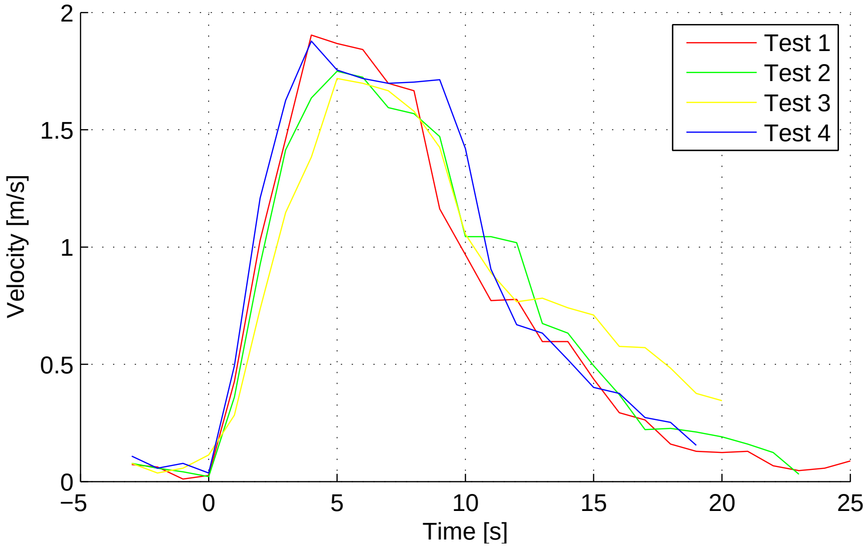

Figure 6.7: Surge tests with constant input followed by zero input.

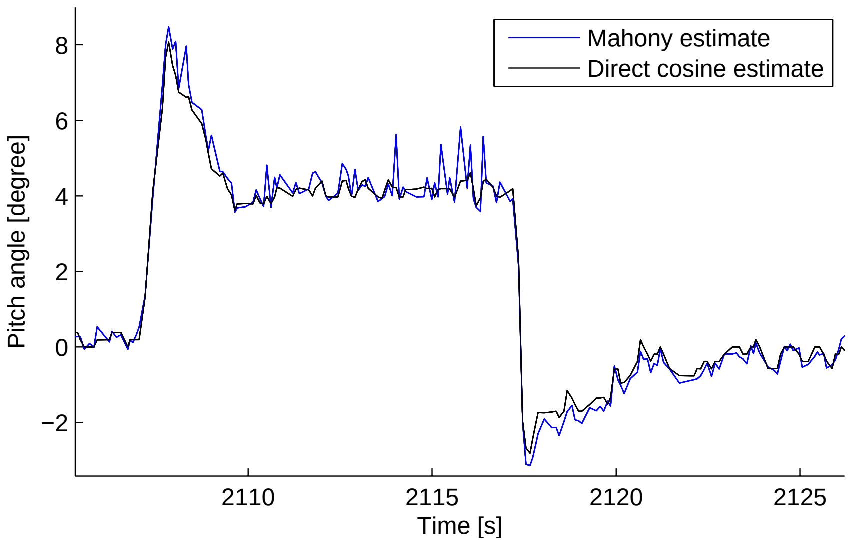

Figure 6.8: Surge tests with constant input followed by zero input.

even though the model does not evaluate the correct pitching angle.

6.9 Kalman Filter Design

6.9.1 The Kalman Filter

A KF is used as a type of observer that can be applied to estimate the state vector. This is done to filter the measurements from the vessel and smooth these. If the measurements are too noisy, such that the vessel changes direction suddenly, but should be surging forward, a filter can predict the modelled direction and compare this to the measurement and apply a more correct measurement for the system.

The KF comprises the deterministic part, the measurement noise, of the model, which estimates the state vector. This is corrected by means of measurements to estimate the final state vector.

The KF is drawn as a block diagram as seen on figure 6.9 on the facing page illustrating both the process and the KF together. The upper part represent the process, which can both be a simulated model or the real vessel with measurements, here it is a linear state space model. The lower part is the KF which takes in the measurements and estimates the new state vector based on these measurements. The KF can be of different types: Linear Kalman Filter (LKF), Extended Kalman Filter (EKF) or Unscented Kalman Filter (UKF). The figure illustrates the LKF. Choosing between these types of filters depends on the type of model used and the application.

6.9.2 Linear Kalman Filter

The process model is the usual state space model in discrete form as:

$$x_k = \Phi_{k-1} x_{k-1} + G u_{k-1} + w_{k-1} \tag{6.36}$$
$$z_k = H_k x_k + v_k \tag{6.37}$$

The LKF prediction and update can be written as:

- Prediction

$$\hat{\mathbf{x}}_k^- = \Phi_{k-1}\, \hat{\mathbf{x}}_{k-1}^+ + G u_{k-1} \tag{6.38}$$
$$P_k^- = \Phi_{k-1} P_{k-1}^+ \Phi_{k-1}^\top + Q_{k-1} \tag{6.39}$$

- Update

$$\bar{\mathbf{z}}_k = z_k - H_k\, \hat{\mathbf{x}}_k^- \tag{6.40}$$
$$S_k = H_k\, P_k^- H_k^\top + R_k \tag{6.41}$$
$$K_k = P_k^- H_k^\top S_k^{-1} \tag{6.42}$$
$$\hat{\mathbf{x}}_k^+ = x_k^- + K_k \bar{\mathbf{z}}_k \tag{6.43}$$
$$P_k^+ = (I - K_k H_k) P_k^- \tag{6.44}$$

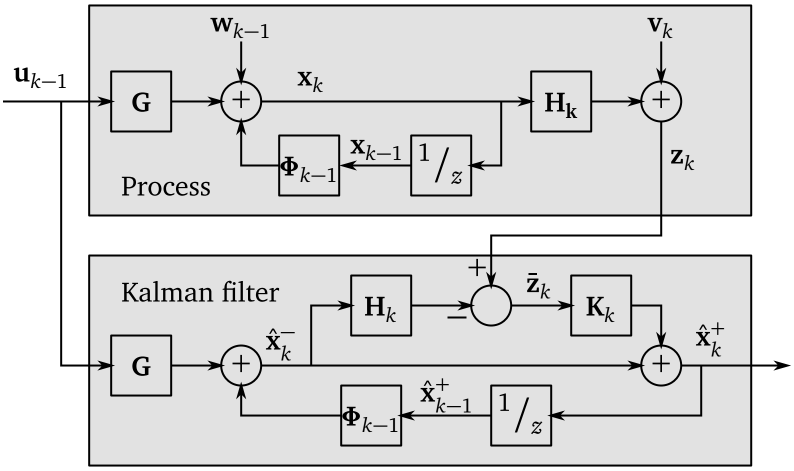

Figure 6.9: Block diagram of a Linear Kalman Filter resulting in the state estimate $\hat{\mathbf{x}}_k^+$.

Where P_k^- is the covariance propagation, P_k^+ is the update of covariance propagation, Q is a covariance matrix with sensor variances and R is a covariance matrix with model variances. Q is a measure of how much the model is to be trusted. If the variance of the sensors are high this will imply that the model are to be trusted more than the noisy sensor measurements. These variances can sometimes be measured directly at the sensors and used in the Q matrix. This leaves the R matrix as the only design matrix left. R is a measure of how much the measurement are to be trusted. If the variance of the model are high it might be better to trust the actual measurements. z_k is the measurements from the sensors and $\bar{\mathbf{z}}_k$ is the difference between the measurements and the predicted state vector, $\hat{\mathbf{x}}_k^-$. S_k is the covariance matrix of the residual with the variance of the model included. K_k is the optimal Kalman gain, in a Minimum Mean Square Error (MMSE) sense.

6.9.3 Extended Kalman Filter

The above mentioned LKF can only be applied on linear systems and transitions. Therefore is this not suited at the AAUSHIP. The position from the GPS and the acceleration measurements needs to be rotated with a rotational matrix, which leads to non-linearities in the system. This can be seen on figure 6.1 on page 44. This entails that a LKF cannot be used and an EKF can be suited. The EKF is used to linearise the non-linear terms in the system around the current estimate. In this case it will linearise the transition around the current measurements from the sensors to estimate the true output. The EKF can be formulated in discrete form with the prediction and an update as:

- Prediction

$$\hat{\mathbf{x}}_k^- = f(\hat{\mathbf{x}}_{k-1}^-, u_{k-1}) \tag{6.45}$$

$$P_k^- = F_{k-1} P_{k-1}^+ F_{k-1}^\top + Q_{k-1} \tag{6.46}$$

- Update

$$\bar{\mathbf{z}}_k = z_k - h(\hat{\mathbf{x}}_k^-) \tag{6.47}$$
$$S_k = H_k\, P_k^- H_k^\top + R_k \tag{6.48}$$
$$K_k = P_k^- H_k^\top S_k^{-1} \tag{6.49}$$
$$\hat{\mathbf{x}}_k^+ = x_k^- + K_k \bar{\mathbf{z}}_k \tag{6.50}$$
$$P_k^+ = (I - K_k H_k) P_k^- \tag{6.51}$$

where the state transition and observation matrices are defined by their respective Jacobians:

$$F_{k-1} = \left.\frac{\partial f}{\partial x}\right|_{\hat{\mathbf{x}}_{k-1}^-, u_{k-1}} \tag{6.52}$$
$$H_k = \left.\frac{\partial h}{\partial x}\right|_{\hat{\mathbf{x}}_k^-} \tag{6.53}$$

6.9.4 Kalman Filter in the Case of AAUSHIP

The input is given by the forces applied to the vessel. On AAUSHIP with the two twin propellers and two side thrusters as illustrated in section 6.7 on page 48. This will result in forces in the surge and sway direction as well as a torque around z, the yaw axis. The roll and pitch torques are neglected, such that the input vector u_k becomes as in equation (6.54).

$$u_k = \tau_k = \begin{bmatrix} X & Y & 0 & 0 & N \end{bmatrix}^\top \tag{6.54}$$

These are the forces that can be applied by the thrusters mounted at the vessel. It should be noted that the pitch and roll are not set as input, since no thrusters can control these directly, and should be treated as model variations. The roll will be affected by the bow thrusters but very little. The pitch is also affected by the two main thrusters, but this is only a product of applying the forces at the main thrusters.

The discrete input matrix Γ is a 15×5 matrix from the discretised B matrix from equation (6.1) on page 43. The Γ matrix takes the forces in X, Y and N as input, and neglects inputs in ϕ and θ. The forces in ϕ and θ are outputs from the system that makes the vessel change in pitch and roll but are not used as inputs. It is not possible to apply a direct force in pitch and roll. It is possible to apply a roll force by actuating the bow thrusters at the same time, but this will mainly result in a sway force. The same goes for the pitch force, where both main thrusters can be actuated and result in a pitch force, but this will mainly result in a surge force. Therefore are these seen as a result of using the surge and sway, and only a output of the system.

The discrete system $\mathbf{\Phi}$ is a 15×15 from the discretised A matrix from equation (6.1) on page 43, and expanded to contain the full state vector calculations.

The dimensions of the different matrices used are checked as a type of sanity check and verify that the matrices are in correct size.

The covariance propagation matrix, the uncertainty of the estimated state, is given by:

$$P_k^- = F_k\ P_{k-1}^- F^\top + Q_k \tag{6.55}$$

$$\dim(P_k^-) = [15 \times 15] \cdot [15 \times 15] \cdot [15 \times 15]^\top + [15 \times 15] \tag{6.56}$$

The Q is the variances of each of the states from the full state vector.

The posteriori error covariance matrix, the update, is given by:

$$P_k^+ = (I - K_k\ H_k) P_k^- \tag{6.57}$$

$$\dim(P_k^+) = ([15 \times 15] - [15 \times 7] \cdot [7 \times 15]) \cdot [15 \times 15] \tag{6.58}$$

which is a measure of the estimated accuracy of the state estimate. Adding a middle calculation as the residual covariance:

$$S_k = H\ P\ H^\top + R \tag{6.59}$$

$$\dim(S_k) = [7 \times 15] \cdot [15 \times 15] \cdot [7 \times 15]^\top + [7 \times 7] \tag{6.60}$$

The R is variances from the sensors, which makes it sensor noise terms.

The updated Kalman Gain:

$$K_k = P\ H^\top\ S^{-1} \tag{6.61}$$

$$\dim(K_k) = [15 \times 15] \cdot [7 \times 15]^\top \cdot [7 \times 7]^{-1} \tag{6.62}$$

which is optimal in a MMSE sense.

State vector

$$\hat{\mathbf{x}} = \begin{bmatrix} x_b & y_b & \phi & \theta & \psi & u & v & p & q & r & \dot{u} & \dot{v} & \dot{p} & \dot{q} & \dot{r} \end{bmatrix}^\top \tag{6.63}$$

Measurement vector

$$\mathbf{z} = \begin{bmatrix} x & y & \psi & u & v & a_x & a_y \end{bmatrix}^\top \tag{6.64}$$

Measurement matrix defining the relationship between the state of the dynamic system and the measurements

$$H_k = \begin{bmatrix} 1 & 0 & 0 & 0 & 0 & 0 & 0 & 0 & 0 & 0 & 0 & 0 & 0 & 0 & 0 \\ 0 & 1 & 0 & 0 & 0 & 0 & 0 & 0 & 0 & 0 & 0 & 0 & 0 & 0 & 0 \\ 0 & 0 & 0 & 0 & 1 & 0 & 0 & 0 & 0 & 0 & 0 & 0 & 0 & 0 & 0 \\ 0 & 0 & 0 & 0 & 0 & 1 & 0 & 0 & 0 & 0 & 0 & 0 & 0 & 0 & 0 \\ 0 & 0 & 0 & 0 & 0 & 0 & 1 & 0 & 0 & 0 & 0 & 0 & 0 & 0 & 0 \\ 0 & 0 & 0 & 0 & 0 & 0 & 0 & 0 & 0 & 0 & 0 & 1 & 0 & 0 & 0 \\ 0 & 0 & 0 & 0 & 0 & 0 & 0 & 0 & 0 & 0 & 0 & 0 & 1 & 0 & 0 \end{bmatrix} \tag{6.65}$$

The covariance matrix of observational (measurement) uncertainty R_k is assumed to be uncorrelated with the other states, such that the matrix only becomes the variances, with no covariance elements as:

$$R_k = \operatorname{diag}(\mathbf{v}) = \tag{6.66}$$

$$\operatorname{diag}\left({}^{\mathrm{GPS}}\sigma_x^2,\ {}^{\mathrm{GPS}}\sigma_y^2,\ {}^{\mathrm{GPS}}\sigma_\psi^2,\ {}^{\mathrm{GPS}}\sigma_u^2,\ {}^{\mathrm{GPS}}\sigma_v^2,\ {}^{\mathrm{IMU}}\sigma_{a_x}^2,\ {}^{\mathrm{IMU}}\sigma_{a_y}^2\right)$$

These variances can be found by letting the AAUSHIP be in steady state. The sensor outputs are read while in steady state to check the variances from these. This will be the variances of the individual sensor measurements thus the variances of the particular measurements. The test finding these variances can be found in appendix D on page 123.

The covariance matrix of process noise in the system state dynamics is Q_k and is assumed to be the variances of each individual state:

$$Q_k = \operatorname{diag}(\mathbf{w}) = \operatorname{diag}\left(\sigma_x^2, \sigma_y^2, \sigma_\phi^2, \sigma_\theta^2, \sigma_\psi^2, \sigma_u^2, \sigma_v^2, \sigma_p^2, \sigma_q^2, \sigma_r^2, \sigma_{\dot{u}}^2, \sigma_{\dot{v}}^2, \sigma_{\dot{p}}^2, \sigma_{\dot{q}}^2, \sigma_{\dot{r}}^2\right) \tag{6.67}$$

The variances of the process can be hard to validate since these can include noises as incoming waves and other disturbances from the environment. Therefore is the matrix Q used as a tuning parameter to set the weighting between how much to trust the model and the measurements.

The $\mathbf{F}$, equation(6.52), from the previous calculations, are the $[15 \times 15]$ system matrix, referred to as Φ in discrete case. This system matrix changes over time due the changes in the heading. The change of heading is not a linear transition which makes the system non-linear and therefore needs to be linearised about the given states of the system. Therefore this matrix is used as the system matrix in the EKF, which is implemented in the AAUSHIP. Φ is therefore the discrete system matrix in equation (6.68). The same goes for the rest of the system, which is discretised at a certain sample time. This makes all the system matrices as discrete versions to be used in the calculation and linearisation.

$$\Phi = A_d \tag{6.68}$$

6.9.5 Determination of Observational Uncertainty

The matrix R represents covariance matrix of observational (measurement) uncertainty. This is the matrix which sets the individual variances of the specific measurements from the sensors, the measurements from the output vector z. This means that the coefficients of the R matrix can be determined within some interval. The disturbances of each sensor measurement highly depends on which sensor is implemented in the used system. When looking at the AAUSHIP the sensors are of higher accuracy, which means that the sensors are to some extend trustworthy. There are two types of sensors in the AAUSHIP, one GPS and an IMU. There are two types of GPSs installed; a Real Time Kinematic (RTK) GPS and a standard GPS. At the moment is only the standard GPS used, which estimates having a variance of 3 metres radius in the NED-frame. This is estimated from steady state measurements of the GPS where it will, as all GPSs, drift around a little. The IMU consists of a magnetometer, a gyro and an accelerometer. The magnetometer measurements is not used directly and the variance of this is not needed in the R matrix. The gyro neither used in the R matrix. These are not used as measurements directly and therefore not appears in the R matrix. The accelerometer measurements are used in the x and y directions. These have a measured accuracy of 0.00033 $\mathrm{m/s^2}$. The GPS have different accuracies dependent on which type is used. The RTK GPS has higher accuracy than the standard GPS, but has not for the moment been implemented. The resulting R matrix, with the standard GPS, is estimated from the measurements of z and determined to be

$$\begin{aligned}
&R_k = \operatorname{diag}(\mathbf{v}) = \\
&\operatorname{diag}\left({}^{\mathrm{GPS}}\sigma_x^2,\ {}^{\mathrm{GPS}}\sigma_y^2,\ {}^{\mathrm{GPS}}\sigma_\psi^2,\ {}^{\mathrm{GPS}}\sigma_u^2,\ {}^{\mathrm{GPS}}\sigma_v^2,\ {}^{\mathrm{IMU}}\sigma_{a_x}^2,\ {}^{\mathrm{IMU}}\sigma_{a_y}^2\right) \\
&\operatorname{diag}\begin{pmatrix}3 & 3 & 13.6\cdot 10^{-6} & 0.2 & 0.2 & 0.00033 & 0.00033\end{pmatrix}
\end{aligned} \tag{6.69}$$

6.9.6 Determination of Process Noise

The matrix Q represents the covariance matrix of process noise in the system state dynamics. This matrix includes parameters as disturbances in the process itself. When looking at the AAUSHIP this could for instance be the incoming waves acting as disturbances both in the roll, pitch and the heading. These types of disturbances can be hard to measure and put a precise number to. Instead, this matrix is used as a tuning parameter for the KF, where it sets a weighting of how much the process, and therefore the model, are to be trusted. If the sensors has a high accuracy, it would be of benefit to trust these more than the process, thus setting the parameter of this specific measurement in the Q matrix high. But the Q matrix is used to combine the measurements and the model prediction together. This means that based on the variances from the Q matrix, based on the values from the R matrix, it is tuned to get the best performance from the combination of the model and the measurements

As the model of the AAUSHIP is made, it becomes possible to tune the parameters of Q in a systematic way. The model decouples the acceleration from the velocity, and the velocity from the position. Therefore it is of benefit to tune the acceleration noise variance firstly, such that this makes a proper fit to a step function. A test can be simulated where the AAUSHIP accelerates to a certain velocity and keeps this velocity. This needs to fit such that it makes the AAUSHIP follow a satisfying curve in each of the acceleration, velocity and position tests. The simulation curve is both based on measurements and model predictions. A wanted acceleration curve, for instance in surge and sway, will look like on figure 6.10. Afterwards is the velocity of the AAUSHIP tuned. This is done in the same manor, where the velocity of a step function needs to look like on figure 6.11. At last is the position tuned, which is the one with largest relative noise from the measurements. This forces the value in Q to be smaller thus making the AAUSHIP trust the model prediction more than then measurements. A position plot with two different values in Q can be seen on figure 6.12. The one with the lowest value in Q gives the best position fit of these, which also follows the intuition of how the KF should work. The resulting Q matrix is tuned to be

$$\begin{aligned}
&Q_k = \operatorname{diag}(\mathbf{w}), \text{ where} \\
&\sigma_{x_b}^2 = 0.001, \quad \sigma_{y_b}^2 = 0.001, \quad \sigma_\phi^2 = 0.01, \quad \sigma_\theta^2 = 0.01, \quad \sigma_\psi^2 = 0.000001, \\
&\sigma_u^2 = 0.01, \quad \sigma_v^2 = 0.01, \quad \sigma_p^2 = 0.001, \quad \sigma_q^2 = 0.001, \quad \sigma_r^2 = 0.001, \\
&\sigma_{\dot u}^2 = 0.01, \quad \sigma_{\dot v}^2 = 0.01, \quad \sigma_{\dot p}^2 = 0.01, \quad \sigma_{\dot q}^2 = 0.01, \quad \sigma_{\dot r}^2 = 0.01
\end{aligned}$$

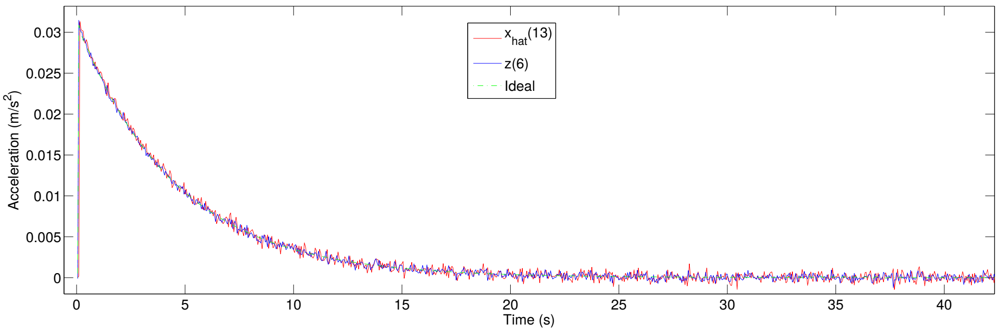

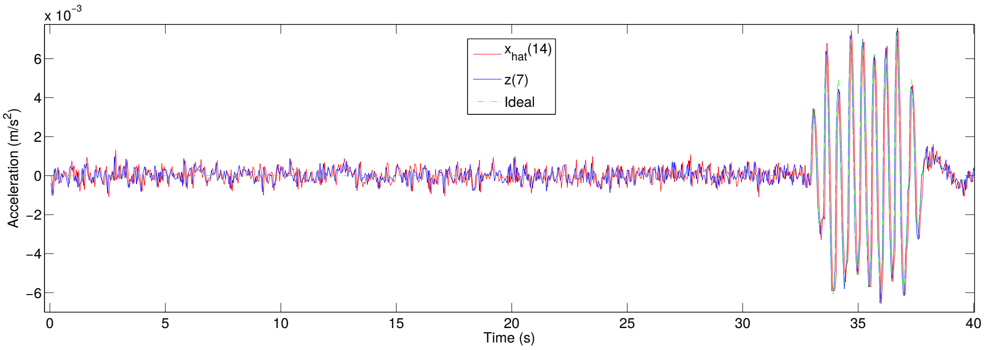

Figure 6.10: Measurement and estimate of acceleration in surge and sway.

6.9.7 GPS in the Closed Loop

The precision of the normal GPS receiver is some times bigger than the desired resolution of the measurement resolution. The means that has been chosen to resolve this problem, is to use a kind of absolute positioning system which has better performance in this respect. A solution to his is the RTK GPS which can achieve way better positioning precision. This system uses a technique with a base station and a rovering device to correct for disturbances present in the local working area, such as atmospheric phenomena that can disturb the receiver. This system requires a direct data connection between the base station and the device on the rover (European Space Agency (ESA), 2014).

Some experiments with this setup has been performed by the authors using RTKLIB and LEA-4T receivers, but this has proven to be problematic as soon as the rover is moving. This is kind of a do it yourself way of getting a RTK system. Commercial systems do exist that work better, but these are fairly expensive to acquire. Therefore it has been decided to make the system such that is will work with a standard GPS module, and optionally use the RTK with logging, where it is possible to post process the data to get the exact positions of where the ships has actually sailed.

This can be done, because the lawnmower reference trajectory the ships shall follow is not a hard requirement from the mapping point of view, they are only intended to distribute the scanning area such that it is scanned fairly even. The reference trajectory generation is described in chapter 3 on page 17. The ship is also pitching an rolling, which cannot be

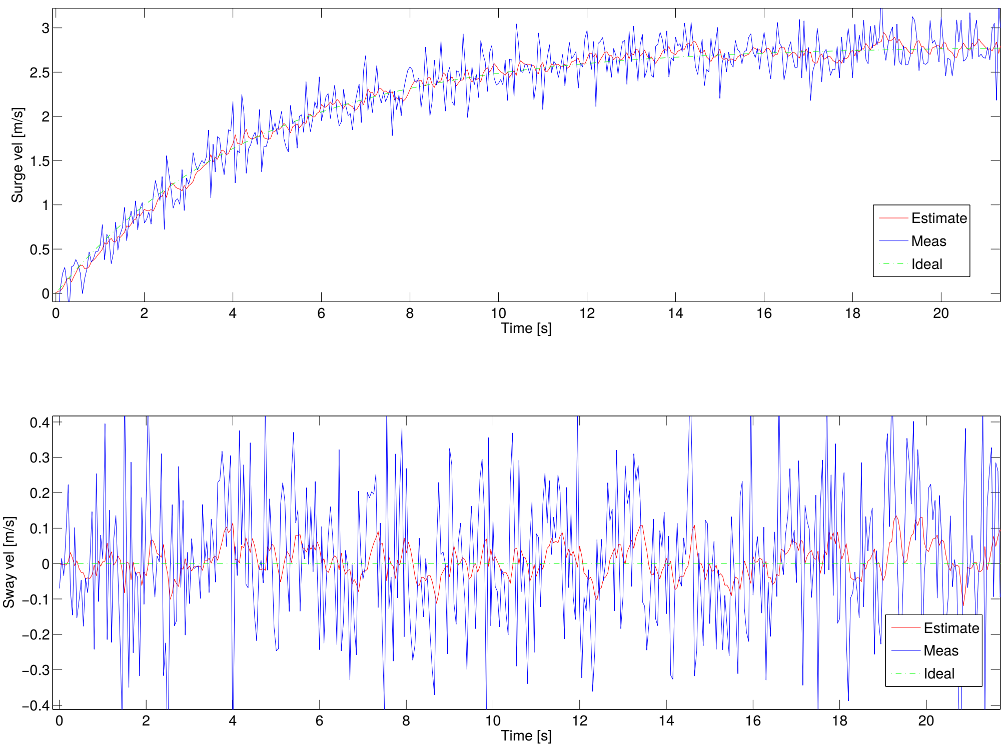

Figure 6.11: Measurement and estimate of velocity in surge and sway.

controlled, and hence it makes no sense to make the ship positioning overly accurate. This is seen from the perspective that the ships main task is to cover the seabed with measurements, thus it is only important to know the actual position and attitude of the ship. This can be logged from the RTK GPS and then used to determine the actual position and therefore the actual measurement point of the seabed can be calculated.

6.9.8 In Absence of GPS Signal

When there is no GPS signal it is not possible to make any new estimates based from the measurements. This results in a model based phase of the controlling of the AAUSHIP. Therefore the AAUSHIP needs to converge to the predetermined trajectory based on how the model of the ship would do it. When a new GPS signal is present this needs to be taken into account and thereby used as a correction to the model prediction. When the signal is absent there are different ways to handle this in the model. One of the ways is to set the variance of the sensor noise from the GPS high. This value could be around $10 \cdot 10^9$ to ensure that the model does not take the measurement from the GPS into account.

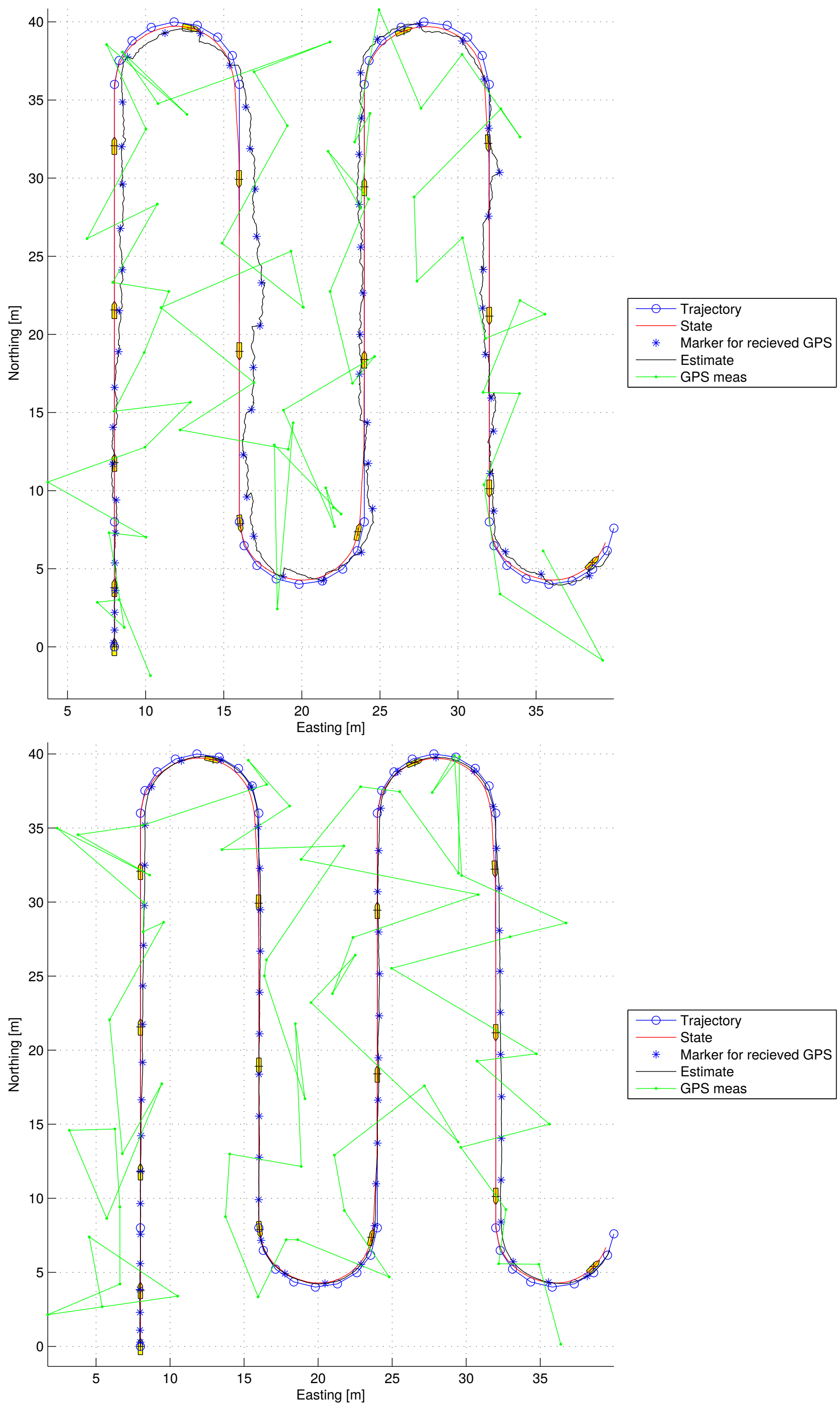

Figure 6.12: Simulated and filtered measurements of AAUSHIP tracking a trajectory. First figure is with low sensor variance of the NED measurement, and second figure is with high sensor variance of the NED measurement.

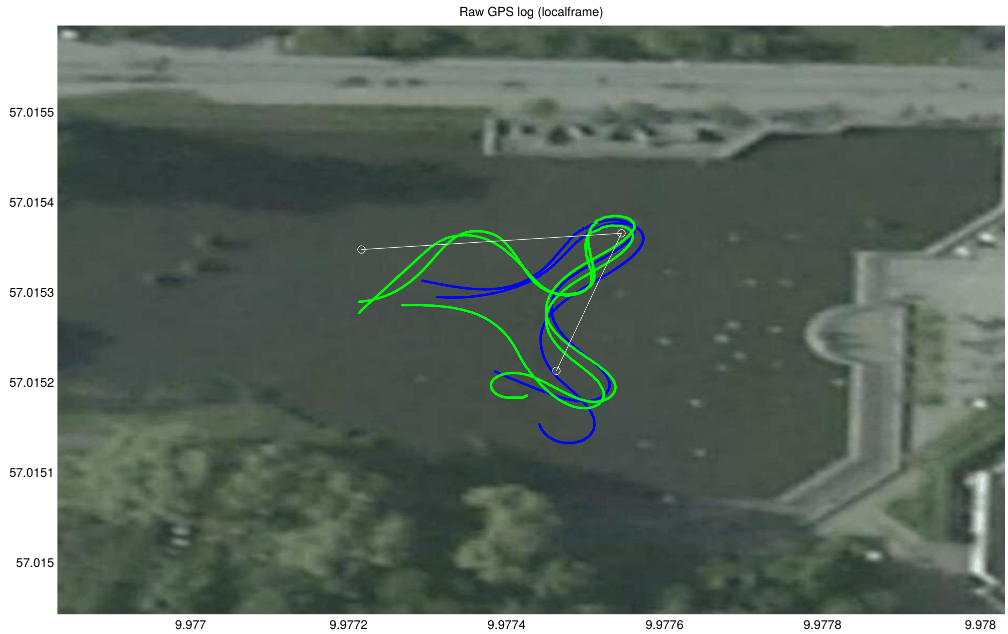

Figure 6.13: Tests with different control parameters for the heading controller. As for initial test the Klingenberg lake seems too small.

6.9.9 Sample Rates

If the different sensor measurements are not sampled with the same rate will the lower sample rates be untrue. This induces the same situation as if the GPS signal is absent, thus setting the variances of these measurements high. The same situation will occur as with the missing GPS signal, making the measurement be highly untrusted and only taking in the model prediction for that particular sample.

6.9.10 Overall filter and conclusion

The filter is implemented with the final results simulated in the first figure on figure 6.12. It can be seen, as a difference to the second figure on figure 6.12, that the estimate takes in the measurement from the GPS and is not totally model based. It is not wanted to have a fully model based KF since the model may not be the perfect match to the real world environment and does not include disturbances as incoming waves etc. Therefore it is important that the filter takes in the measurements from the GPS and IMU to correct the model with respect to the real world measurements. It can be seen on figure 6.12 that the filter corrects the estimate with the GPS measurement. A received GPS measurement is marked with a star on the estimate and it can be seen that the estimate corrects in the direction of the GPS measurement. The KF works as intended in the simulations and is the one to be implemented on the AAUSHIP. Sea trials with this filter will be performed to verify that the filter works as intended from the simulations. On figure 6.13 are four tests performed with the KF from above. The white line, between the three dots, are the line segments of three waypoints to the AAUSHIP to follow. The tests in the Klingenberg Lake was hard to perform and evaluate results from. This needs to be seen in respect to the limited area of testing in the lake. The two green paths are with one set of control parameters for the heading controller, and the two blue paths are for a different set of control parameters. It can be noted that the AAUSHIP performs steady and with the same errors in the same type of tests. It can be seen that the controller tries to turn onto the line segments as intended. The tests are to be performed in more open areas to be able to tune in the parameters even more to the model. The risk of going too close to the sides of the Klingenberg Lake was evaluated too high thus tests need to be moved out in the fjord. Although a final conclusion can be made that the AAUSHIP tracks the waypoints as intended, but more tuning is needed.

6.10 Addition to the Kalman Filter

The heading reference can be estimated both from the GPS measurements and the from the IMU measurements. The simulation model is using the measurement from one GPS, due to the implementation of the single GPS. The noise have been measured from the GPS thus setting the accuracy based on this. When the RTK GPS will become implemented this can lower the noise variance from the measurements by fusing the two GPSs. The measurements from the IMU can too be used to estimate the attitude and the heading. All of these sensor measurements can be fused together in the KF, such that the two GPSs can give an estimate of the heading and include the IMU. The GPSs will also be used to estimate the SOG together. When the RTK GPS is expected to have a lower variance both in position and SOG measurements thus making the fusion of this preferable and resulting in a better estimate of both position and SOG. Since the variance from the normal GPS seems relatively high, it is expected that the main GPS will be the RTK GPS.

Chapter 7

Control

This chapter describes the selected strategy from chapter 4 on page 23 in more detail, describing the exact algorithm and the implemented simulation.

7.1 One Approach for Potential Fields

In the following approach a potential field is generated for each agent including obstacles, formation span, desired, and actual position. It will be a combination of virtual leader and potential field. The principle generates a potential field to keep the formation and that field is moved around as a virtual leader. When the virtual leader is moved around it results in a deflection of the desired position and causes the affected agents to get back into position. The positions of the agents in the field is given individually to the specific agents relative to the virtual leader. The approach generates a single resulting vector for each agent which is used to guide the agent. The potential field for each agent is generated from four components:

$$\tilde{\mathbf{F}}_i^{tot} = \mathbf{F}_{vl} + \mathbf{F}_{ij}^{tot} + \mathbf{F}_{ca}^{tot} + \mathbf{F}_{oa}^{tot} \tag{7.1}$$

where:

- $\mathbf{F}_{vl}$ virtual leader force
- $\mathbf{F}_{ij}^{tot}$ inter-agent forces
- $\mathbf{F}_{ca}^{tot}$ agent-agent collision avoidance forces
- $\mathbf{F}_{oa}^{tot}$ agent-obstacle collision avoidance forces

7.1.0.1 Virtual Leader, $\mathbf{F}_{vl}$

The virtual leader is an anchor of each formation, the FRP, and controls the movement of this. This movement can be given as a full trajectory of as a set of way points. The local virtual leader's contribution to the field is defined as:

$$\mathbf{F}_{vl} = K_{vl}(p_{vl}^n - p_i^n - [p_{vl}^n - p_{i0}^n]) \tag{7.2}$$
$$= K_{vl}(\mathbf{d}_i - \mathbf{d}_{i0}) \tag{7.3}$$

K_{vl} is a tuning parameter. p_{vl} is position of the virtual leader, p_i is position of agent i, p_{i0} is desired position of agent i and the d is a shorter notation for the distances in between. The virtual leader component guides the agents directly to their desired positions relative to the virtual leader.

7.1.0.2 Inter Vehicle Influence, $\mathbf{F}_{ij}$

This is the contribution of other vehicles to the potential field, which is expressed as:

$$\mathbf{F}_{ij} = K_{ij}(p_j^n - p_i^n - [p_{j0}^n - p_{i0}^n]) \tag{7.4}$$
$$= K_{ij}(\mathbf{d}_{ij} - \mathbf{d}_{ij0}) \tag{7.5}$$

Similar to previously the ps are positions, K_{ij} is a tuning parameter and d is a shorter notation for the distances in between. This component preserves the formation by affecting the agents to keep their respective desired distances among themselves. The weighting on each goal can be adjusted by K_{vl} and K_{ij}, hence this weighting is a weighting that causes the agents to either follow the virtual leader or to preserve their desired formation. In a swarm of N agents the total field for agent i given by:

$$\mathbf{F}_{ij}^{tot} = \sum_{j=1}^{N} \mathbf{F}_{ij}(i,j) \text{ for } j \neq i \tag{7.6}$$

7.1.0.3 Collision Avoidance, $\mathbf{F}_{ca}$

The collision avoidance takes effect when the agents get closer than a pre defined distance of each other. It generates an additional field component for the vehicle i which points away from the entering agent causing the agents to move away from each other. To ensure the avoidance the component converges towards infinity in the centre of the i'th agent. The $\mathbf{F}_{ca}$ is expressed as:

$$\mathbf{F}_{ca}^{ij} = \begin{cases} \left(\frac{K_{ca} r}{||\mathbf{d}_{ij}||} - K_{ca}\right) \frac{\mathbf{d}_{ij}}{||\mathbf{d}_{ij}||}, & \text{for } ||\mathbf{d}_{ij}|| < r \\ 0, & \text{otherwise} \end{cases} \tag{7.7}$$

where K_{ca} is a tuning parameter. r is the safety radius for collision and $\mathbf{d}_{ij}$ is the distance between the individual agents. The collision avoidance can be expressed in a total term of the collision avoidance:

$$\mathbf{F}_{ca}^{tot} = \sum_{j=1}^{N} \mathbf{F}_{ca}^{ij} \text{ for } i \neq j \tag{7.8}$$

7.1.0.4 Obstacle Avoidance, $\mathbf{F}_{oa}$

The same principle as for collision avoidance can be applied to obstacle avoidance. Now each obstacle needs to be handled as an agent, which will make the same result, but the reference is a little different:

$$\mathbf{F}_{oa}^{ik} = \begin{cases} \left(\frac{K_{oa}}{||\mathbf{d}_{ki}||} - \frac{K_{oa}}{r}\right)\frac{\mathbf{d}_{ki}}{||\mathbf{d}_{ki}||}, & \text{for } ||\mathbf{d}_{ki}|| < r \\ 0, & \text{otherwise} \end{cases} \tag{7.9}$$

where k denotes the counter for obstacles instead of other agents. K_{oa} is also a tuning parameter for the obstacle avoidance. $\mathbf{d}_{ki}$ is the vector between an agent and the obstacle, which in a total term is summed up as:

$$\mathbf{F}_{oa}^{tot} = \sum_{k=1}^{M} \mathbf{F}_{oa}^{ik} \text{ for } i \neq k \tag{7.10}$$

Here d_{ki} represents one of the M place vectors which has the effect of a detected obstacle.

It can be noticed that there is a difference between $\mathbf{F}_{ca}$ and $\mathbf{F}_{oa}$. The two forces applies the same directions of forces, making the agents repulse from another agent or an obstacle. Though there is made a difference between them. It can be seen that the safety radius is moved from a multiplication to a division from the $\mathbf{F}_{ca}$ to the $\mathbf{F}_{oa}$. This will, dependent on the choices of K_{ca} and K_{oa}, allow agents to move further into the safety radius of an obstacle than into the radius of another agent. This is due to the fact that the repulsing forces from agents needs to be larger in the case that two agents moves toward each other. In this case the agents need to react with higher aggression to ensure that they will repulse enough to not collide. This will not be the case for obstacles since these are defined with a constant position. The 2-D representation of Fca and Foa in their safety radius can be seen on figure 7.1.

It can be seen that the force of Fca are greater than the force of Foa, although their gains Kca and Koa have been chosen equally. This is due to the difference of their structure and ensures that no agents collide even though they are on a collision course.

The distance r can be determined dynamically depending on the velocity of the agent:

$$r = r^{min} + K_r||\dot{\mathbf{p}}^n|| \tag{7.11}$$

Still will ensure that the agents have the possibility to decelerate from their absolute velocity in the safety radius such that they can turn away from each other.

7.1.0.5 Potential field

The forces are summed together to get $\tilde{\mathbf{F}}_i^{tot}$, which is an intermediate vector which gives the magnitude and direction of the potential field for vehicle i at its current position.

$$\mathbf{F}_i^{tot} = \min\{\ ||\tilde{\mathbf{F}}_i^{tot}||\ ,\ F_{max}\ \}\frac{\tilde{\mathbf{F}}_i^{tot}}{||\tilde{\mathbf{F}}_i^{tot}||} \tag{7.12}$$

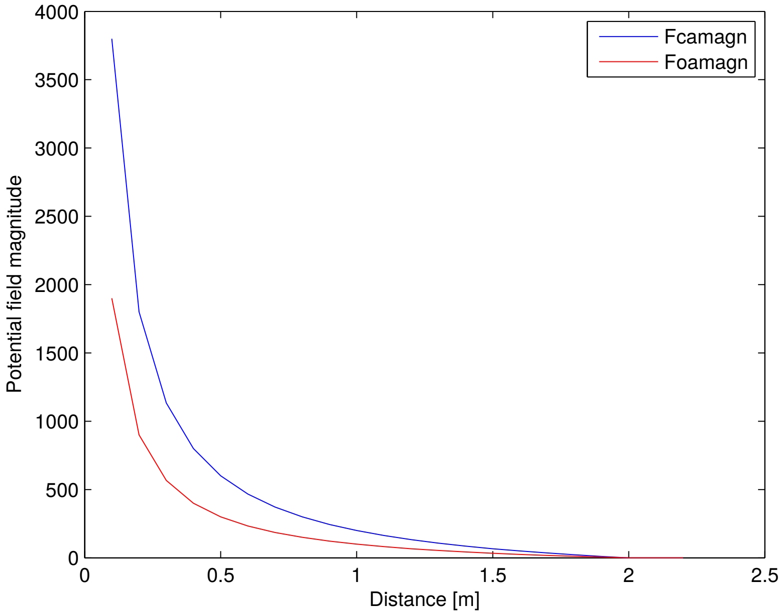

Figure 7.1: The magnitude of the forces Fca and Foa. This force applies when an agent or an obstacle enters within the safety radius.

The $\tilde{\mathbf{F}}_i^{tot}$ denotes that it is a middle variable and not the final value of the potential calculation, thus not the one used by the controller yet. As the potential field does not need to expand to infinity it is reasonable to define a maximum amplitude for the vector, while still keeping its direction, F_{max}. This will be a limitation of the agents' speed. As a start in the simulation phase is F_{max} chosen as a constant, but in the fully implemented system it can be of benefit to adjust this maximum speed dynamically, for instance as in equation (7.13), as an example from (Paul et al., 2008).

$$F_{max} = F_{min} + K_{vl}||\dot{p}^n|| \tag{7.13}$$

where the F_{min} is a minimum value for the upper limit and then with an applied gain of the speed. The reference trajectory is used by the controller to calculate the agent's control input which can be based on the desired movement in the NED frame as:

$$\mathbf{p}_{i,r}^n = \mathbf{p}_i^n + \mathbf{F}_i^{\text{tot}} \tag{7.14}$$

where their positions are added together with the potential field, such that the position and the potential field becomes linked.

7.2 The Potential Field Strategy

The theory of potential fields are implemented with the strategy proposed in section 4.4. The potential field is generated for each individual agent at every update step to make the formation move and converge to a specified formation and position. The field is generated based on forces acting in an overlying potential field structure where one force converges the agent to a desired position, a force attracting the agent to obtain the desired formation along the trajectory, a force repelling the agent from other agents if their distance is too small and finally a force repelling the agents from static objects. The latter two can seem the same, but the repelling force will be larger for the agent-agent force due to the fact that two agents could have course directly toward each other and a more aggressive avoidance can be needed.

To be able to generate and simulate the potential field the implementation needs to be generic. First it was developed with one agent that needs to converge to a desired position and afterwards were other agents added as obstacles and some static objects were added in extend. From these obstacles it can be seen that a single agent is able to converge to a position which makes it possible to expand such that more agents can converge into formation with reference from either a virtual leader or from each other. This will solve the formation coordination task, where the following task will be the group coordination task. The group coordination task has the goal to move the formation around, which here will be done by making the virtual leader, or an actual leader of the formation, follow a specified trajectory. This will make the other agents follow this leader and keep their formation on the trajectory.

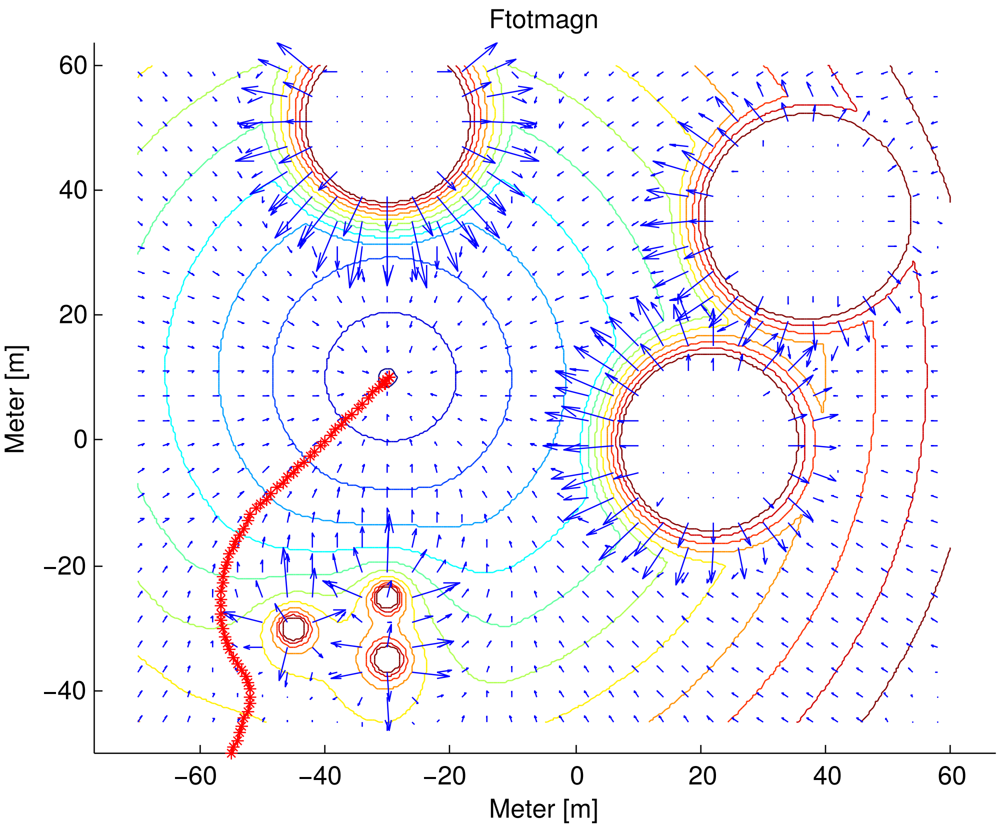

Figure 7.2: Plot of one agent's trajectory with a desired position with obstacles to avoid

A plot for a total potential reference field for a single agent can be seen on figure 7.2. The red line made of crosses is the trajectory that one single agent will follow, if the obstacles to avoid in the plot are static. In the plot every object, either another agent or an object, are kept static. So it shows how the trajectory will be in one single time step. This will change in the next time step if the other agents also move in the potential field. The agent avoids obstacles on the way, where it can be seen that it does not get into the safety radius of the obstacles. In this specific plot is a safety radius (r) of 20m chosen, such that the distance from agent p_i (red trajectory) to any obstacle always will be larger than 20m.

The same algorithm is applied where agent i avoids other agents, agent j, $j+1$. This can be seen on figure 7.3.

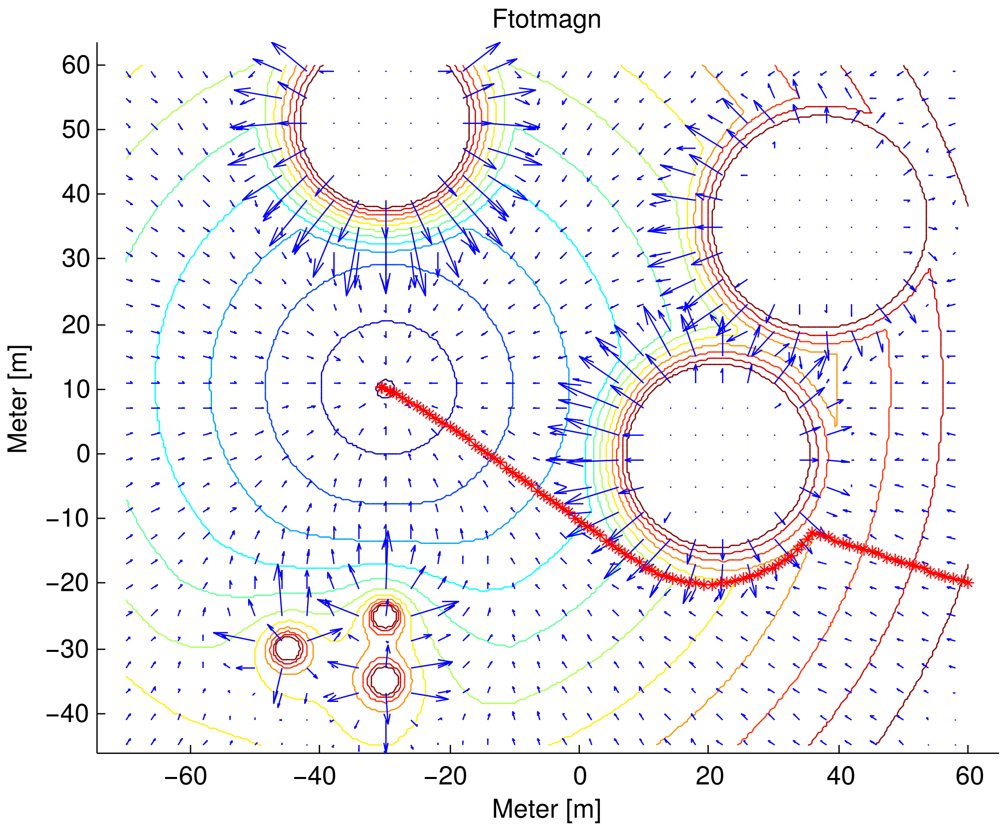

Figure 7.3: Agent i avoids agent j and converges to the minima at the virtual leader

Agent i takes a direct course toward the virtual leader but meets another agent as an obstacle. Agent i moves on the boarder of agent j with the defined safety radius and afterwards diverges from agent j towards the virtual leader. This is all done by following the lowest gradient at all times.

The gain of K_{ij} is not to be interpret from figure 7.2. K_{ij} is the gain to the force that attracts the agents together by minimizing the distance in between them. By doing this the agents will get faster into the desired formation. The gain K_{vl} does at some point the opposite. This gain adjusts the weighting of how fixated the agents should be to converge to the desired position. If this gain is relatively larger than K_{ij} then the agents will converge directly to their position around the virtual leader and not converge to the desired formation on the way. This implies that the scaling between K_{vl} and K_{ij} controls if the formation should converge to the desired formation on the way to the desired position, or if agent i should only have the desired position in focus.

7.2.1 Numerical Solution

The grid in which the potential field is generated are limited with a certain resolution while simulating the agents movement. This reduces the directions of where the agents can move, which will not arise a problem on the same level when implemented in reality. In the simulation environment it reduces the resolution such that a single field in the grid contains one value of magnitude of the potential field, which makes the basis of a certain gradient to the field. The agents are following the implementation of the steepest decent. This generates a gradient towards the steepest decent, which the agent tracks. The analogy can be seen as a bowl, or sphere in this case, where a ball will converge towards the lowest point in the direction of the minimum gradient.

The method of applying the grid with magnitude of the potential field rises a problem with resolution, and therefore also a problem that makes the 'corners' of the grid around the agent to have the steepest decent. This is seen as if the agent is placed in the middle of a 3-by-3 matrix, and have eight placements around it. The placements around the agent will then be checked. The magnitude of the vector from the agent and outgoing will therefore be biggest in the corners since the distance to those are greater than the distances to the sides, up and down. This problem has been expanded with a solution such that a certain radius in the potential field around an agent will be checked. The value at the radius around the agent can be checked, and due to the newly equal distance to every point, these will be weighted equally with respect to their value. This makes in principle the possibility to make the agent go in all directions which will be closer to the reality. When testing the two methods against each other it is clear that the first proposed with the grid structure did not have the same mobility thus not preferable in simulations though it is simpler. The first made the agents move only in the diagonals of their local placement, where the latter makes the agents able to move in a number of directions specified in the algorithm.

7.2.2 Local Minima Problem

A problem that can become crucial arises when two agents or two objects are within the radius of each other. This will result in a local minima in the potential field between those objects. This will create a local minima in between these agents or objects. If an agent converges toward this minima they cannot get out again. The problem can be seen on figure 7.4. The gains here are chosen exactly the same as in figure 7.2.

The scenario on figure 7.4 has the following steps. The agent i moves in the direction of the steepest decent. Then it gets to the border of another agent where it cannot go through thus starts to go around this agent. The problem arises when agent i reaches another agent

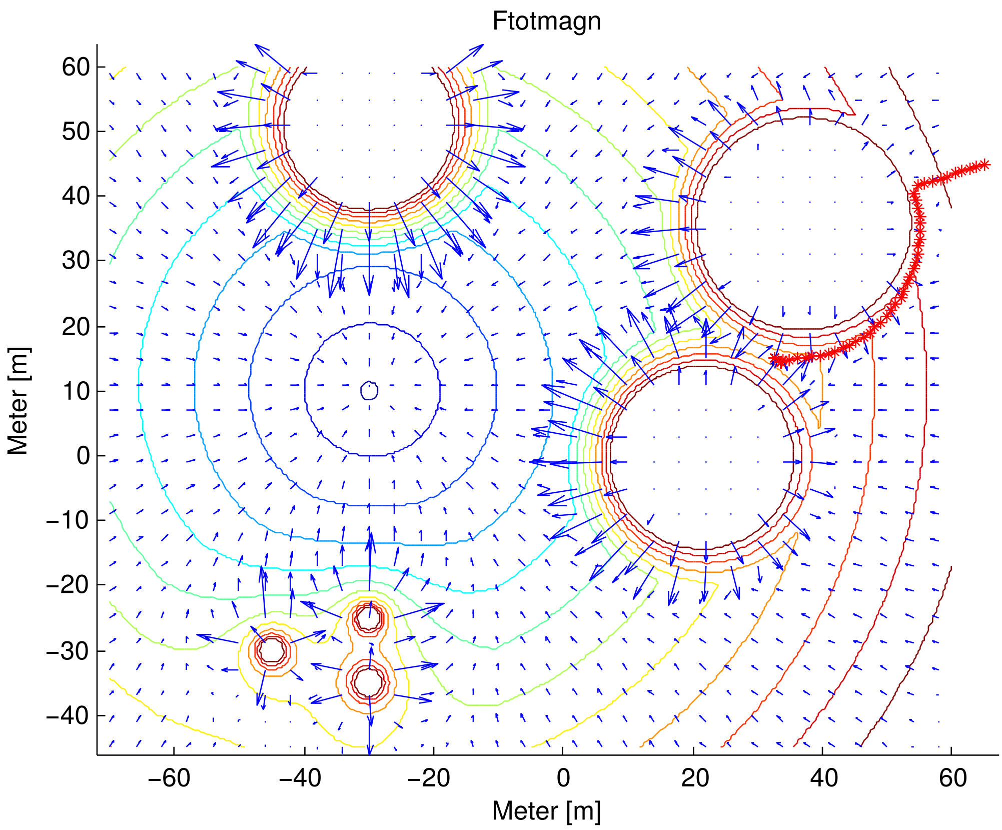

Figure 7.4: An agent gets stuck due to a local minima between two other agents. The agent cannot get out of this minima unless the other two agents makes the space for the agent to pass through

on the way where it now has reached a local minima. Now the steepest gradient will point at the position where the agent already is thus making it think it has reached the end point. Solutions to this problem can be formulated in different ways.

One solution could be to cluster the two objects together and instead of making their potential field individually, then combine those together and make an ellipsoid or even a circle formed obstacle of those objects. This will ensure that the local minima disappears thus not making an agent get stuck between those objects.

Another solution is to make an exception handler that can tell if agent i has reached the desired position. If it has not reached its end point, and the position is constant on the same placement, it perturbs the desired position of the agent until the direction of the steepest decent changes more than a predefined value. This will mean that the agent is out of the local minima and can continue on the trajectory. The solution of clustering the objects, that are too close, can be seen on figure 7.5.

Here the first solution is applied where the two agents, that were too close to each other, have been clustered into one, seen from the i'th agent. Now the local minima between the agents have been neglected and the i'th agent can generate its trajectory around the agents

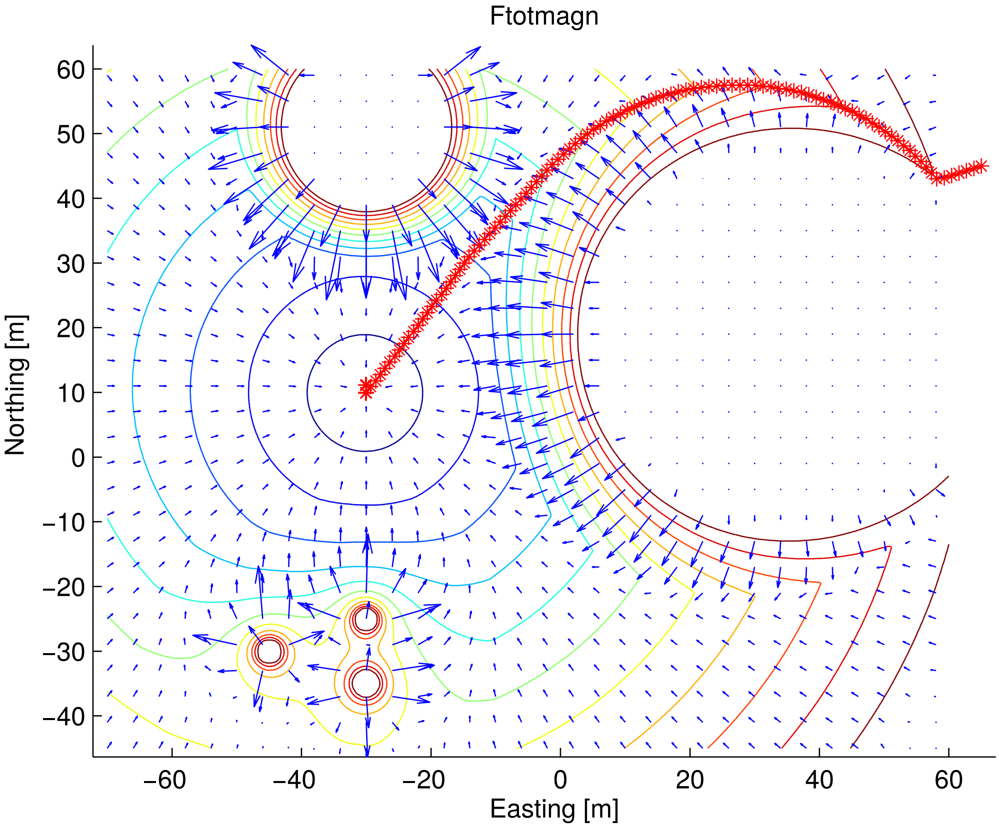

Figure 7.5: An agent that before was stuck now does not get into a local minima close to the agents, as it now sees the two other agents as one larger agent.

and continue to the endpoint of the potential field. The algorithm checks if the distances between the agents are lower that $2 \cdot r$. If this is the case it means that the i'th agent cannot generate a trajectory in between these agents, which can lead to a local minima. Therefore is the agents that are too close combined into one by generating the middle point between their positions and generating a new radius. This makes a larger circle where the two agents are in the subset. This circle will be larger depending on the wanted safety radius thus rises the need to recheck the potential field again after have generated a new combined agent. If the radius of the new agent places it close to one of the single agents, these also might need to cluster. Thus the algorithm needs to run until no distances between agents are $< 2 \cdot r$.

The algorithm generating this combined agent can be seen in pseudo code in algorithm 1.

Data: clustering of agents
initialization;
if $||\mathbf{p}_i, \mathbf{p}_j|| < 2 \cdot r$ **then**
  $\mathbf{p}_{j,new} \leftarrow$ mid point between $\mathbf{p}_i$ and $\mathbf{p}_j$
  $r_{new} \leftarrow$ calc new r for $\mathbf{p}_{j,new}$
  delete $\mathbf{p}_i$ and $\mathbf{p}_j$with $\mathbf{p}_{j,new}$
end

Algorithm 1: This pseudo code describes how agents that are too close to each other are getting clustered and seen as one. The algorithm can also be applied for obstacles in the potential field.

Firstly every distance between the agents are checked if it is lower than $2 \cdot r$. If the distance is lower, a new coordinate set needs to be calculated. The coordinates for the $\mathbf{p}_{j,new}$ is generated to the middle value of the two points

$$\mathbf{p}_{j,new} = \frac{\mathbf{p}_i + \mathbf{p}_j}{2} \tag{7.15}$$

and afterwards can the new radius for $\mathbf{p}_{j,new}$ be found from

$$r_{new} = \frac{||\mathbf{p}_i, \mathbf{p}_j||}{2} + r \tag{7.16}$$

The r_{new} is visualized on figure 7.6 This shows the relation between the normal safety radius

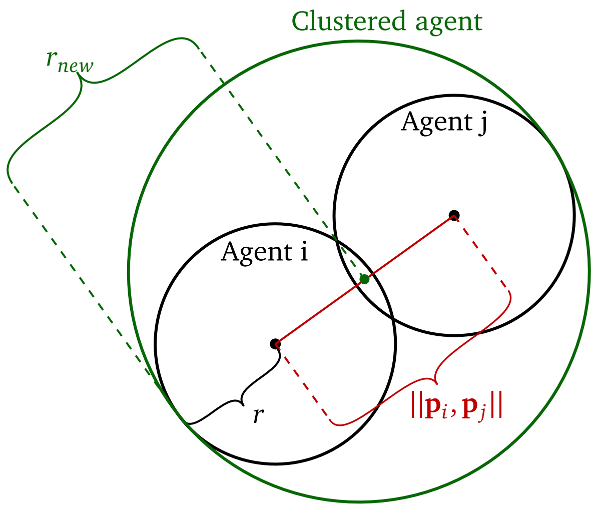

Figure 7.6: Illustration of two agents close to each other clustering into one new agent. The two original agents, i and j are coloured in black and the new clustered object are coloured in green. The distance between i and j is coloured in red.

and the new radius defined for the new clustered agent.

7.2.3 Summary

In the end this results in that the every agent needs a magnitude and a direction of which they should move. This will be given depending on the total environment where the agents are manoeuvring, and will be assigned by the gradient vector. When applying this formation strategy a collision free movement is guaranteed which is one of the more critical criteria to be fulfilled.

7.2.4 Algebraic Solution

In the previous section 7.2.1 the problem is solved in a numerical manor, where the functions are evaluated in single steps in a grid, to see the individual potential field magnitudes. Afterwards they are added together to get the total potential field in that specific point. This is one way to implement the potential field algorithms and within this section another approach is analysed.

The other solution could be to investigate the problem analytically, where the potential fields are calculated from the derivatives of the potential field functions. By doing this the direct gradient of the individual potential field function can be calculated, and added together to get the total gradient at a specific point. The potential field functions are summarized in the following where their derivatives are calculated.

7.2.4.1 Collision Avoidance

The repulsive forces from the collision avoidance is given from equation (7.17). It only applies when the distance from the i'th agents to agent j is smaller than the safety radius. The last term multiplied at the parenthesis is a directional vector, which can be seen as a sign function both in the scalar and the vector case.

$$\mathbf{F}_{ca}^{ij} = \begin{cases} \left(\frac{K_{ca} r}{||\mathbf{d}_{ij}||} - K_{ca} \right) \frac{\mathbf{d}_{ji}}{||\mathbf{d}_{ji}||}, & \text{for } ||\mathbf{d}_{ij}|| < r \\ 0, & \text{otherwise} \end{cases} \tag{7.17}$$

The derivative of F_{ca} can be seen in equation (7.18), where the direction vector have been neglected due to the fact that it is a sign function to be added later, and the derivative of a sign function is still the sign function. This can be seen in section 7.2.4.2 on the following page.

$$\frac{\delta F_{ca}}{\delta d} = -\frac{K_{ca} r \cdot \frac{d}{||d||}}{||d^2||} \tag{7.18}$$

where $\frac{d}{||d||}$ still is a sign function. The derivation can be done by seen in equation (7.19), where equation (7.17) have been split up to make the derivative.

$$F_{ca} = \left(K_{ca} r \cdot \frac{1}{||d||} - K_{ca}\right) \frac{d}{||d||} \tag{7.19a}$$

$$= K_{ca} r \cdot \frac{1}{||d||} - K_{ca} \tag{7.19b}$$

$$\frac{\delta F_{ca}}{\delta d} = -\frac{K_{ca} r \cdot \frac{d}{||d||}}{||d^2||} \tag{7.19c}$$

This applies since the derivative of $\frac{1}{||d||}$ with respect to d can be seen in equation (7.20) and the K_{ca} becomes zero when differentiated with respect to d.

$$\frac{\delta}{\delta d}\left(\frac{1}{||d||}\right) = -\frac{\frac{d}{||d||}}{||d^2||} \tag{7.20}$$

In equation (7.18) the $\frac{d}{||d||}$ enters again by applying equation (7.20) which still is the form of the sign function.

7.2.4.2 The Sign Function

The sign function, also known as the signum function, is an odd function that returns the sign of a real number. The sign function can be split up into three parts, depending on the argument to the function:

$$\text{sign}(x) = \begin{cases} -1, & \text{if } x < 0 \\ 0, & \text{if } x = 0 \\ 1, & \text{if } x > 0 \end{cases} \tag{7.21}$$

Thus it is given in the scalar case that for every $x \neq 0$:

$$\text{sign}(x) = \frac{x}{|x|} = \frac{|x|}{x} \tag{7.22}$$

The derivative of the sign function can be split up in the individual regions and be given as:

$$\frac{\delta \text{sign}(x)}{\delta x} = \begin{cases} \left(\frac{\delta \frac{x}{|x|}}{\delta x}\right) = -1, & \text{if } x < 0 \\ \text{Undefined}, & \text{if } x = 0 \\ \left(\frac{\delta \frac{x}{|x|}}{\delta x}\right) = 1, & \text{if } x > 0 \end{cases} \tag{7.23}$$

7.2.4.3 Obstacle Avoidance

By the applying the same principle as with the collision avoidance, the obstacle avoidance can be determined by taking the derivative of the forces applied by the F_{oa}. The F_{oa} is summarized in equation (7.24).

$$\mathbf{F}_{oa}^{ik} = \begin{cases} \left(\frac{K_{oa}}{||\mathbf{d}_{ki}||} - \frac{K_{oa}}{r}\right)\frac{\mathbf{d}_{ki}}{||\mathbf{d}_{ki}||}, & \text{for } ||\mathbf{d}_{ki}|| < r \\ 0, & \text{otherwise} \end{cases} \tag{7.24}$$

The total derivative can be seen in equation (7.25).

$$\frac{\delta F_{oa}}{\delta d} = -\frac{K_{oa} \cdot \frac{d}{||d||}}{||d^2||} \tag{7.25}$$

The derivation of F_{oa} can be done as in equation (7.28), where the outer sign function is neglected and put back into the derivative afterwards due to the property of the sign function.

$$F_{oa} = \left(\frac{K_{oa}}{||d||} - \frac{K_{oa}}{r}\right)\frac{d}{||d||} \tag{7.26}$$

$$= K_{oa}\frac{1}{||d||} - K_{oa}\frac{1}{r} \tag{7.27}$$

$$\frac{\delta F_{oa}}{\delta d} = -\frac{K_{oa} \cdot \frac{d}{||d||}}{||d^2||} \tag{7.28}$$

The difference between F_{ca} and F_{oa}, equation (7.18) and equation (7.25), lies in the factor of r. This is also the interpretation of the repulsing forces since the F_{ca} should apply a larger force to ensure that no collision will happen between agents that are on collision course.

7.2.4.4 Virtual Leader

The virtual leader force is the contribution as a cone toward the point of virtual leader. The virtual leader force, F_{vl}, is given as:

$$F_{vl} = K_{vl}(d_i - d_{i0}) \tag{7.29}$$

and the derivative is then given in equation (7.30), where the slope is a constant.

$$\frac{\delta F_{vl}}{\delta d} = K_{vl} \tag{7.30}$$

7.2.4.5 Inter Vehicle

The inter vehicle forces are the ones that makes the agents converge toward the formation along the tracking phase. The forces are given as:

$$F_{ij} = K_{ij}(d_{ij} - d_{ij0}) \tag{7.31}$$

and the derivative is therefore also a constant, as seen in equation (7.32).

$$\frac{\delta F_{ij}}{\delta d} = K_{ij} \tag{7.32}$$

7.2.4.6 Summation of the Derivatives

Since the respective derivatives now have been calculated, these can be summed into a combined derivative being the slope in one specific point on the track. By doing this the derivative can be expressed in pure algebra and thereby the ability to calculate the slope by this instead of a numerical solution. The respective derivatives can be seen in equation (7.30), (7.32), (7.18) and (7.25). The summation to find the absolute slope can be seen in equation (7.33).

$$\frac{\delta F_i^{tot}}{\delta d} = \frac{\delta F_{vl}}{\delta d} + \frac{\delta F_{ij}}{\delta d} + \frac{\delta F_{ca}}{\delta d} + \frac{\delta F_{oa}}{\delta d} \tag{7.33}$$

This will be a more direct calculation method compared to the numerical method. Though the numerical method is chosen to be implemented due to a more interpreting idea of how the potential field algorithms should be carried out.

7.2.5 Adding the Dynamics for Simulation

The potential field control system consists of multiple elements as seen with the flow which is illustrated on the block diagram on figure 7.7. The first block is the potential field gener-

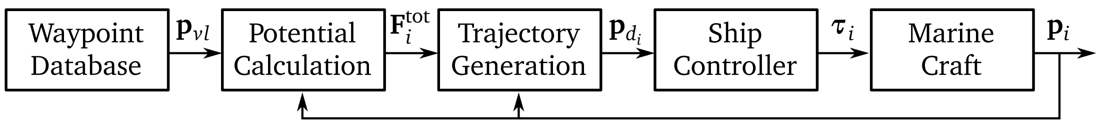

Figure 7.7: Block diagram showing the iteration process of using the potential fields for computation of the input vector

ator. This is the potential field calculation to compute the magnitude of the global potential field. This information is passed to a trajectory generator, which generates the reference trajectory. This reference trajectory is where the i'th agent needs to move. This is passed to the controller of the vessel, which then computes the input to the actuators on the vessels. The position of the vessels are then fed back, both to the potential field calculation, the trajectory generation and the controller. The potential field needs to be calculated from the vessels relative position, the trajectory generation needs the position for the intermediate reference position and the controller will need it for i.e. error calculations.

Part of this flow can be computed by the i'th ship themselves, but the overlying trajectory generation needs to be handled by the virtual leader, or one leader in the formation.

The implementation of this is tested in matlab, using the m-files;

potfield.m, pathgen.m, shipcontroller.m, simaauship.m, simaauship2.m.

The potfield.m is the potential field algorithm, where the magnitudes of the field is generated. The pathgen.m is the trajectory generation, which takes in a set of waypoints and generates the line segments that the vessels needs to follow. The controller applied at the AAUSHIP is a heading controller, which is handled in the shipcontroller.m. To simulate the AAUSHIP is two files used; simaauship.m and simaauship2.m. The first is used to simulate the individual vessel and verify the dynamics of a single ship, and the latter is for simulating the formation with the potfield.m and pathgen.m applied.

The simulation algorithm for the multiship potential field should keep in mind that it is necessary to save the time series for the ship's states, the control inputs and the local reference trajectory for the i'th ship. This needs to be done since the ships need to calculate individual trajectories dependent on the overlying trajectory, which only the virtual leader follows.

Ignoring the initialization of all the variables, the outer loop guidance navigation and control algorithm using potential fields are as follows.

The Guidance, Navigation and Control (GNC) works by an array of mission specific waypoints given, usually computed from a desired area used to create a lawnmower pattern described in chapter 3 on page 17. This trajectory becomes the area of interest, and is the one overlying trajectory that the virtual leader has to follow. The other ships will need to maintain their individual positions at all time steps respective to the virtual leader. Dependent of how the position is formed, the ships needs to go into formation before or during the trajectory tracking phase.

Waypoint Database Different methods can be used to steer ships after this path. The simplest is the usual heading autopilot, which will just steer the reading of the ship to the course angle to the waypoint. Or more elaborate, ways is the use of the waypoints as line segments that the ship should follow. This is implemented with a LOS algorithm. This algorithm, can work, but it is too simple to include obstacle or inter vehicle collisions. A way proposed to solve this issue is to use the concept of potential fields.

Potential Field The potential field itself is merely some functions describing the repulsive and repelling forces between points of interest in the map. These points of interest are all objects that matters for the navigation, that is all ships, the anchor point (virtual leader) of the formation, and other point obstacles. This using the methodology described in the paper (Paul et al., 2008).

The potential field is used in an iterative algorithm which can calculate the direction (from the i'th boat to the desired position spanned by a potential field defining the formation.

Trajectory Generation In the end, a reference path is calculated by the means of the previous position and the result from the potential field solver. It is calculated as the paper presents, (Paul et al., 2008, eq. 48) and described in section 7.1 on page 65.

$$\mathbf{p}_{i,r}^{n} = \mathbf{p}_{i}^{n} + \mathbf{F}_{i}^{\mathrm{tot}} \tag{7.34}$$

This is passed to the ships inner control loop.

When the trajectory is generated from a series of way points, which is not ordered as a series of equidistant way points, it means that some handling of when or how to update the position of the virtual leader is needed.

For example; in the case, where the way points are far from each other, it is still desired to make the virtual leader trajectory converge to the line between these two way points, kind of like the LOS guidance. Earlier a path following algorithm using a LOS principle was used, to calculate a course angle to a point projected into the line between two way points with a specified lookahead distance. The projection with the lookahead ensures convergence to the line. But in the case of controlling the virtual leader, it is not necessary to calculate the course angle from the virtual leader to the projected point, because this is only a virtual anchor of the formation, hence this only specifies where the geometry of the formation is calculated from.

For the inner loop, a heading based LOS method can still be used, but this should be calculated for every ship, with each their reference position $\mathbf{p}_{i,r}$.

```
Data: track as global mission trajectory as way points
initialization;
while m <= length of track do
    for every i-th boat do
        if formation is ok then
            if p_vl is inside the way point acceptance radius of the track then
                m ← m + 1;
                p_vl ← LOS( p_vl , track(m) );
            end
        end
        ( p_d,i , F_tot,i ) ← pathgen( p_i , p0_i );
        p_r,i ← p_i + F_tot,i;
        ψ_d,i ← heading from p_i to p_d;
        u_i ← controller( ψ_d );
        send input u to ship;
        x_i ← sense ship states;
        p_i ← position of x_i;
    end
end
```

Algorithm 2: This pseudo code describes how the potential field is used for each boat to calculate the reference for the inner controller for every boat at every time step. Every iteration in the while loop is a time step.

The algorithm 2 describes how the potential field strategy can be simulated, were each iteration of the while loop is a time step, which means that the control will continue until the formation has reached the way point acceptance radius of the track. This is to ensure that the formation anchor do not move forward if the ships are not properly in formation. This is analogous with the group coordination task as defined by (Thorvaldsen, 2011), and described in section 2.1.2.

A simulation of the algorithm with the dynamics of the AAUSHIP can be seen on figure 7.8. The red crosses are waypoints that have been targeted as the next waypoint to reach. The line connecting those waypoints are the virtual leader movement, which changes position

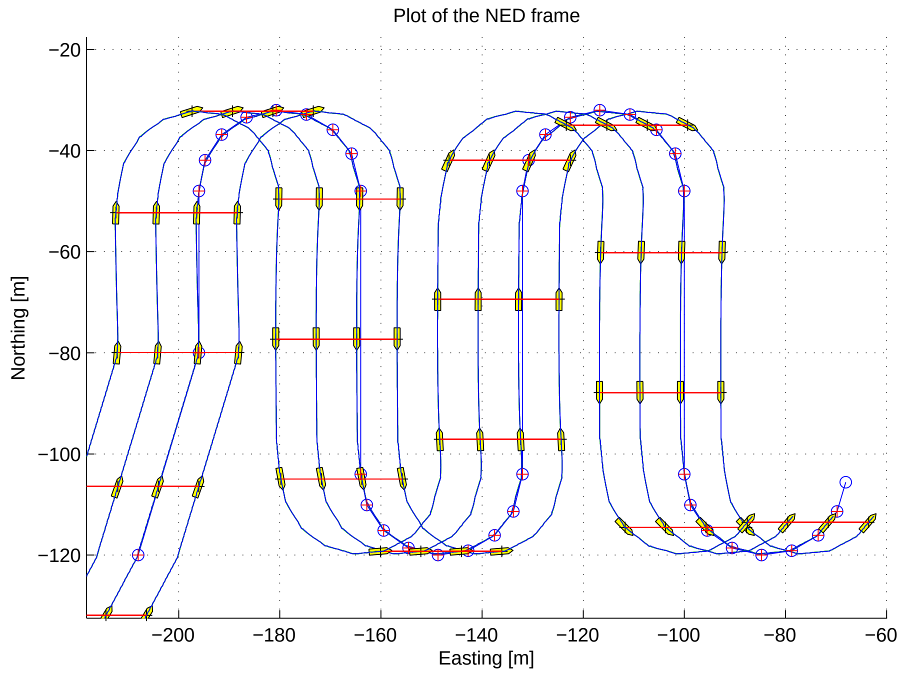

Figure 7.8: Four agents are placed relative to the middle point of the formation, the virtual leader. This leader moves at the trajectory with the waypoints, but only changes to the next waypoint if the agents are in formation.

from waypoint to waypoint to generate the straight line segments for the formation to follow. Every of the four agents have a relative position placement to the virtual leader, the agents positions are p_{ij} and given as $p^n_{vl} + offset$ and the position of the virtual leader is given as p^n_{vl}. The ships are shown as yellow ships and the ships in formation is connected with a red line.

The formation have started at position $[-250, -150]$ and has the first waypoint in $[-208, -120]$. When the agents are close to reach the waypoint at $[-208, -120]$, they ensure that every agent are in formation by waiting for the last to catch up, if needed. Then all of them are in formation with respect to the virtual leader and this changes waypoint such that the agents needs to go toward the next waypoint. This waypoint shifting continues until no more waypoints are available.

It can be seen that there is a little divergence of the ships to the line segments which is mainly due to the dynamics of the AAUSHIP. Their respective line segments are not shown on the figure, while this would make the figure confusing. Though the agents will follow a line segment from their position in the formation to the new position in the formation. This is due to the movement of the virtual leader where this only moves in straight lines, thus the following agents pursue to do the same. The trajectory the ships follow is plotted beneath the third vessel from the left from where it can be seen that this vessel is placed on top of the virtual leader, and almost makes this vessel serve as the leader of the formation. Due to the formation setup the following ships will follow the same trajectory as the leader but only in this case shifted in the easting position.

Chapter 8

ROS Design

This chapter describes the details of the implementation level, which is done on a Robot Operating System platform. This should provide all the information needed to complete the implementation.

It was decided to use Robot Operating System (ROS) in the implementation. It is used as an other abstraction layer on top of the Low Level Interface (LLI). In turn it makes AAUSHIP modular and make it easy for others to write parts of the control system without reimplementing basic components. This in turn makes it an extensible platform, that should be easy to extend. ROS is a project available at `http://ros.org`, which describes itself in short as following:

> *ROS (Robot Operating System) provides libraries and tools to help software developers create robot applications. It provides hardware abstraction, device drivers, libraries, visualizers, message-passing, package management, and more. ROS is licensed under an open source, BSD license.*
>
> ROS.org

8.1 ROS Terminology

To start working with ROS it is important to use the terminology used by ROS to avoid confusion. Therefore these will be stated in this section. The idea of ROS is to make it easy to build a system modularly, and this is achieved by using almost "self-contained" code segments called *nodes*, which is application parts that is run as its own process. A node should be designed to execute limited tasks such as image processing or similar atomic processes. These nodes can then communicate with other nodes by the means of two main communication forms called *topics* and *services*. A good introduction to the base components of ROS and overview of how it works is also described by the (Quigley et al., 2009) conference paper.

The topic is an asynchronous connection, that can *publish* from many nodes and be *subscribed* by many nodes. This means that it is a multicast form for providing data.

The service is a synchronous connection that is used between one node to another node. This is only unicast.

An illustration of multiple nodes connected via topics and a service is on figure 8.1. This concept can also be used across multiple machines. This is illustrated in figure 8.2 on the facing page. On this a new type of unique node is introduced, this is the ROS master. This is a required component for a ROS system to run. The master's only purpose is to make the nodes connect together via the topics or services. There can only be one master per ROS system. This also enables multiple machines to share topics, by connecting the masters that runs on the individual machines. In short the masters sole purpose is to make these connections. It is illustrated by the dashed arrows. Each node says that it want to i.e. publish or subscribe to a certain topic. To connect a node from one machine to another, the environment variable `ROS_MASTER_URI` has to be set to the host with the master running, and the `/etc/hosts` file has to be set on all machines with the other machine's hostnames.

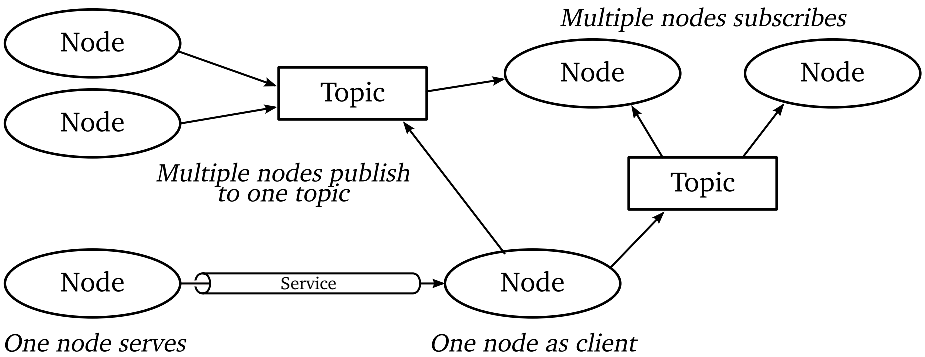

Figure 8.1: Basic principle of the node abstraction illustrating a service and two topics. The topology chosen here is only to illustrate the possibilities.

When that is said, that is not the whole picture of the topology. In a need to make this flexible ROS has made it such that the nodes can be started and stopped kind of "runtime". That is such that it is possible to have different configurations of nodes to run in different scenarios, i.e. in development with debugging nodes and virtual sensor nodes versus in the real mission where no debugging nodes is used and real sensor nodes that use real sensor data is used.

8.2 ROS on AAUSHIP

`/lli_node`
: This is responsible for communicating with the LLI. It publishes sensor data from the LLI and receives various input commands and forwards them to the LLI.

`/sensor_decode_node`
: This decodes the samples from the LLI and publishes this to the relevant topics.

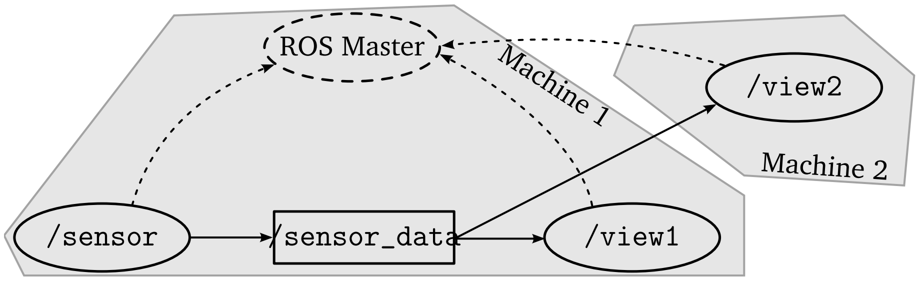

Figure 8.2: Concept showing the ROS master together with the nodes, also illustrating the masters role with multiple machines. Dashed lines hows that the node will either subscribe or publish to the topic. This only happens initially when connecting to a topic. Gray area is two physical separate but networked machines.

`/joy`
: This is a node from ROS that is a generic interface to various joystick inputs. Here it is used to get data from a PS3 controller.

`/joy_teleop_node`
: This is node parses some data from the PlayStation 3 controller, and formats those as messages that is to be sent to the LLI.

`/kf_node`
: This node is the running the KF iteration with the attitude estimate and the decoded IMU samples.

`/gnc_node`
: This node runs the GNC algorithm, basically the controller.

`/rqt_mission_planner_node`
: This node is an rqt plugin used to specify the mission.

`/ahrs_mahony`
: This node is the attitude observer described in section 6.6 on page 47.

8.3 Multiple AAUSHIP's

All of the above design only describes the ROS layout on one ship. Given that this project is about formation control, that implicitly means that multiple ships has to operate at the same time, which in the case of cooperative formation some information has to be shared between ships. AAUSHIP is equipped with Wi-Fi, which in turn means that it uses an Internet Protocol (IP) based networking scheme. This means that one can easily add up to 255 ships on one subnet with Internet Protocol version 4 (IPv4). If the formation needs to scale to more than that, some networking design is needed maybe using Internet Protocol version 6 (IPv6).

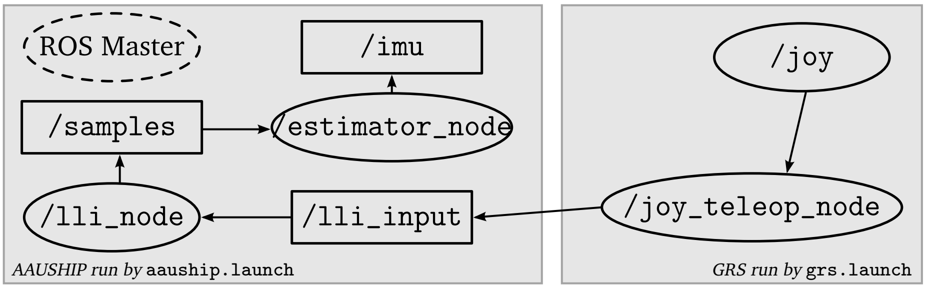

Figure 8.3: ROS configuration on AAUSHIP for manual tele operation. AAUSHIP and GRS are connected via a Wi-Fi connection.

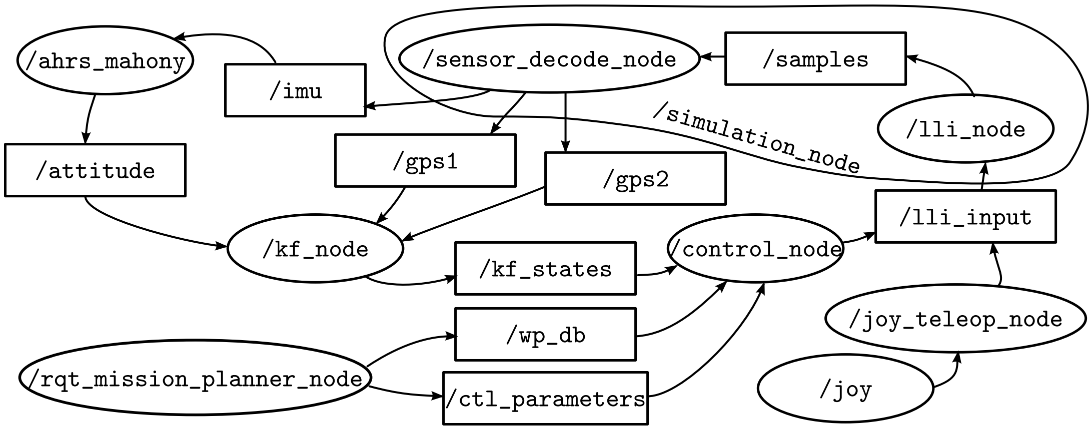

Figure 8.4: Closed loop ROS system on one ship. The blob representing the `/simulation_node` is what where the simulation fits in, that is it replaces the `/lli_node` and the `/sensor_decode_node`.

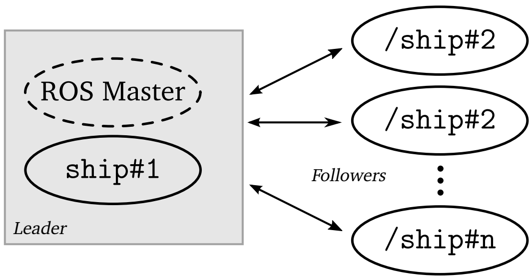

Figure 8.5: ROS configuration on AAUSHIP for with multiple ships. It show that there is only one master, for example the lader, but not limited to the leader ship.

launch

GRS run by g

The degree of information of the information that needs to be share depends on the formation method chosen. The ROS system should accommodate some arbitrarily defined schemes in a way that is defined by the control node of the ship. Since every boat is connected with a via Wi-Fi it is assuming that all ships can reach everyone. This simplification is used for the testing implementations for now. A more advanced system, that should take into account that not every ship can communicate with each other can be developed for large formations or scalability, but in this project the implementation assumes small formations with small distance, that is that all ships are reachable on the whole network. In practice the networks consists of an access point on any random ship where the others connects to.

Part III

Conclusion

The end of the project is the discussion, conclusion and future work.

Chapter 9

Conclusions

This section contains the discussion, conclusion and future work. The discussion and conclusion evaluates what have been done and the future work states where to start a further investigation and additional work.

9.1 Summary of the Project

Within the work of the AAUSHIP project several aspects has been worked on. A summary and further work on the platform will be a discussed in the following,

9.1.1 Path Generation

For the AAUSHIP to follow a given path this needs to be described and carried out to the use case. The vessel is intended for surveying purposes in the Limfjord, where the path for the vessel to track have been designed as a lawnmover pattern. This have been described in chapter 3 after the previous analysis.

9.1.2 Hardware Upgrades

For the AAUSHIP to be fully operational some hardware upgrades have been implemented. Among others is a new computer mounted at the vessel, for the implementation of the ROS, and for the need to process more data. Previously an Raspberry Pi was used. The mounting of a RTKGPS is also completed but has not been used on a verification sea trial. A new Wi-FI module have been implemented, since the older one used seemingly could not handle the warm weather and dropped out.

9.1.3 Design

In this work a 5 DOF model has been made established from measurements of the ship. It does not include the heave, since this is not in focus to control. To make this model have the needed model parameters been estimated based on measurements and tests of the AAUSHIP.

This includes Bollard Pull tests and Start/Stop tests to determine the damping coefficients. The restoring forces acting on the vessel have also been estimated from tests of rolling and pitching tests.

A simulation environment have been set up in ROS to verify this model and test how controlling will act on the vessel. This gives the project group a chance to implement different types of controlling at the single vessel before testing, to have an idea of how the AAUSHIP will perform. The ROS environment has also been tested with multiple instances of AAUSHIPs in one simulation, and a fast simulation of a Duckling formation have been performed. This was done to give the project group the verification that the ROS environment was ready to implement a fleet of vessels.

The model is tested with a working KF both in the simulation environment but also in real life, where observations shows positive results for the model to converge to a given path.

The inner loop control, the LOS controller for each ship is a PID heading controller, which have been implemented to track the line segments between the given waypoints from the path generation. This is a rather simple heading controller which have been evaluated sufficient to the purpose.

Lastly a design phase of formation strategies has been carried out. The first part of the design phase is an analysis of which type of formation control is needed from a set of different types. Afterwards is one of those chosen, the potential field strategy, and worked on further. This strategy have first been simulated with a single ship, which needs to track a reference calculated by the potential field. After is this simulation expanded to include four vessels, potentially more. The work in this field have caused problems in the implementation phase, but as seen on figure 7.8 have the simulation proven results. The dynamics of the AAUSHIP is included in the simulation, but further work within this field is needed. The potential field strategy is the acting controller to the fleet of AAUSHIPs, and the benefit of the potential field algorithm is that it includes object avoidance to ensure a collision free trajectory.

9.2 Future Work

The future work will state the natural expansion of the project, where a perspective to the future work is commented. Areas where future work are needed is:

9.2.1 Sea Trials

There have been performed trials both in the Klingenberg Lake, but also in the fjord. Due to technical errors have the tests from the fjord not been documented, which are still to come. The tests from the smaller lake shows the potential of the implemented system to be working, and the observations from the fjord trials does the same.

More tuning is needed of the heading controller and more investigation to the minimum velocity at the vessel is needed. This can be done with more trials in the fjord and should be possible with the system as it works now without any technical issues. The observations from the trials of the fjord showed that the vessel was able to converge to the determined path and maintain until the next waypoint and continue on the path.

Although was the program loaded onto the AAUSHIP of older date thus not working as intended when performing the trials. It is in the believe that with the updated program the AAUSHIP is capable to fulfil the trajectory tracking on the level of acceptance that is wanted in the scope of the project.

9.2.2 Model

As for now is the model a five DOF model, that does not include any disturbances, and is linearised to low speed manoeuvring. A natural improvement will be to expand the model parameters to perform at higher speeds such that the model becomes more non linear, thus also will be in need of an updated KF to estimate the states of the vessel. The model does not track the correct pitch angle while surging, which have caused trouble to the project group. This problem has not yet been solved which is also a model parameter that needs the correct update.

9.2.3 ROS Integration

The intermediate results of having more AAUSHIPs in one simulation in ROS was promising. It showed that it was possible to implement several ships in to one environment, which have been a problem in the beginning of the project. As a part to work on with the ROS is to investigate the network stability while having the communication layer up and running with the vessels. In all the simulations performed until now it is assumed that there are full network communication which in reality might not be as ideal as assumed.

9.2.4 Formation with Potential Field

The formation control strategy implemented with the potential field algorithm has for a start not reached the level where any conclusions can be made. To make the formation control more complete a first step is to perform more intermediate results where the formation is tested in different situations.

It can be seen from the result for now that the four vessels can stay in formation, and that the virtual leader can track a path given, such that vessels keep formation and generates trajectories that seem viable. The result for now was deduced late in the process and therefore have further work with the error checking not been performed.

Although the initial formation strategy is included to show that it is possible now to apply the single ship potential field control to a formation and make several vessels converge into formation and keep the desired formation. Further work could be to investigate different cases of how the formation should move during turns, i.e. implement the different situations analysed in the introduction in chapter 2.

For now is the formation fixed around the virtual leader, where the orientation of the formation does not change. This is done by giving the formation an offset from the position of the virtual leader. Instead this might be done by applying a rotational matrix to generate the relative position of the vessels in the formation, to make the formation turn about the leader, instead of keeping the relative position fixed.

Other things to test is the obstacle avoidance which have been shown with the single AAUSHIP in a potential field. The theory behind this can also be applied to the formation, such that if an obstacle is on the path of the lawnmover pattern, the formation will diverge from their reference to avoid the obstacle, and then afterwards get into formation again. Error analysis of the included dynamics is also of interest and so is situations where the algorithm requires the vessels to be fully actuated, which they are not.

9.2.5 Building the Fleet

Since a formation strategy implies more than one vessel will a natural expansion to the project be to duplicate the AAUSHIP. This will have the benefit of knowing the errors at the working AAUSHIP since this version has several quick fixes. This means that the next versions can be more complete and probably working more stable than this version. The expansion of one AAUSHIP into several will make the fleet of AAUSHIPs that are needed to perform the formation control strategies analysed in this project.

The shortcoming of the project is mainly two aspects, the sea trials in the fjord and verification of the formation control with potential field implementation.

It was a goal to get the fully functional AAUSHIP tested on the fjord and make a survey of the seabed in a lawnmover pattern. This is yet to come with the final AAUSHIP up and running, but observations from the initial testing of the AAUSHIP shows promising intermediate results.

The formation control strategy by applying a potential field algorithm has not been tested enough to conclude if an implementation is applicable. The result shown on figure 7.8 was generated too late in the working process to be able to verify anything concluding about this. A goal was to have a fully working simulation running with the AAUSHIPs in formation, but have only been verified for a single vessel, and the short result for formation of four vessels.

The benefit of the research with the AAUSHIP have improved the basis of the project. The AAUSHIP platform has been upgraded both with a newer model with five DOF, integrated in a ROS environment for the purpose of future work and the hardware of the ship has been upgraded. The hardware upgrades have been done to improve the performance of the ship during the warm days in Denmark where the communication module had problems with dropouts. Before was a Raspberry Pi integrated with the ship but this has been upgraded to a ieee PC to enhance processing power. This was needed to both run the new ROS implementation but also to handle the local data sampling on the vessel. The second part of the project was to investigate formation control strategies for further expansion of the single AAUSHIP to an AAUSHIP fleet. The benefit of having a fleet of vessels have been investigated with focus on the case set up with Port of Aalborg, thus making the focus of expansion to a fleet and to draw industrial attention.

Part IV

Appendix

The appendix includes chapters which are important for the project, but not necessarily interesting to the reader of the report.

Appendix A

Identification of Hydrodynamic Coefficients

A.1 Objective

The purpose with this test is to identify the hydrodynamic coefficients used in the linear model for AAUSHIP, being the hydrodynamic damping coefficients for the 5 DOF damping matrix (5.16) on page 40 and the restoring force during pitch and roll. This is accomplished by three sea trails; a surge test, a sway test and a yaw test, performed in a lake, and two tests to determine pitch and roll, performed in a small pool.

A.2 Theory

The surge, sway and yaw tests are performed with theory of one method of testing, and theory of another method is used when determining pitch and roll. The damping in surge, sway and yaw is estimated by fitting data to a first order differential equation where the pitch and roll dampings are determined from fitting onto a second order differential equation. These two ways of determining the damping coefficients will be denoted *method one* for the first order fitting and *method two* for the second order fitting.

A.2.1 Which Parameters to Determine

The parameters that needs to be determined is the damping coefficients from the damping matrix. The 5 DOF damping matrix is reduced from the 6 DOF damping matrix from (5.11):

$$D = -\begin{bmatrix} X_u & 0 & 0 & 0 & 0 \\ 0 & Y_v & Y_p & 0 & Y_r \\ 0 & K_v & K_p & 0 & K_r \\ 0 & 0 & 0 & M_q & 0 \\ 0 & N_v & N_p & 0 & N_r \end{bmatrix} \tag{A.1}$$

and the coefficients from the restoring force matrix G, (5.17), being:

$$G = -\begin{bmatrix} 0 & 0 & 0 & 0 & 0 \\ 0 & 0 & 0 & 0 & 0 \\ 0 & 0 & K_\varphi & 0 & 0 \\ 0 & 0 & 0 & M_\theta & 0 \\ 0 & 0 & 0 & 0 & 0 \end{bmatrix} \tag{A.2}$$

The different coefficients can be found by writing the complete dynamic system:

$$M_{RB}\,\dot{\nu} + D\,\nu + G\eta = \tau \tag{A.3}$$

where:

$$\nu = \begin{bmatrix} u & v & p & q & r \end{bmatrix}^\top \quad , \quad \eta = \begin{bmatrix} x & y & \varphi & \theta & \psi \end{bmatrix}^\top \tag{A.4}$$

and

$$M_{RB} = \begin{bmatrix} m & 0 & 0 & mz_g & -my_g \\ 0 & m & -mz_g & 0 & mx_g \\ 0 & -mz_g & I_x & -I_{xy} & -I_{xz} \\ mz_g & 0 & -I_{yx} & I_y & -I_{yz} \\ -my_g & mx_g & -I_{zx} & -I_{zy} & I_z \end{bmatrix} \tag{A.5}$$

The full 5 DOF dynamic system equations can then be written as:

$$M_{RB1}\,\dot{\nu} + D_1\,\nu = \tau \tag{A.6}$$
$$M_{RB2}\,\dot{\nu} + D_2\,\nu = \tau \tag{A.7}$$
$$M_{RB3}\,\dot{\nu} + D_3\,\nu + G_3\eta = \tau \tag{A.8}$$
$$M_{RB4}\,\dot{\nu} + D_4\,\nu + G_4\eta = \tau \tag{A.9}$$
$$M_{RB5}\,\dot{\nu} + D_5\,\nu = \tau \tag{A.10}$$

The equations equal τ, being the input to the vessel. Some of the contributions cannot have an input, since actuators for controlling pitch and roll is not implemented.

From the first row can the following be outlined:

$$m\dot{u} - X_u u = \tau_u \tag{A.11}$$

From the second row can the following be outlined:

$$m\dot{v} - Y_v v = \tau_v \tag{A.12}$$
$$-mz_g\dot{p} - Y_p p = 0 \tag{A.13}$$
$$mx_g\dot{r} - Y_r r = \tau_r \tag{A.14}$$

From the third row can the following be outlined:

$$-mz_g\dot{v} - K_v v = \tau_v \tag{A.15}$$
$$I_x\dot{p} - K_p p - K_\varphi \varphi = 0 \tag{A.16}$$
$$-I_{xy}\dot{q} = 0 \tag{A.17}$$
$$-I_{xz}\dot{r} - K_r r = \tau_r \tag{A.18}$$

From the forth row can the following be outlined:

$$mz_g\dot{u} = \tau_u \tag{A.19}$$
$$-I_{yx}\dot{p} = 0 \tag{A.20}$$
$$I_y\dot{q} - M_q q - M_\theta \theta = 0 \tag{A.21}$$
$$-I_{yz}\dot{r} = \tau_r \tag{A.22}$$

From the fifth row can the following be outlined:

$$-my_g\dot{u} = \tau_u \tag{A.23}$$
$$mx_g\dot{v} - N_v v = \tau_v \tag{A.24}$$
$$-I_{zx}\dot{p} - N_p p = 0 \tag{A.25}$$
$$-I_{zy}\dot{q} = 0 \tag{A.26}$$
$$I_z\dot{r} - N_r r = \tau_r \tag{A.27}$$

These equations can be utilized to calculate the coefficients from the damping matrix D and the restoring force matrix G. The coefficients regarding surge, sway and yaw, u, v and r, will be determined by *method one* and coefficients regarding pitch and roll, q and p, and the restoring force coefficients K_φ amd M_θ will be determined by *method two*.

A.2.2 Method One

This method is used to fit a first order differential equation to be able to estimate the damping coefficient. This is done by performing a test of the vessel. The vessel is accelerated from zero velocity to a constant velocity from where the input is taken away. This will make a velocity curve as seen on figure A.1. From this it is possible to fit the dynamic model including

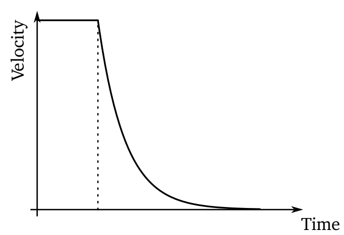

Figure A.1: Constant velocity followed by zero input.

damping of the vessel such that the damping coefficient can be determined. When looking at the motion in surge, this should be fitted by the following method. The dynamic equation in surge, as a homogeneous equation, is given by:

$$m\ddot{x} + D\dot{x} = 0 \tag{A.28}$$

A guess to fit such a first order differential equation could be:

$$u = k \cdot \mathrm{e}^{-st} \tag{A.29}$$

This is the expression of the surge speed, as seen from figure A.1. This is substituted into the dynamic equation to be able to fit the dynamic equation to the differential equation.

$$m\dot{u} + Du = 0 \tag{A.30}$$

$$m \cdot (-ks\mathrm{e}^{-st}) + D \cdot k \cdot \mathrm{e}^{-st} = 0 \tag{A.31}$$

$$-ms + D = 0 \tag{A.32}$$

$$s = \frac{D}{m} \tag{A.33}$$

This makes the surge velocity to be expressed as:

$$u = k \cdot \mathrm{e}^{-\frac{D}{m}t} \tag{A.34}$$

By setting the time to zero gives the initial velocity:

$$u_0 = k \tag{A.35}$$

After the damping is determined is the input force the only unknown in the dynamic equation ((A.28)). The input force, to reach the constant velocity u_0, can be determined by the same principle but should be applied to a curve rising from zero velocity to the constant velocity. This would look as seen in figure A.2. The differential equation to fit this curve would be

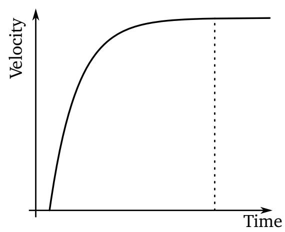

Figure A.2: Zero velocity followed by constant velocity.

given by the inhomogeneous equation:

$$u_{\mathrm{inh}} = u_0 - u_{\mathrm{h}} \tag{A.36}$$

$$u = u_0 - k \cdot \mathrm{e}^{-st} \tag{A.37}$$

where the s still would be given as:

$$s = \frac{D}{m} \tag{A.38}$$

From this is the input force, to reach u_0, given from:

$$m\dot{u} + Du = \tau \tag{A.39}$$

A.2.3 Method Two

The second method is used to determine the coefficients Y_r, K_r, N_r, Y_p, K_p, and N_p for the pitch and roll cross terms in the damping matrix ((5.16)) and the restoring forces from G being K_φ and M_θ. In these tests is the vessel put to a certain angle in pitch and roll and hereafter released. This will make the vessel go back to the buoyant steady state, as seen on figure A.4 on page 103. The damping must be determined by fitting ((A.41)) to the measured data, then this can be used to identify the coefficients for the second order differential equation. The procedure is illustrated by calculating it with the example of K_p and K_φ. The two coefficients from the restoring matrix is given in (5.17).

The damping coefficients K_p and K_φ can be found from the dynamic equation of roll by utilizing M_{RB}, D and the restoring matrix G:

$$I_x\dot{p} + K_p p + K_\varphi \varphi = 0 \tag{A.40}$$

φ is angle position of the vessel. This is the position that needs to follow the damping as seen on figure A.4 on page 103. This can be fit to a second order differential equation. The position of the angle can be expressed as:

$$\varphi = k\mathrm{e}^{-\sigma t} \cdot \cos(\omega_d t) \tag{A.41}$$

This is an under damped system, which is described by a second order homogeneous linear equation given by:

$$a\ddot{y} + b\dot{y} + cy = 0 \tag{A.42}$$

Which can be normalized with the coefficient of a, such that it takes the form:

$$\ddot{y} + \frac{b}{a}\dot{y} + \frac{c}{a}y = 0 \tag{A.43}$$

For an under damped system this can be seen as:

$$\ddot{y} + b\dot{y} + cy = 0 \tag{A.44}$$

$$\ddot{y} + 2\zeta\omega_0\dot{y} + \omega_0^2 y = 0 \tag{A.45}$$

Where ζ is the exponential damping ratio of the system and ω_0 is the undamped natural frequency. The solution to this is guessed as:

$$y(t) = k\mathrm{e}^{-st} \tag{A.46}$$

This will make the curve as the damping from the pitch and roll dampings. Substituting this into (A.45), and transforming, gives:

$$s^2 k\mathrm{e}^{-st} + 2\zeta\omega_0 s k\mathrm{e}^{-st} + \omega_0^2 k\mathrm{e}^{-st} = 0 \tag{A.47}$$

Which can be divided by $k\mathrm{e}^{-st}$:

$$s^2 + 2\zeta\omega_0 s + \omega_0^2 = 0 \tag{A.48}$$

The solution for the second order polynomial in (A.48) is then:

$$s = \frac{-2\zeta\omega_0 \pm \sqrt{4\zeta^2\omega_0^2 - 4\omega_0^2}}{2} \tag{A.49}$$

where:

$$a = 1 \tag{A.50}$$
$$b = 2\zeta\omega_0 \tag{A.51}$$
$$c = \omega_0^2 \tag{A.52}$$

Which for an under damped system can be expressed in the complex form:

$$s \overset{\zeta<1}{=} -\zeta\omega_0 \pm \omega_0\sqrt{1-\zeta^2} \tag{A.53}$$
$$= -\sigma \pm j\omega_d \tag{A.54}$$

Where:

$$\zeta\omega_0 = \sigma \text{ from equation}(A.41), \text{which is the real part} \tag{A.55}$$
$$\omega_0\sqrt{1-\zeta^2} = \omega_d \text{ from equation}(A.41), \text{which is the imaginary part} \tag{A.56}$$

By comparing (A.43) and (A.48) it can be seen that:

$$a = 1 \tag{A.57}$$
$$b = 2\zeta\omega_0 = \frac{K_p}{I_x} \tag{A.58}$$
$$c = \omega_0^2 = \frac{K_\varphi}{I_x} \tag{A.59}$$

From the fitting of data is two variables known:

$$\sigma = \zeta\omega_0 \tag{A.60}$$
$$\omega_d = \omega_0\sqrt{1-\zeta^2} \tag{A.61}$$

This makes it possible to determine K_p by:

$$b = 2\zeta\omega_0 = 2\sigma = \frac{K_p}{I_x} \tag{A.62}$$
$$K_p = 2\sigma I_x \tag{A.63}$$

The coefficient K_φ can be determined by:

$$\omega_d = \omega_0\sqrt{1-\zeta^2} \tag{A.64}$$
$$\omega_d^2 = \omega_0^2 - (\zeta\omega_0)^2 = c - \sigma^2 = \frac{K_\varphi}{I_x} - \sigma^2 \tag{A.65}$$
$$K_\varphi = \omega_d^2 I_x + \sigma^2 I_x \tag{A.66}$$

This makes the dynamic equation with roll as:

$$I_x\ddot{\varphi} + K_p\dot{\varphi} + K_\varphi\varphi = 0 \tag{A.67}$$

$$I_x\ddot{\varphi} + (2\sigma I_x)\dot{\varphi} + (\omega_d^2 I_x + \sigma^2 I_x)\varphi = 0 \tag{A.68}$$

A.2.3.1 Surge Test

$$m\dot{u} + X_u u = \tau_u \tag{A.69}$$

where only *method one* is used.

A.2.3.2 Sway Test

$$m\dot{v} + Y_v v = \tau_v \tag{A.70}$$

$$-mz_g\dot{v} + K_v v = \tau_v \tag{A.71}$$

$$mx_g\dot{v} + N_v v = \tau_v \tag{A.72}$$

where only *method one* is used.

A.2.3.3 Yaw Test

$$mx_g\dot{r} + Y_r r = \tau_r \tag{A.73}$$

$$-I_{xz}\dot{r} + K_r r = \tau_r \tag{A.74}$$

$$I_z\dot{r} + N_r r = \tau_r \tag{A.75}$$

where only *method one* is used.

A.2.3.4 Pitch Test

$$I_y\dot{q} + M_q q + M_\theta\theta = 0 \tag{A.76}$$

$$\tag{A.77}$$

where only *method two* is used.

A.2.3.5 Roll Test

$$-mz_g\dot{p} + Y_p p = 0 \tag{A.78}$$

$$I_x\dot{p} + K_p p + K_\varphi\varphi = 0 \tag{A.79}$$

$$-I_{zx}\dot{p} + N_p p = 0 \tag{A.80}$$

where only *method two* is used.

A.3 Tools

Tools needed are:

- AAUSHIP equipped with:
    1. Capability to set thrusters to equal setpoints and stop at the same time.
    2. Logging capability for IMU, GPS1, GPS2 with UBX data and control inputs.
- Computer to set remote parameters and tele operation.
- RTK base station logging UBX data.

To be able to make the tests the AAUSHIP needs to have both forward thrusters and sideways thrusters. These are implemented and can be controlled from a computer.

A.4 Method

Two different types of measurements needs to be made. These are dependent on which coefficients that is wanted. The first type of test is split into three phases, as seen on figure A.3, and is approximated from a first order fitting. The second type of test is made as seen on figure A.4, and is approximated from a second order fitting.

In the first type of test is the vessel accelerated to constant velocity. When the constant velocity is ensured, the input force to the vessel is removed and zero input is therefore applied. This will correspond to a model like:

$$M_{RB}\,\dot{\nu}_r + D\,\nu_r = 0 \tag{A.81}$$

An acceleration, constant velocity and deceleration will look like figure A.3. This makes it

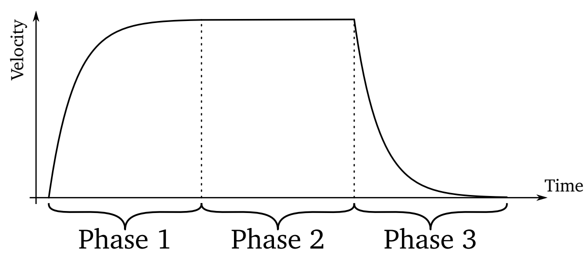

Figure A.3: An acceleration followed by constant velocity followed by zero input.

possible to determine some of the coefficients of the D matrix. e.g. is the damping in the x direction determined by:

$$M_{11}\ddot{x} + D_{11}\dot{x} = 0 \tag{A.82}$$

The mass of the vessel can be measured, being the M_{11}. The velocity and acceleration can be estimated from measurements of the positions measured by the GPS at the vessel. This makes

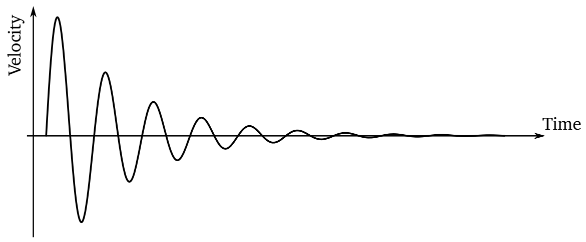

Figure A.4: Pitch and roll response.

the damping coefficient D_{11} the only unknown in equation (A.82). From this a linearisation can be made, see appendix A. From this can the damping coefficient be determined.

This makes it possible to determine the input force by applying a step input on the motors and let the vessel accelerate to the same constant velocity. This can be done since, due to the previous test, only the input is unknown. A model of this will look like:

$$M_{11}\ddot{x} + D_{11}\dot{x} = \tau \tag{A.83}$$

From this it is possible to estimate the input force as a linearisation, since this is the only unknown from equation (A.83).

This type of procedure is used in all of the first types of tests and can be put into steps.

1. Step one is to apply force in one direction until a constant velocity is achieved and then measure the damping while the vessel is decelerating to estimate the damping coefficient.

2. Step two can be made after knowing the damping coefficient. Then is only the input unknown and a step can be applied to accelerate the vessel to constant velocity again. From this step input can a input force be estimated.

The second type of test is used when determining coefficients as pitch and roll, r and p. In these tests is the vessel put to a certain angle in pitch or roll and is afterwards released. This will make the vessel converge to steady state, as seen on figure A.4. This is due to the acting restoring force due to that the vessel is perturbed away from its equilibrium and converges back to it. The convergence is dependent on the angle of either pitch or roll of the vessel, and therefore the tests need to be made from the same angle every time.

One of the important things are to decouple the tests such that the damping coefficients can be measured. This can, as a start, be performed in x-, y- and z-directions. The mixed damping coefficients, as the Y_r (the force in y-direction due to a rotation), has got many components as shown above. But, after have performed the previous tests, these will become the next unknowns to be determined. Looking at the system as a 5 DOF will make it possible to determine the coefficients needed. Some of the coefficients can be found from measurements made by (Nielsen and Lundgaard, 2013). The decoupled coefficients are tested from the equations in (A.85).

$$M_{11}\ddot{x} + D_{11}\dot{x} = \tau \tag{A.84a}$$
$$M_{22}\ddot{y} + M_{23}\ddot{\psi} + D_{22}\dot{y} + D_{23}\dot{\psi} = \tau \tag{A.84b}$$
$$M_{45}\ddot{y} + M_{55}\ddot{\psi} + D_{45}\dot{y} + D_{55}\dot{\psi} = \tau \tag{A.84c}$$

being

$$m\ddot{x} - X_u\dot{x} = \tau \tag{A.85a}$$
$$m\ddot{y} + mx_g\ddot{\psi} - Y_v\dot{y} - Y_r\dot{\psi} = \tau \tag{A.85b}$$
$$mx_g\ddot{y} + I_z\ddot{\psi} - N_v\dot{y} - N_r\dot{\psi} = \tau \tag{A.85c}$$

The tests performed are as follows:

A.4.1 Test 1

The first test is a *surge* test. This test is done to test the forward damping coefficient being X_u from the damping matrix D. The vessel will accelerate to a certain velocity and keep this. Then all input is put to zero and the vessel will decelerate. This will, as described in section 5.4, give a damping coefficient in the forward motion. This is expressed as $m\ddot{x} - X_u\dot{x} = 0$ and X_u can be estimated. A step input is now set on the vessel to see the acceleration from zero velocity to the same constant velocity as before. This now gives the input force at the vessel, which is the last unknown in $m\ddot{x} - X_u\dot{x} = \tau$. Both X_u and τ is estimated by fitting to a first order differential curve, as described in A.2.2. To make this test and data fitting is only position data in the forward motion from the GPS of importance. The position can be differentiated twice, to give both velocity and acceleration of the vessel and cab be used to fit the acceleration and deceleration of the vessel.

A.4.2 Test 2

The second test is a purely *sway* test. The vessel will make use of the sideways thrusters to move strictly sideways. This implies that there is no rotation or movement in ψ and x. Thus makes the moving equation as $m\ddot{y} - Y_v\dot{y} = 0$. Here is the vessel again accelerated to a constant velocity and the input is then set to zero, and Y_v can be determined. After this the sideways thrusters can be used to accelerate the vessel to the same constant velocity and the input can be estimated by $m\ddot{y} - Y_v\dot{y} = \tau$ where τ is the only unknown. K_v and N_v can be determined from the same test, though the fitting needs to be changed due to the new parameter from M_{RB}. The fitting should be done to the same type, namely like procedure *method one* in A.2.2. To make this test and data fitting is only position data in sideways motion from the GPS of importance. This can be differentiated twice to give both velocity and acceleration in the sideways direction. This can be fitted to a acceleration and deceleration of the vessel when only moving in the sideways direction.

A.4.3 Test 3

The last test to perform is the *yaw* test. In this test it is of importance to control the sideways thrusters such that the vessel will keep the position at both x and y, such that only rotation is used to move the surrounding water. The vessel is accelerated to a constant angular velocity and the input is then set to zero. The damping of this will determine N_r from $I_z\ddot{\psi}-N_r\dot{\psi}=0$. Now the vessel needs to reach the constant angular velocity again from zero, and the input can now be estimated from $I_z\ddot{\psi}-N_r\dot{\psi}=\tau$. Y_r and and K_r can be determined from the same test, but the fitting is a little different due to the new parameter from M_{RB}. These fittings should be done as procedure *method one* in A.2.2. To make these should the position from the GPS be measured to ensure that the vessel does not move of greater importance in forward and sideways directions. Measurements from the magnetometer and accelerometer is used to determine the heading and thereby the change on heading and the acceleration. The accelerometer is used to compensate the pitch and roll in the magnetometer measurements.

The parameters in pitch and roll is determined by fitting data to *method two* as described in A.2.3. Previous work done by (Nielsen and Lundgaard, 2013) has provided the data to be fitted. The data is dependent of the position on the angle of the vessel and the equations is therefore formulated to fit these measurements. The fitting of the data is done as procedure *method two* and no further tests needs to be performed. The tests shows pitch and roll, measured in a vicon motion tracking lab. The vessel is put to a maximum angle without level it into the water. Afterwards it is released and the vessel will damp to zero angle, being horizontal in steady water. To verify the data from (Nielsen and Lundgaard, 2013) accelerometer will be collected both in pitch and roll from two simpler tests without the vicon motion tracking lab.

A.5 Results

A.5.0.1 Surge Test

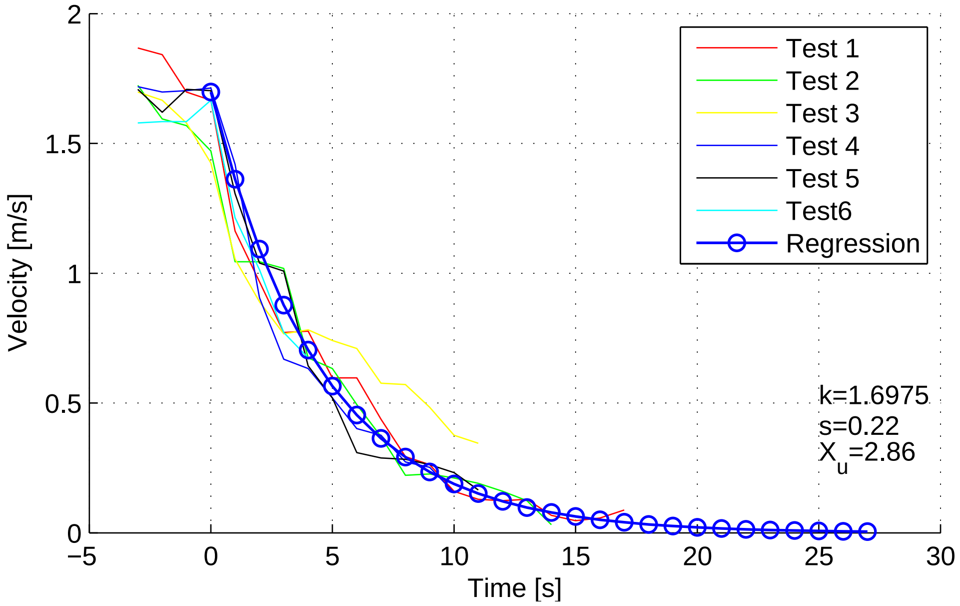

Figure A.5: Surge tests with input on both thrusters.

A.5.0.2 Sway Test

While performing tests with sway it was rather difficult to get any reliable data from measurements. Weather conditions was almost perfect but there was a slight wind. This seemed from measurements to be enough to counteract the forces added by the bow thrusters. The vessel was not moving much over time, thus the measurements seems unreliable. Therefore is the parameters from sway approximated from observations of how fast the vessel was moving over time. The constants which needs to be approximated manually is Y_v, K_v and N_v.

it is assumed, from observations, that the vessel moves in sway with a constant velocity being $0.1\frac{m}{s}$. From this velocity it is estimated that the vessel was on hold after a few seconds. This gives the following damping:

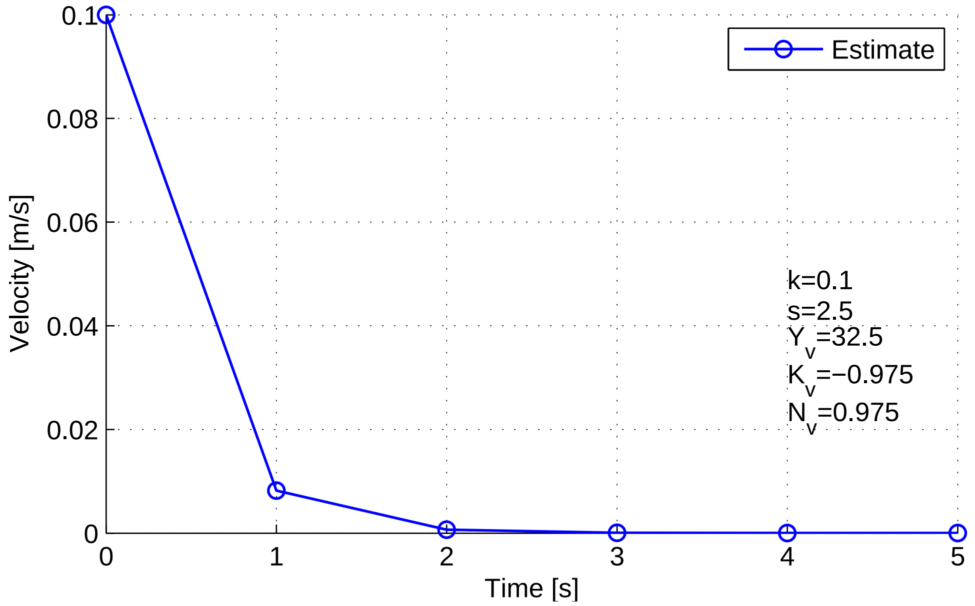

Figure A.6: Estimated sway velocity. The performed tests did not give enough response amplitude to estimate this, so it is deducted from observations.

A.5.0.3 Yaw Test

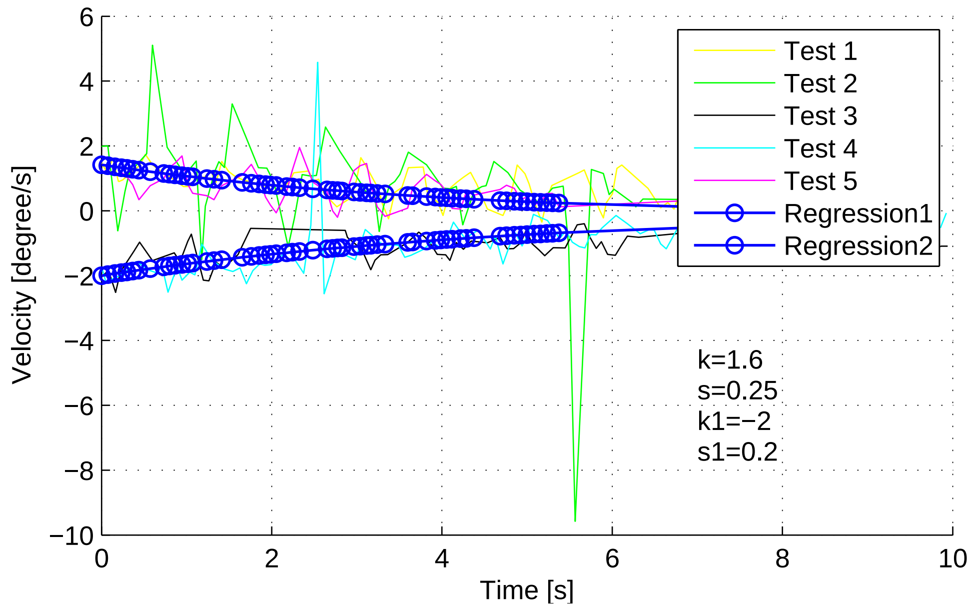

Figure A.7: Yaw tests with bow thrusters, both cw and ccw.

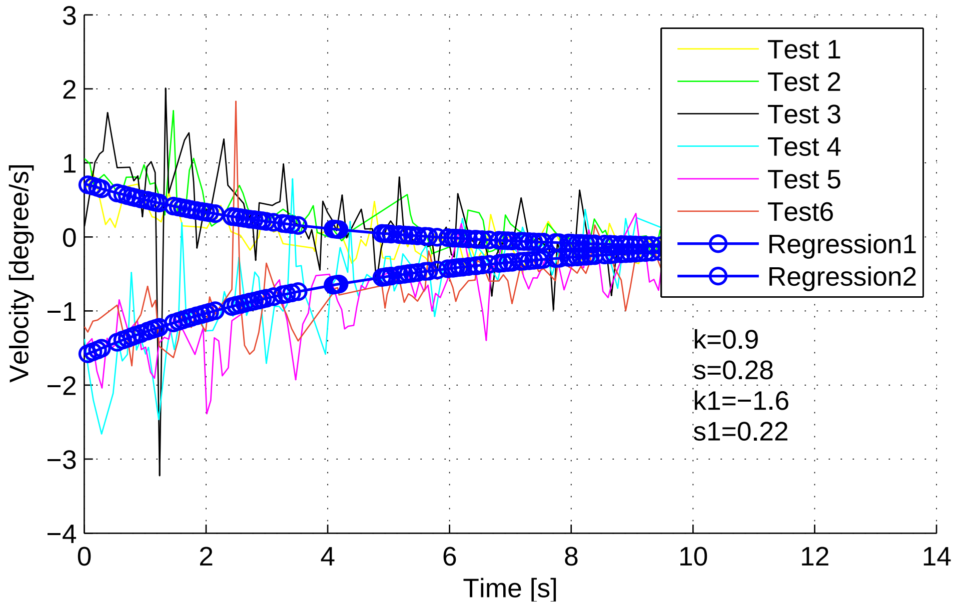

Figure A.8: Yaw tests with propellers, both cw and ccw.

A.5.0.4 Pitch Test

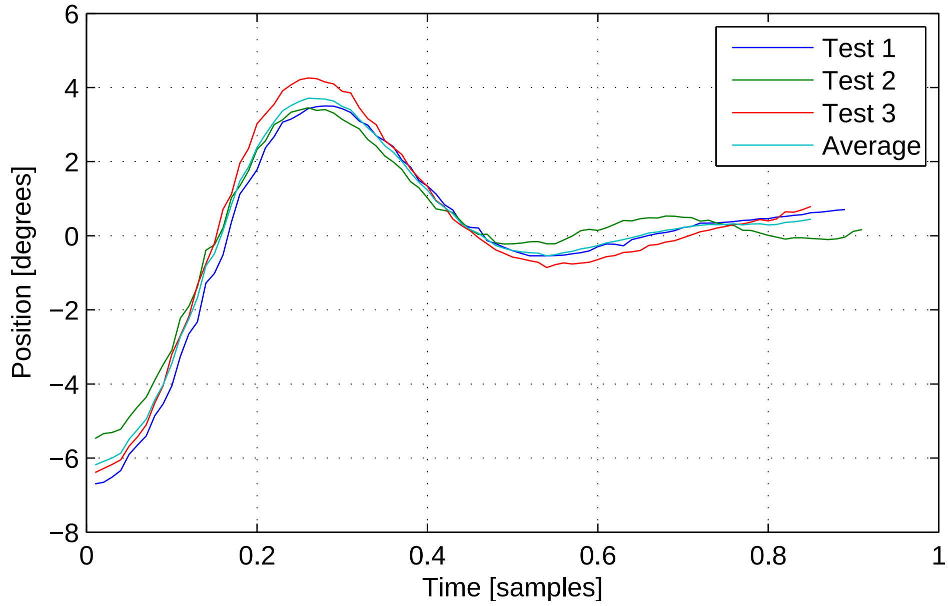

Figure A.9: Pitch test with Vicon, Bow pushed down.

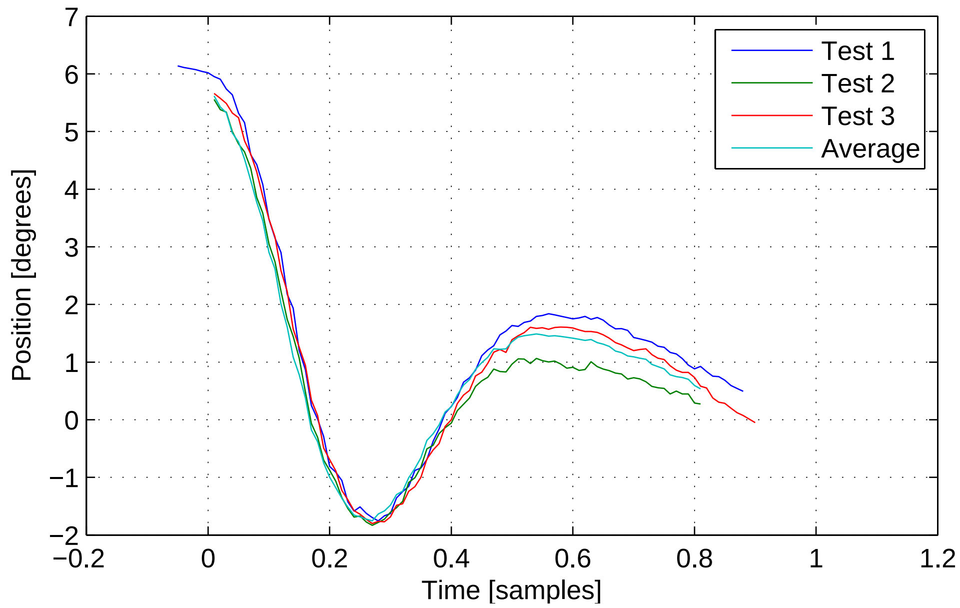

Figure A.10: Pitch test with Vicon, Stern pushed down.

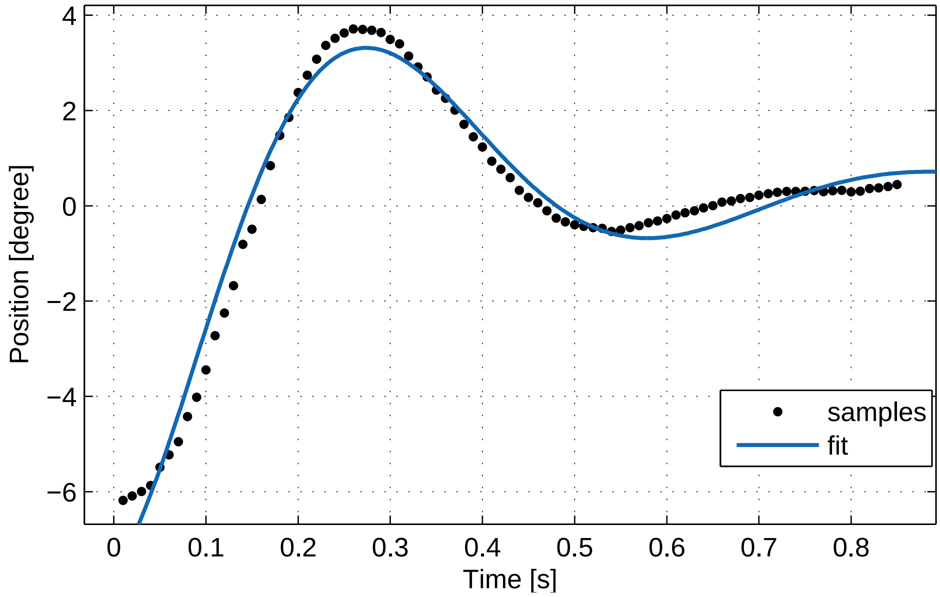

Figure A.11: Regression to the average from the bow pitch test. Coefficient of determination: $R^2 = 0.9729$.

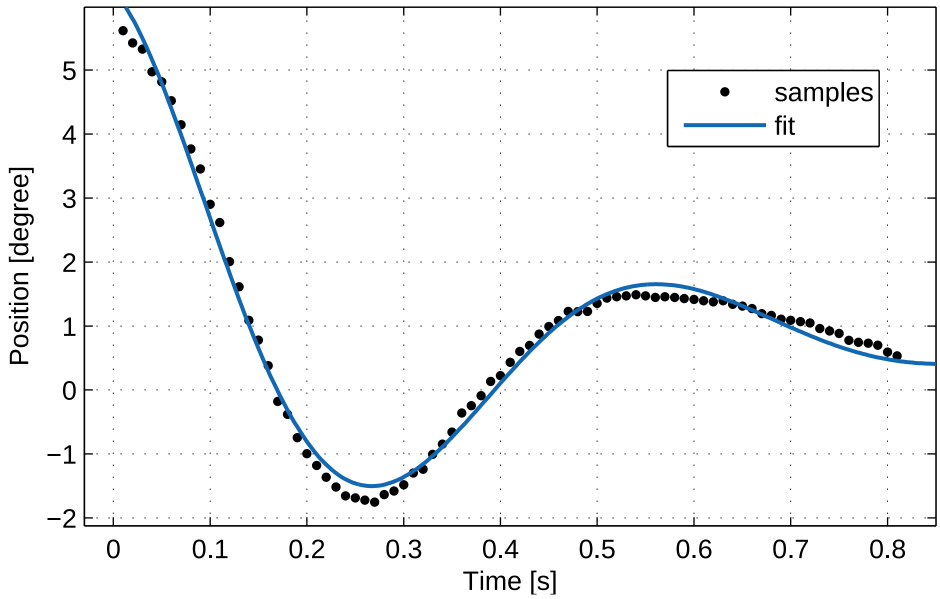

Figure A.12: Regression to the average from the stern pitch test. Coefficient of determination: $R^2 = 0.9905$.

A.5.0.5 Roll Test

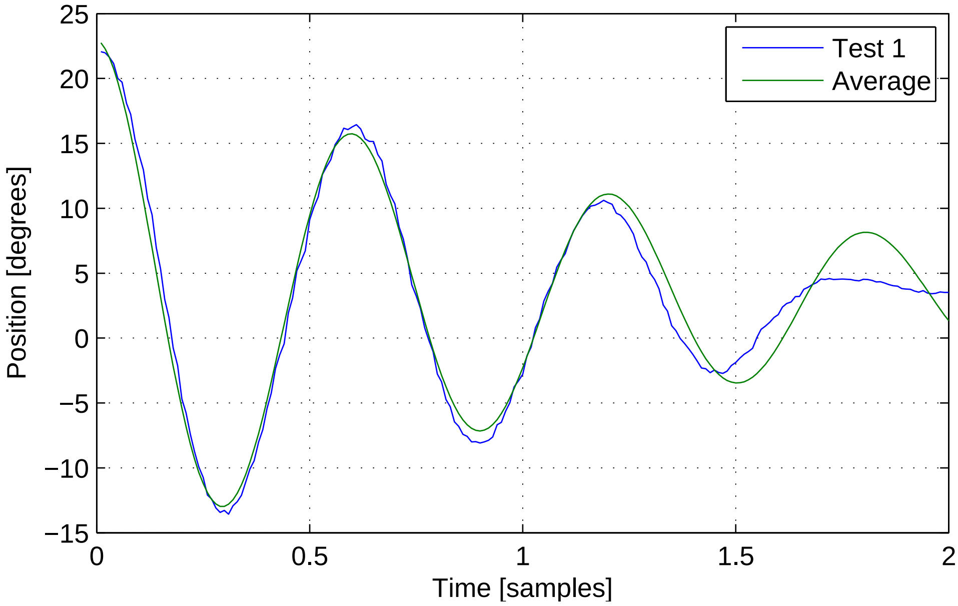

Figure A.13: Roll left test with Vicon, Port side pushed down.

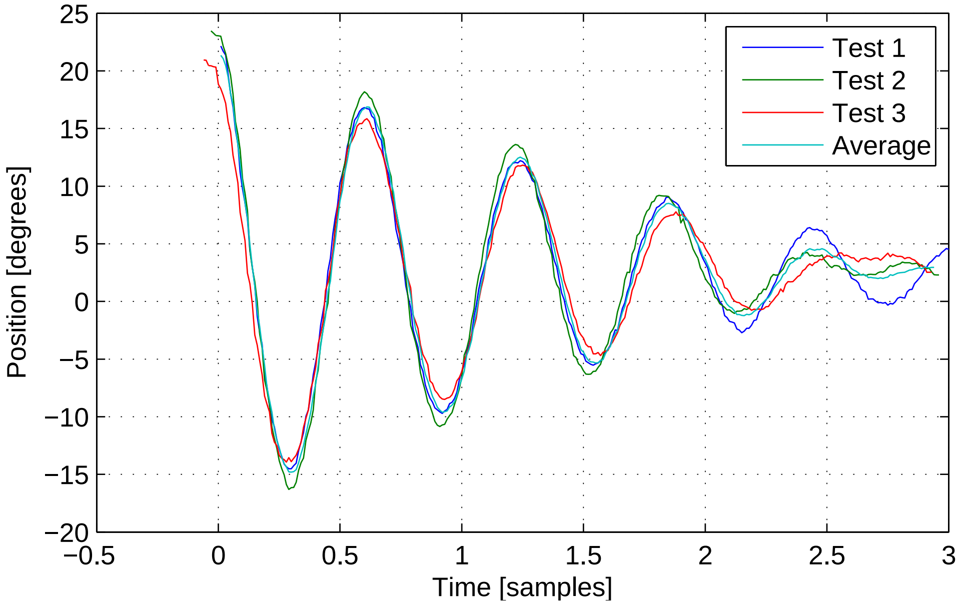

Figure A.14: Roll right test with Vicon, Starboard side pushed down.

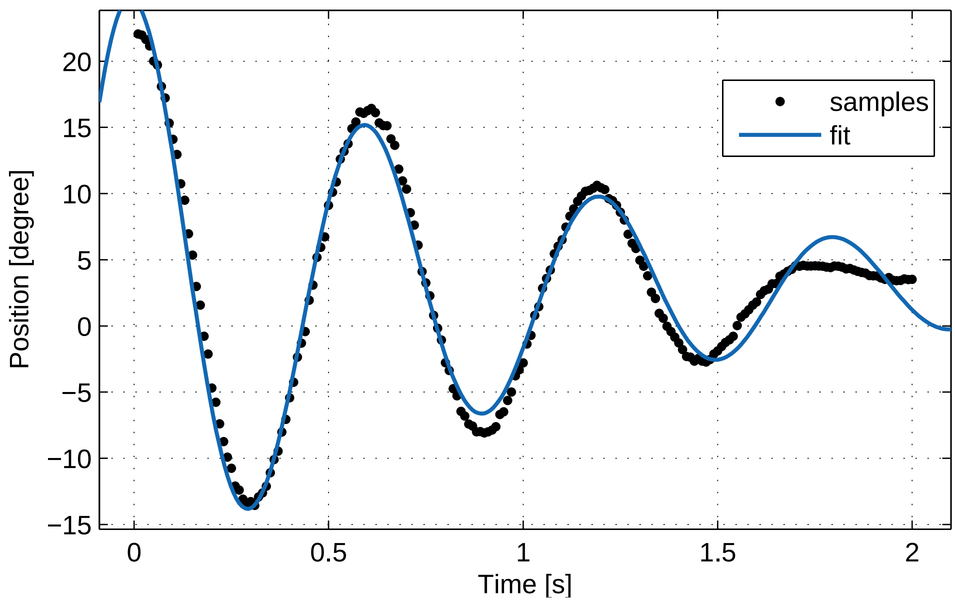

Figure A.15: Regression to the average from the left roll test. Coefficient of determination: $R^2 = 0.9754$.

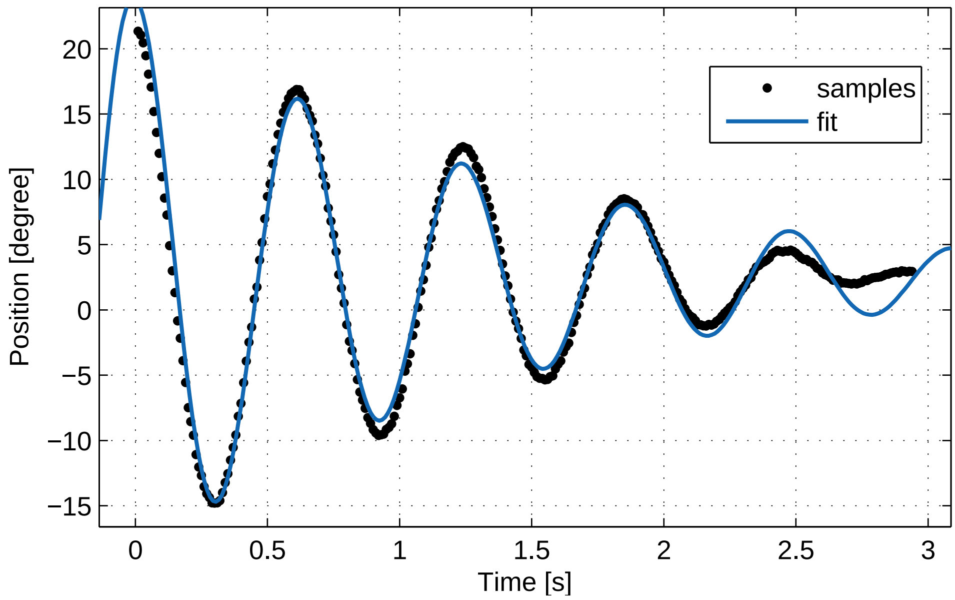

Figure A.16: Regression to the average from the right roll test. Coefficient of determination: $R^2 = 0.9765$.

The coefficients that are fitted can be found in table A.1. It can be seen how well the fitting matches the data, and from this are the damping coefficients determined.

Test	R^2	RMSE	Function
Pitch, bow A.11	0.9729	0.4041	$f(t) = -8.029\exp(-3.45t)\cos(10.29t) + 0.3544$
Pitch, stern A.12	0.9905	0.1721	$f(t) = 5.492\exp(-3.163t)\cos(10.69t) + 0.7605$
Roll, left A.15	0.9754	1.256	$f(t) = 21.93\exp(-0.9482t)\cos(10.45t) + 2.734$
Roll, right A.16	0.9765	1.133	$f(t) = 21.43\exp(-0.7242t)\cos(10.13t) + 2.475$

Table A.1: Coefficient of determination, Root Mean Square Error and the functions to the fittings.

The rigid body constants for the vessel can be found in table A.2 and the results from measurements and estimation can be found in table A.3.

Coefficient	Value	Coefficient	Value	Coefficient	Value
m	13	I_{zx}	-0.05359	I_z	1.10675
x_g	0.03	I_{xy}	-0.01260	I_y	1.08921
y_g	0	I_{yx}	-0.01260	I_x	0.06541
z_g	0.03	I_{yz}	-0.00108		
I_{xz}	-0.05359	I_{zy}	-0.00108		

Table A.2: Rigid body mass matrix constants for M_{RB}

Coefficient	Value	Coefficient	Value	Coefficient	Value
X_u	2.86	N_r	0.26285	K_p	0.1094
Y_v	32.5	Y_r	0.09263	N_p	-0.00069
K_v	-0.975	K_r	0.01273	M_q	7.2030
N_v	0.975	Y_p	-0.00503		

Table A.3: Results of fitted values and the calculated hydrodynamic coefficients.

Restoring force Coefficient	Value
K_φ	6.9736
M_θ	131.8316

Table A.4: Results of fitted values and the calculated restoring coefficients.

This makes the linear damping matrix as:

$$D = \begin{bmatrix} 2.86 & 0 & 0 & 0 & 0 \\ 0 & 32.5 & -0.00503 & 0 & 0.09263 \\ 0 & -0.975 & 0.1094 & 0 & 0.01273 \\ 0 & 0 & 0 & 7.2030 & 0 \\ 0 & 0.975 & -0.00069 & 0 & 0.26285 \end{bmatrix} \tag{A.86}$$

and the restoring force matrix as:

$$G = \begin{bmatrix} 0 & 0 & 0 & 0 & 0 \\ 0 & 0 & 0 & 0 & 0 \\ 0 & 0 & 6.9736 & 0 & 0 \\ 0 & 0 & 0 & 131.8316 & 0 \\ 0 & 0 & 0 & 0 & 0 \end{bmatrix} \tag{A.87}$$

and the rigid body matrix as:

$$M_{RB} = \begin{bmatrix} 13 & 0 & 0 & -0.39 & 0 \\ 0 & 13 & 0.39 & 0 & -0.39 \\ 0 & 0.39 & 0.06541 & -0.01260 & -0.05359 \\ -0.39 & 0 & -0.01260 & 1.08921 & -0.00108 \\ 0 & -0.39 & -0.05359 & -0.00108 & 1.10675 \end{bmatrix} \tag{A.88}$$

A.6 Discussion and Conclusion

The tests regarding surge, sway and yaw have been performed in a lake, where wind could have had an influence on the measurement data. The disturbance from the wind would dominate most in the sway tests due to the lack of power from the bow thrusters. The wind was not of greater speed at the day of testing, but yet could make the vessel stand still during sway tests. Thus have the sway parameters been estimated from observations and not from trustworthy measurement data. The wind did not have any significant impact of measurements during surge and yaw tests.

The pitch and roll tests have been made in a pool in a lab with Vicon system. These tests is not as precise as they could be, due to reflecting waves from the side of the pool. Though is the dampings determined from these data, but only from the first part of the data. Therefore is the regressions made to fit the first part of the data more than the later part of the data. Thus are these taken as approved regressions and a fair approximation of the angular positions.

The coefficients found are compared with coefficients from other models of ships to verify the operational signs. Almost all the signs of the coefficients are of the same operational sign, thus is the parameters approved. The coefficients with changed sign may arise from symmetry and asymmetry of the vessels compared.

Appendix B

Bollard Pull

B.1 Objective

The purpose of this measurement journal is to test if the force, which is generated from the vessel, is linear with the control input to the thrusters or if there should be a mapping between these.

B.2 Theory

If the linear stepped input to the thrusters ends out in a linear output of the vessel it can be approximated that the translation from input to output is linear. This makes some of the controlling of the vessel less complicated due to the non existing non linear mapping from input to output. If a mapping is needed this needs to be taken care of in the control of the vessel, which needs to be compensated at least in the simulations of the vessel. This makes it possible to take it into account in the plant model of the vessel but might be neglected in the control model.

B.3 Tools

Tool
Test vessel
Dynamometer
Rod to apply on the vessel

Table B.1: Tools needed to test the forces generated by the vessel.

B.4 Method

The first tests, utilizing the thrusters forward, was performed by applying a rod symmetric at the stern of the vessel. The rod was extended such that it was possible to measure the force generated by the vessel from the bay, while the vessel was in the middle of the lake. This is done to make the reflecting waves as little as possible. The same procedure are used when testing the vessel while thrusting backwards. The test setup can be seen on figure B.1.

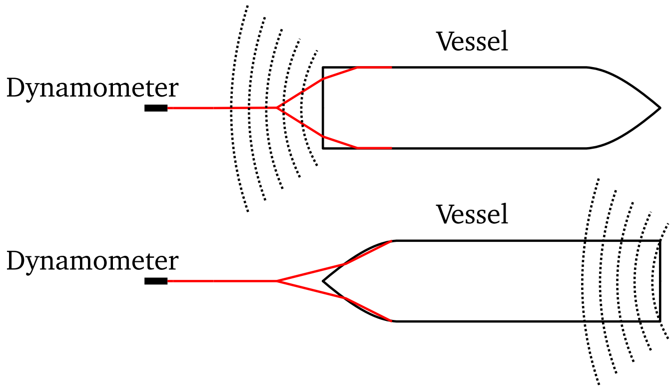

Figure B.1: Setup while testing bollard pull, forward and backward motion.

B.5 Results

Figure B.2: Forward motion tests.

B.6 Discussion and Conclusion

The fitting maps from motor Pulse Width Modulation (PWM) input to force output in N. When looking at the two first regressions at the forward motion it can be chosen to either

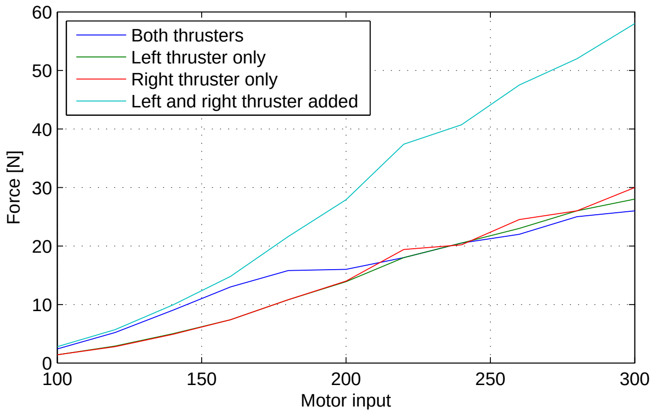

Figure B.3: Backward motion tests.

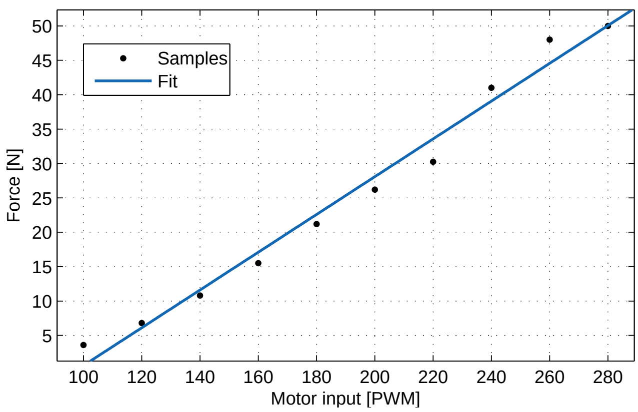

Figure B.4: Forward motion test with 1 order polynomial fitting.

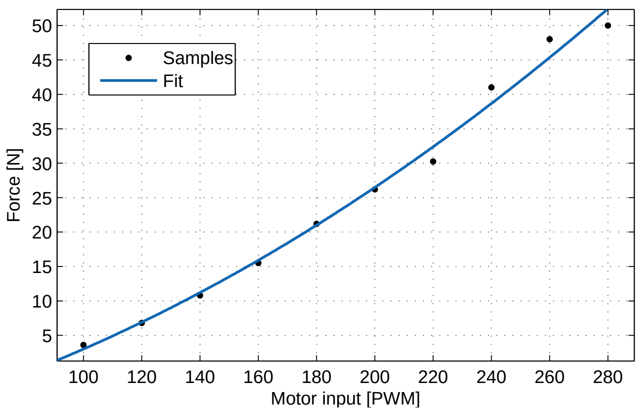

Figure B.5: Forward motion test with 2 order polynomial fitting.

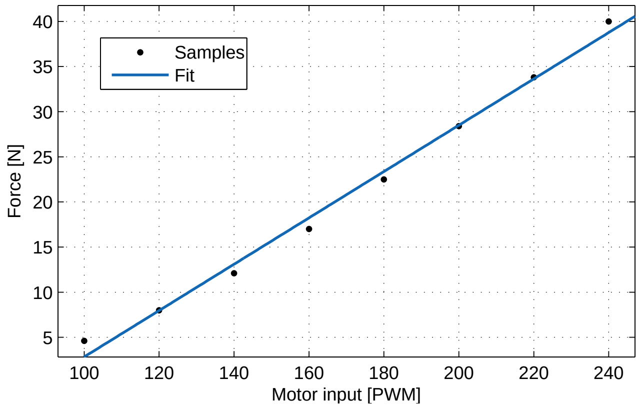

Figure B.6: Forward motion test with 1 order polynomial fitting.

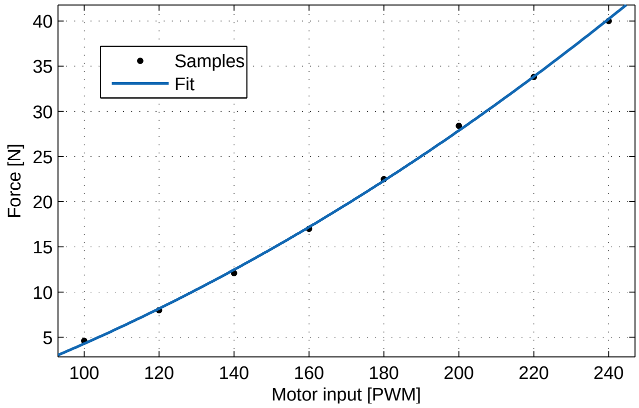

Figure B.7: Forward motion test with 2 order polynomial fitting.

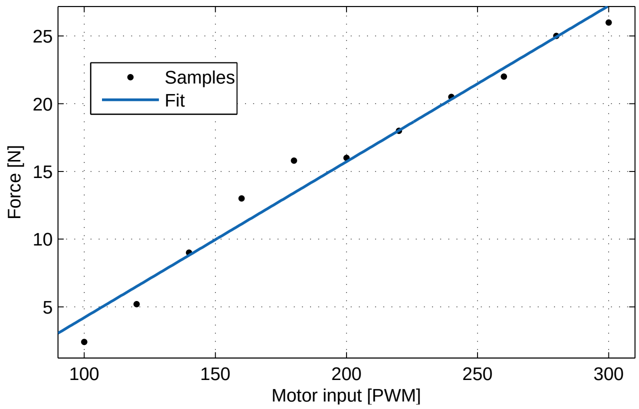

Figure B.8: Backward motion test with 1 order polynomial fitting.

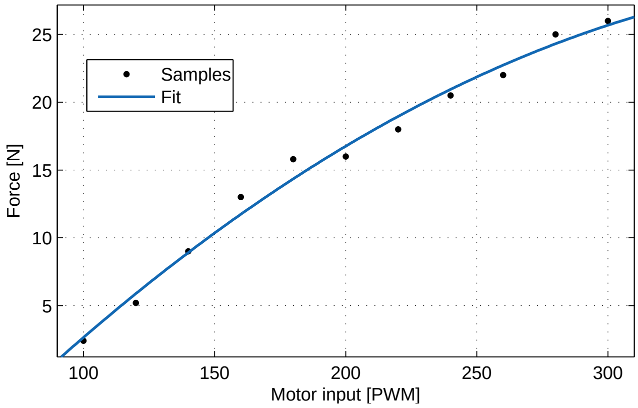

Figure B.9: Backward motion test with 2 order polynomial fitting.

Test	R^2	RMSE	Function
Both thrusters, forward B.4	0.9824	2.3626	$f(x) = 0.2746 \cdot x - 26.84$
Both thrusters, forward B.5	0.9906	1.8414	$f(x) = 0.0004976 \cdot x^2 + 0.08552 \cdot x - 10.52$
Both thrusters, forward B.6	0.9929	1.1513	$f(x) = 0.2567 \cdot x - 22.83$
Both thrusters, forward B.7	0.9994	0.3638	$f(x) = 0.0005208 \cdot x^2 + 0.07958 \cdot x - 8.875$
Both thrusters, backward B.8	0.9729	1.345	$f(x) = 0.1152 \cdot x - 7.318$
Both thrusters, backward B.8	0.9883	0.9383	$f(x) = -0.0002593 \cdot x^2 + 0.2189 \cdot x - 16.65$

Table B.2: Coefficient of determination, Root Mean Square Error and the functions to the fittings.

use the first order fitting or the second order fitting. The coefficient of determination and the RMSE does not deviate much from the samples in either cases. Thus it is concluded that the first order fitting can be as good as the second order fitting, and the first order is chosen as fitting.

When looking at the regression for the backward motion it can be seen, that the second order fitting estimates the a coefficient of the fitting to be negative. This is due to the backward test. At a PWM input above 160 is applied, the vessel starts to ventilate from the propellers. This makes the force, which the vessel's pulls with, be lesser than it actually would if it did not ventilate. Therefore is the first order also seen as the most reliable while going backwards.

Appendix C

Verification of Attitude with a Camera

This is a description of a technique to verify an attitude estimator by using a camera. It utilizes the horizon as the reference.

C.1 Objective

It is wanted to have a means to verify the attitude estimator, which is independent of other inertial measurements. This can be done i.e. with a verification using a camera.

C.2 Method

While testing it is of importance to make some verifications. When implementing an attitude estimator for pitch and roll, it is hard to verify whether it works as intended or not. A simple way to test it is to put the sensor in positions that can be measured in a static environment, that is by i.e. putting in on a table on what is to be defined as flat, then angle it some known degrees and see if the estimator agrees.

Depending on how exotic the estimator is, it might utilise a dynamic model in an attempt to improve the accuracy of the estimates. It is harder to measure the dynamic model in a static lab setup. Another way is to record the attitude with another setup that is known to work, but that could not exist, hence the need to implement a new one. Another setup could be made by utilizing a Vicon system. Alternatively a method with a camera is proposed. This is the method to be described in the following. This should provide a visual means of determining the heading.

The idea here is to mount a camera on the rigid body object containing the sensor in the longitudinal direction of the axis of interest. That is a camera pointing forward for the roll determination or a camera pointing to one side for the pitch determination. This is intended for use on ships.

This method relies on a known reference, that is stationary or at least known at all time. The most ideal scenario is to be in open water where the horizon is between the sea and the sky. This is guaranteed to be horizontal, giving an absolute reference to compare against.

A non ideal scenario is to e.g. use the harbour quay. This works if the ship is not moving a lot around relative to the quay, else it is needed to know the exact position to the quay to determine the angle the camera should see as zero. This is also possible but is out of scope of this description.

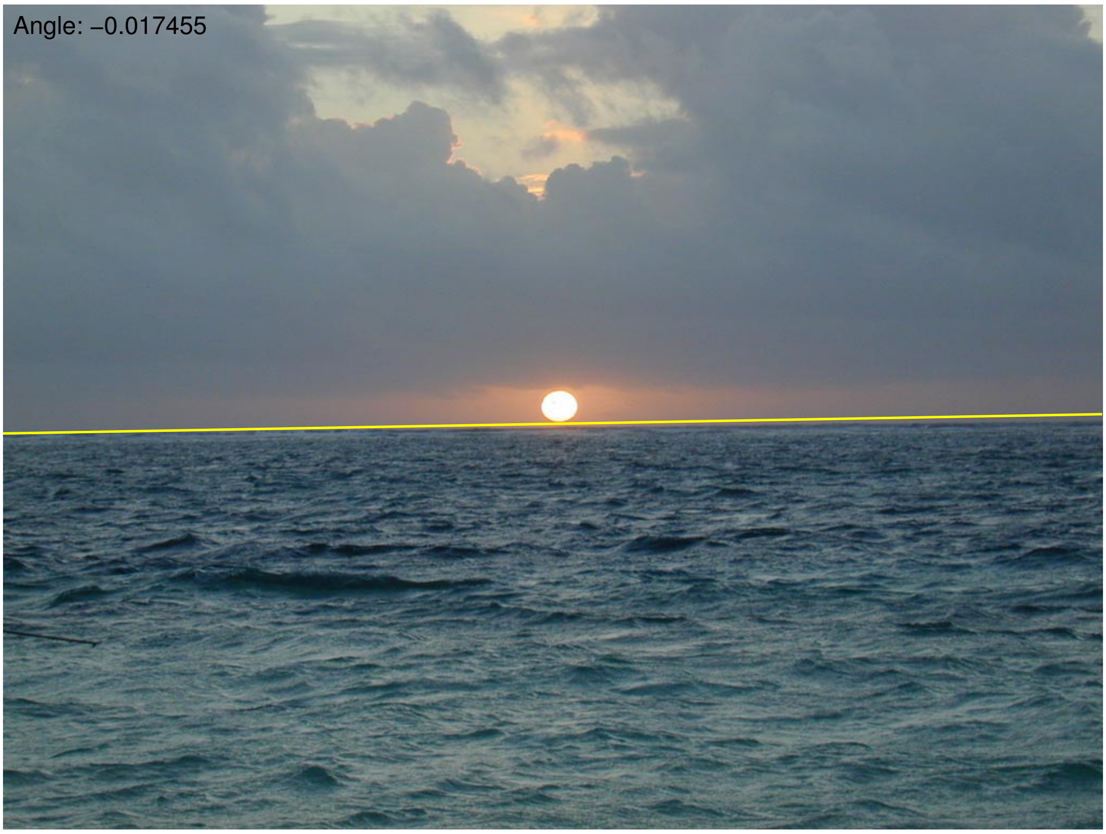

Figure C.1: Example plot of the angle calculated and overlaid on a frame from the video recorded by the camera. The example image is fetched from (poslarchive.com, 2003).

The idea is that the angle should be calculated from the image by some means of image processing, but this has not been implemented, hence there is not nice plot of this in action.

When this is done it should be possible to get time series of the angles estimated from the image processing and compare it with the time series from the observer on the same sea trail.

Appendix D

Test Journal for Sensor Variances

D.1 Objective

The objective is to determine the measurement variances on the sensors that can be used for state estimation of the ship for control purposes. This is the IMU and GPS measurements.

D.2 Theory

The variance is a key constant that state estimators rely on to make a weighting of how much it should trust a measurement, hence the value must be known.

The variance is the standard deviation squared, and can be determined from a time series of measurements from the sensors. The variance for a discrete random variable can be calculated as:

$$\mathrm{Var}(X) = \frac{1}{n}\sum_{i=1}^{n}(x_i - \mu)^2 \tag{D.1}$$

where the expected value μ is for example

$$\mu = \frac{1}{n}\sum_{i=1}^{n} x_i. \tag{D.2}$$

D.3 Tools

1. One AAUSHIP with sensors and High Level Interface (HLI) to log the data.
2. The data was processed in MATLAB with the command `var()`.

D.4 Results

The computed vales is;

$$
\begin{aligned}
&{}^{\mathrm{IMU}}\sigma^2_{m_x} = 1.0415e^{-6}, && {}^{\mathrm{IMU}}\sigma^2_{m_y} = 544.2176e^{-9}, && {}^{\mathrm{IMU}}\sigma^2_{m_z} = 419.2507e^{-9},\\
&{}^{\mathrm{IMU}}\sigma^2_{g_x} = 94.0726e^{-3}, && {}^{\mathrm{IMU}}\sigma^2_{g_y} = 28.1434e^{-3}, && {}^{\mathrm{IMU}}\sigma^2_{g_z} = 99.3437e^{-3},\\
&{}^{\mathrm{IMU}}\sigma^2_{a_x} = 285.4267e^{-6}, && {}^{\mathrm{IMU}}\sigma^2_{a_y} = 264.4893e^{-6}, && {}^{\mathrm{IMU}}\sigma^2_{a_z} = 317.1120e^{-6},\\
&{}^{\mathrm{GPS}}\sigma^2_{x} = 5.3135, && {}^{\mathrm{GPS}}\sigma^2_{y} = 593.8035e^{-3}, && {}^{\mathrm{GPS}}\sigma^2_{z} = 4.0181e^{-9}.
\end{aligned}
$$

D.5 Discussion and Conclusion

It is seen on the histogram plots that the shapes is not beautifully gaussian shaped. This can be because there is some slow bias drift on the sensor and the fact that the noise is around a few samples. Especially for the accelerometer on figure D.1 on the next page where it is only four samples and most on the middle two.

Variances of the time series for all plots was determined and presented in the results section.

The variances for the GPS might not be a good measure of the noise, since the histogram and ground track looks like a random walk of some form. It should be noted that the GPS under test, was placed in a not so ideal position. It was approximately four meters from a wall of a building on its south facing side. This could be why the variance is bigger in the northing axis.

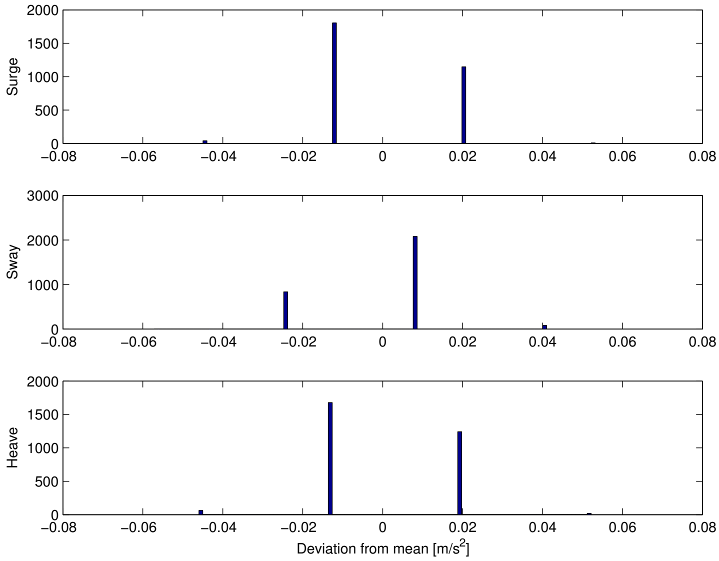

Figure D.1: Histogram of the accelerometer. 100 bins. 3000 samples.

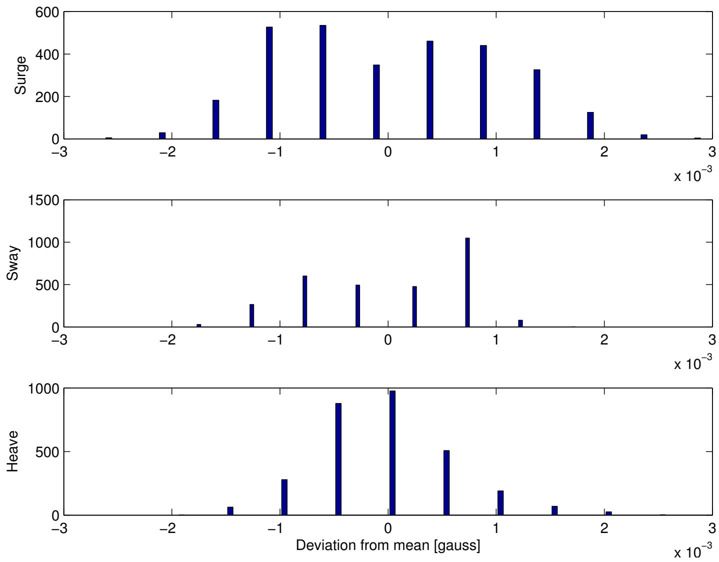

Figure D.2: Histogram of the magnetometer. 100 bins. 3000 samples.

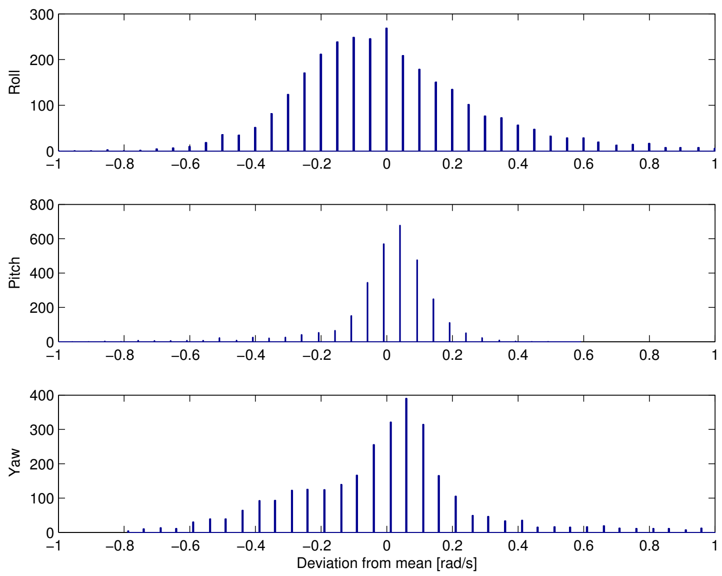

Figure D.3: Histogram of the gyrometer. 1000 bins. 3000 samples.

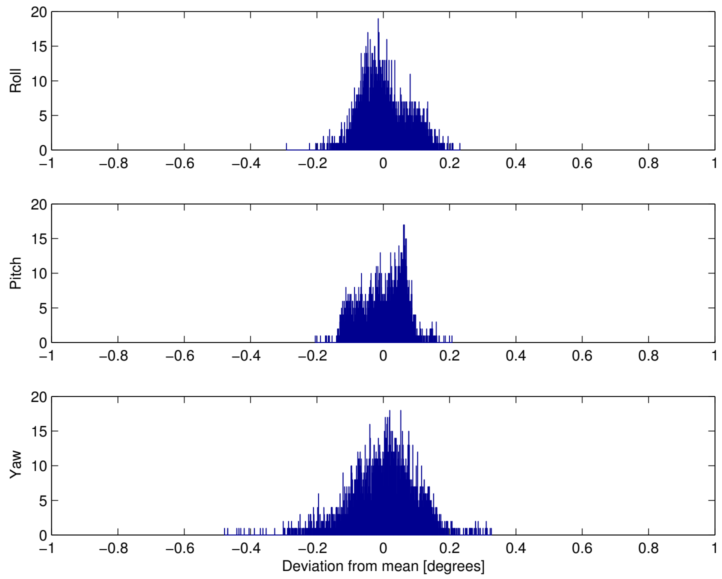

Figure D.4: Histogram of the estimated attitude with the Mahony filter with the filter constants; sample time of 1/20 s, $K_p = 8.8$, $K_i = 0.5$. 1000 bins. 3000 samples.

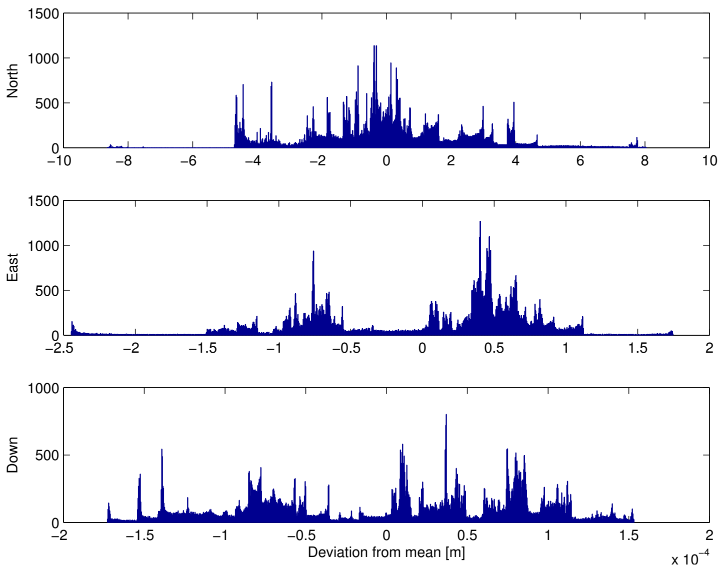

Figure D.5: Histogram of the MB100 RTK GPS. 1000 bins.

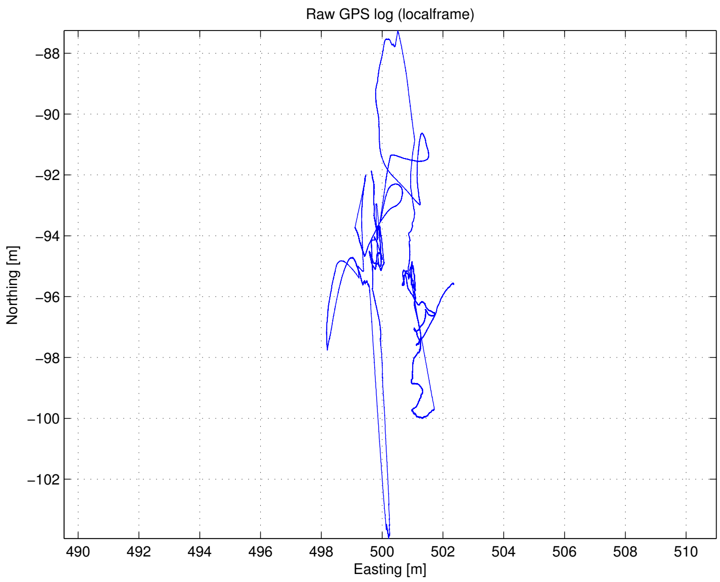

Figure D.6: Ground track from the MB100 RTK GPS.

Appendix E

Hardware Overview of AAUSHIP

E.1 Introduction

Some practical sections in this appendix is based on the writing of Østergaard et al. (2012). Going further to describe the use cases when using AAUSHIP in a formation control setup will be described here.

The use case considered here is that of ASV Formation Control for Surveying Purposes. This task is about using the ASV to scan an area using a “lawnmower”-pattern. This pattern is of course not a very definite pattern, but it basically means that the mowing machine or formation in this case will move across all the area in some structured way.

E.2 Description

The AAUSHIP consists of an approximately 1 meter long vacuum formed hull made of ABS plastic, which contains twin propellers. Additions on some AAUSHIPs include tunneltrusters for those that want to include this option.

E.3 Objective

A use case that is a basis of this project is a service that surveying companies offer, which is to survey and map the seabed of waterways and lakes. Currently they do this very manually my sailing with a boat in the lake after a Global Navigation Satellite System (GNSS) in the boat. In waterways as small rivers and the like in Denmark they do it by a smaller boat or raft, where they are using a prism system and a stick to take point measurements of the river.

These tasks could be automated and probably improve surveying time by using an autonomous system that can cover this. Here focus is on trying to design such a system with small ships sailing in formation to scan a predefined area.

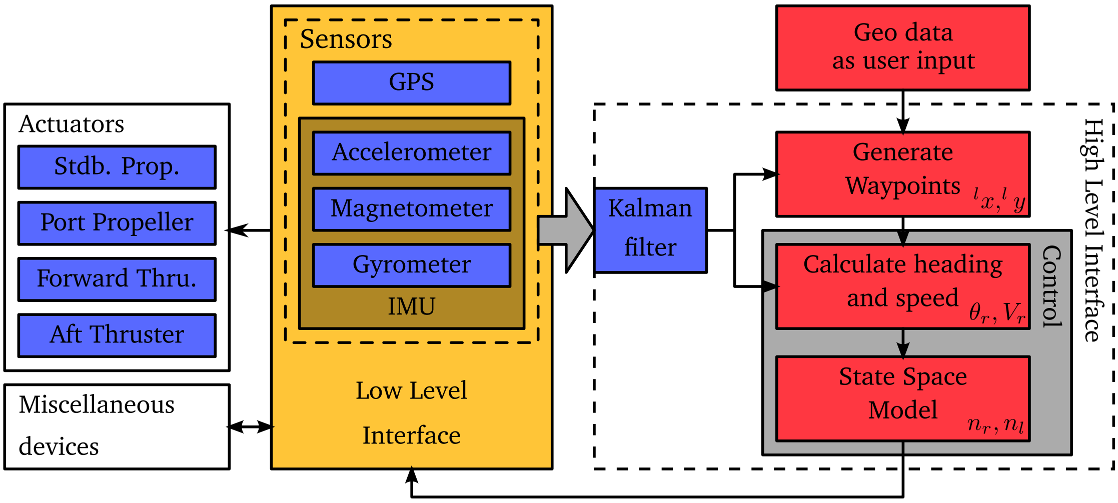

Figure E.1: Overview of the control layout and its interfaces for a single AAUSHIP. Modified version of graphic from (Østergaard et al., 2012).

E.4 Parts list

See table E.1.

#	Model
2	Graupner InIine 750
2	Electronic Speed Controller
2	Propellers
2	Prop Shaft
2	Motor to prop shaft couplings 5mm
6	LiPo 3600 mAh 4S1P batteries
1	Intelligent Charge Port (ICP)
1	Raspberry Pi or similar
1	4-split USB hub
1	Echosounder

Table E.1: Mechanical parts for an AAUSHIP

E.5 Power System

The power source in AAUSHIP is chosen to be LiPo batteries, which is a type of battery chemistry where the operator take great care in not damaging the batteries. If care is not taken they might catch on fire, which cannot easily be extinguished. This can of course be dangerous.

E.5.1 Power Harness

The power system on the ship consists of some somewhat convoluted wiring harnessed loosely in the hull structures. An single line diagram is therefor provided to give an overview of the system. This se seen on the figure E.2, where the most basic elements are presented. The CP is the charge port, used to recharge the batteries. It is also seen that it contains six battieres connected in two banks, see section E.5.2.

The power hub is just a pair of screw terminals as a means of connecting different devices to, on there there is also connected some regulators already, which provides 3.3 and 5.0 V for the auxiliary devices shown in green, which are connected through USB to the HLI. Also the communication in the form of a Wi-Fi access point is powered from a separate DC supply.

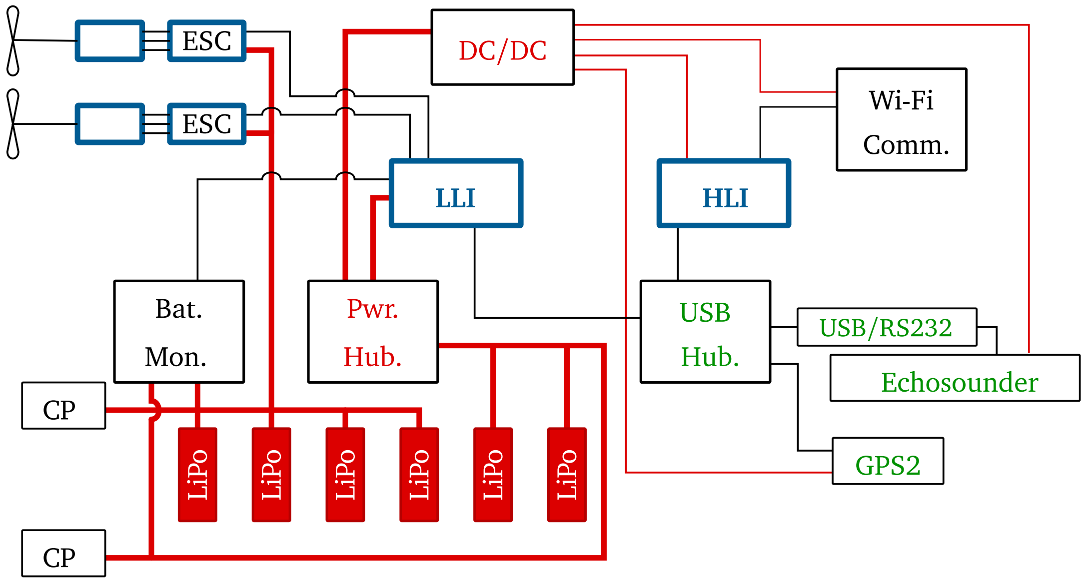

Figure E.2: Single line diagram of AAUSHIP. The red lines are power distribution, whilst the black lines are different kinds of signal lines. Blue elements are required elements for a ship in some form.

E.5.2 LiPo Basics

The LiPo battery packs each consists of four cells in series, which in the LiPo battery world is called “4S1P”. One parallel is what you get when you only have a series connection.

Since each cell is normally not charged individually but across the output terminals of the battery, every pack with more than one series cell is equipped with a so called balance port.

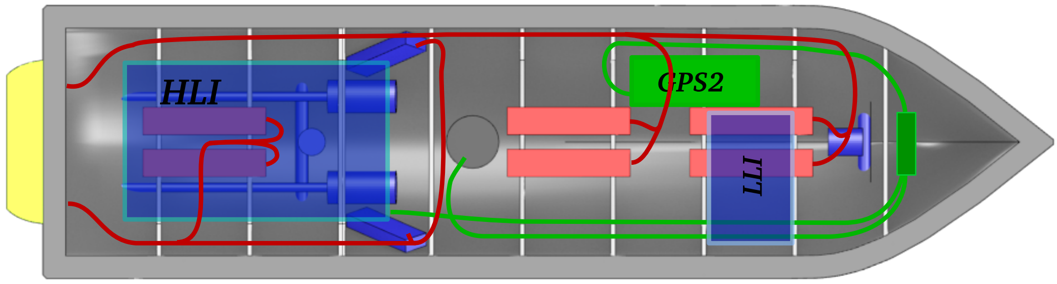

Figure E.3: Power harness system of AAUSHIP

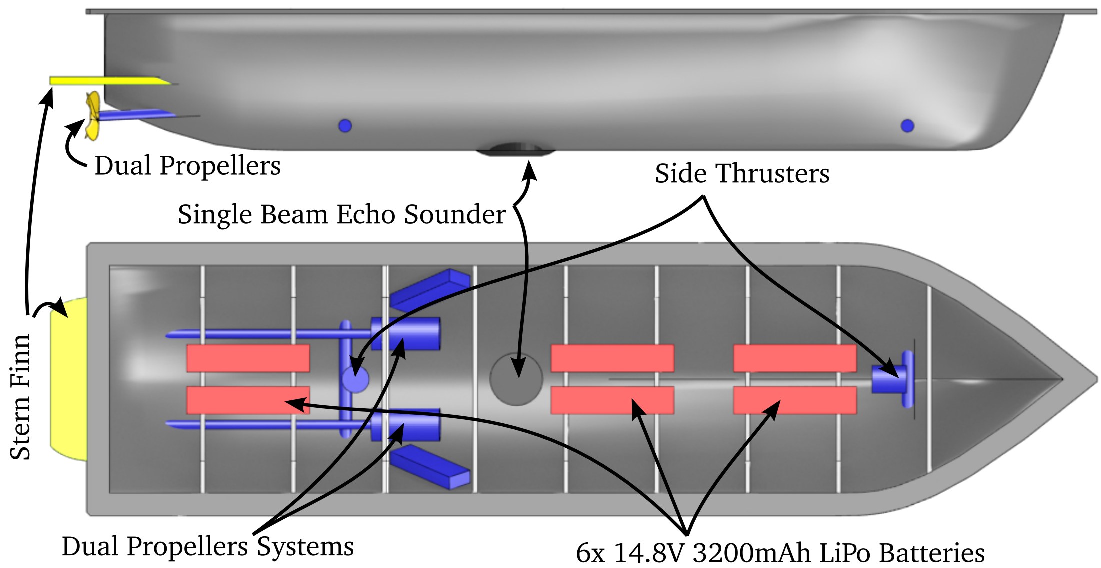

Figure E.4: Overview of the mechanical base components and their arrangement. Side view and top view.

This is basically a smaller multiple pin connector that has a connection to each cell, such that is is possible for a “balancer” to discharge cells that is unbalanced. An unbalanced cell is basically just a cell that does not have the same voltage as the others.

This balancer is usually run whilst one is charging the main connections. The purpose is to eliminate the difference that is inherent in each cell not being exactly the same, such that one cell does not get overcharged, when charging them in series.

E.5.3 LiPo Battery Safety

It is strongly advised not to mess with the LiPo batteries before you have read and understand how to handle them. A good resource for learning some basics and safety about LiPo batteries are (TJinGuy, 2014a) and (TJinGuy, 2014b).

Appendix F

Battery Monitor for AAUSHIP

This appendix is a minor chapter describing a hardware component, the battery monitor, for AAUSHIP which was also devised under the project period. This is not directly a goal according to the project thesis, hence this is included in the appendix as reference.

Since the AAUSHIP is equipped with multiple LiPo cells, it is of high concern to have a means of checking the state of these battery cells. Therefore a battery monitor have been created, that can be hooked onto the LLI via the I^2C bus. This will enable the HLI to report the voltages on the cells. This was implemented with ROS by utilizing the graphical interface for ROS called rqt. In this Qt based environment it is possible to make plugins as easy as it is to create ROS nodes. A screenshot of the plugin in action is seen on figure F.2 on the next page.

The battery monitor is made of two Analog to Digital Converter (ADC) chips, namely the MCP3428, each with four channels and 16-bit resolution. But not all this resolution is of real use as such, because it is implemented with a resistor voltage divider from each cell in series, which basically means that only the top end of the value range is used.

It is designed to measure maximum 4.2 V per cell to the minimum allowed voltage of about 3.6 V per cell. It can of course measure smaller values but the critical value is around 3.6 V. The four cells are connected in series, each with a resistor divider with reference to the negative lead. The division ratio is determined by the maximum voltage present at the cells (which are in series with the lower ones), such that the cell voltages are at the two volt that each ADC can handle. This gives the following ratios for the cells:

$$\#1 = 0.12, \quad \#2 = 0.16, \quad \#3 = 0.24, \quad \#4 = 0.48 \tag{F.1}$$

This means that the voltage on high cell ADC is ranging from about 1.728 V to 2.0 V. In turn meaning that the reading will only use the top 15 % of the capabilities of the ADC. This results in a range for the high side ADC of about 288 when using the exact numbers, which equates to about 8 mV per Least Significant Bit (LSB). The lower ranges are more accurate.

High resistance dividers is used since these are always connected to the battery, and the resistance is adjusted such that the discharge current is very low, in comparison to the self discharge of the battery. The highest discharge rate for the cells are 138 µA, which corresponds to a fully charged pack to discharge over three years. Note if needed to store the batteries for a significant amount of time they should be disconnected completely.

On the following pages are the printed circuit board and schematic attached.

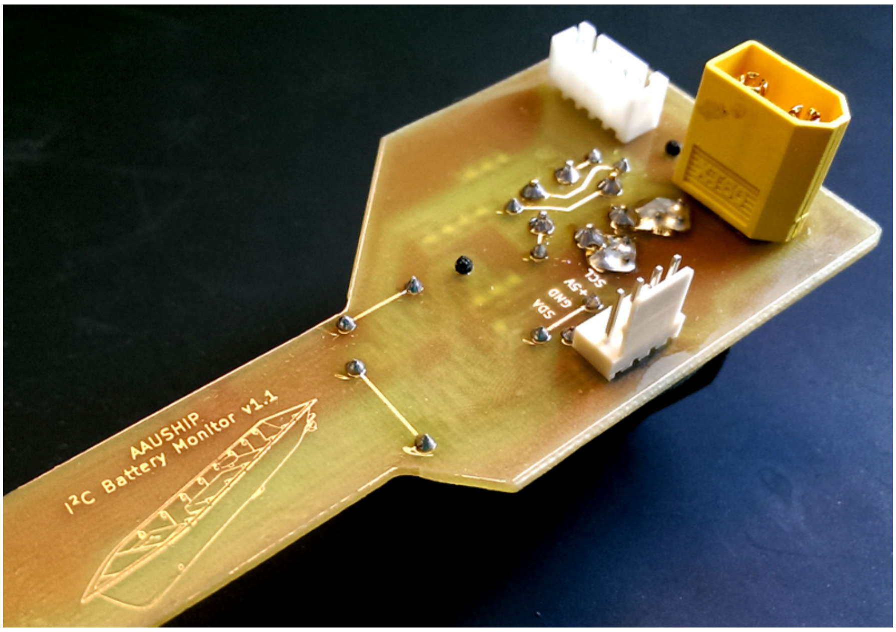

Figure F.1: Macro photo of the finished battery monitor.

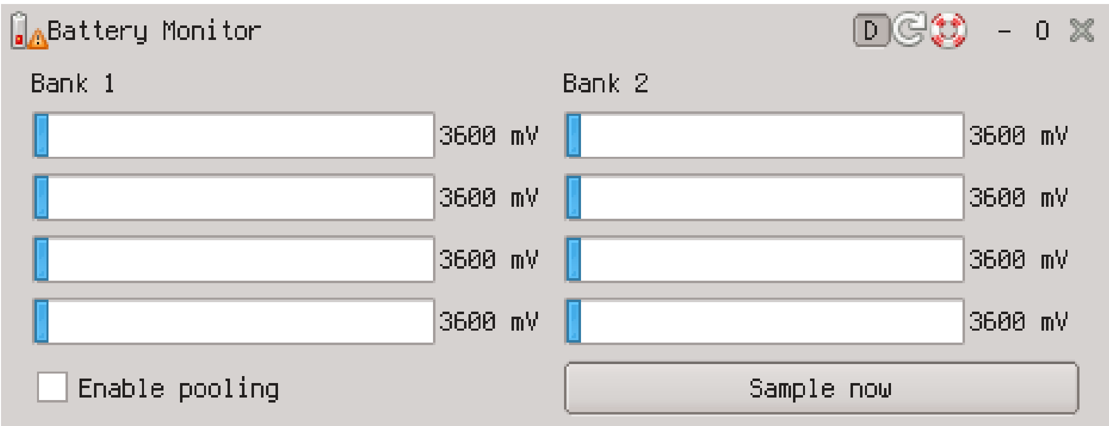

Figure F.2: Screen shot of the battery monitor plugin in rqt.

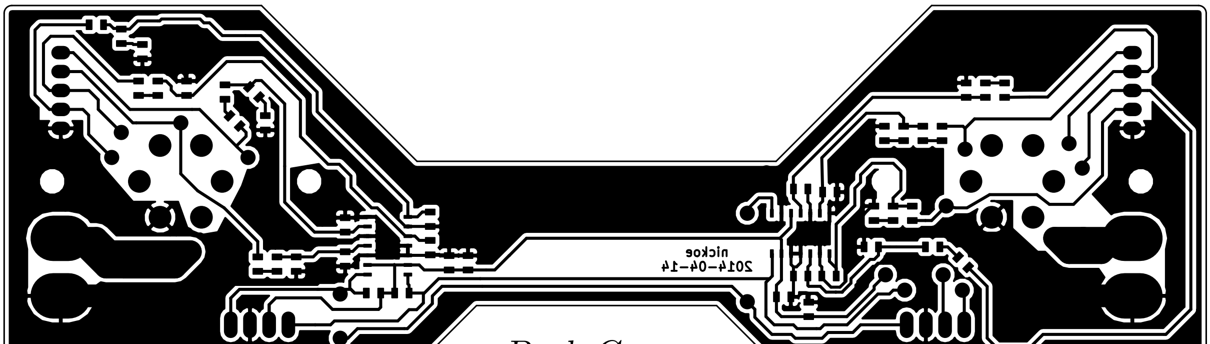

Back Copper

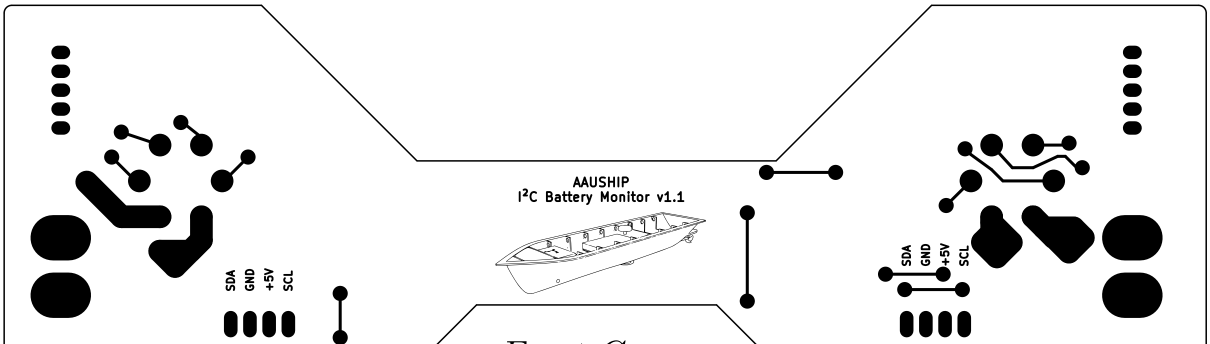

Front Copper

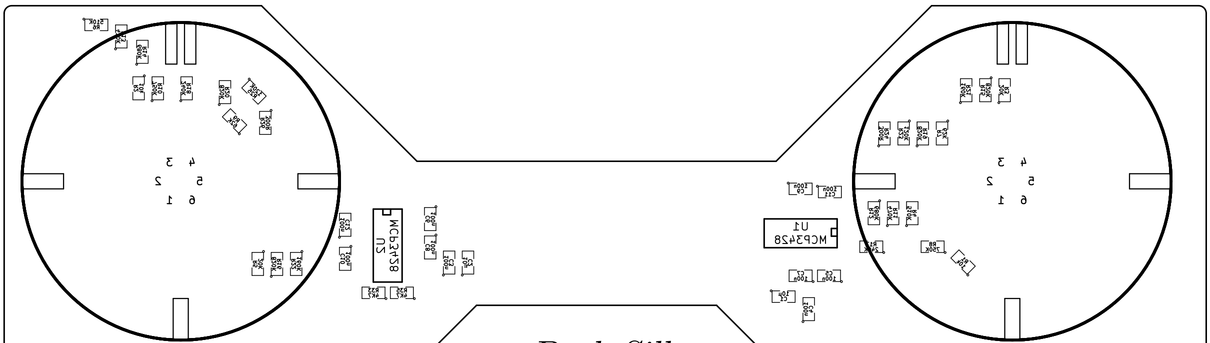

Back Silk

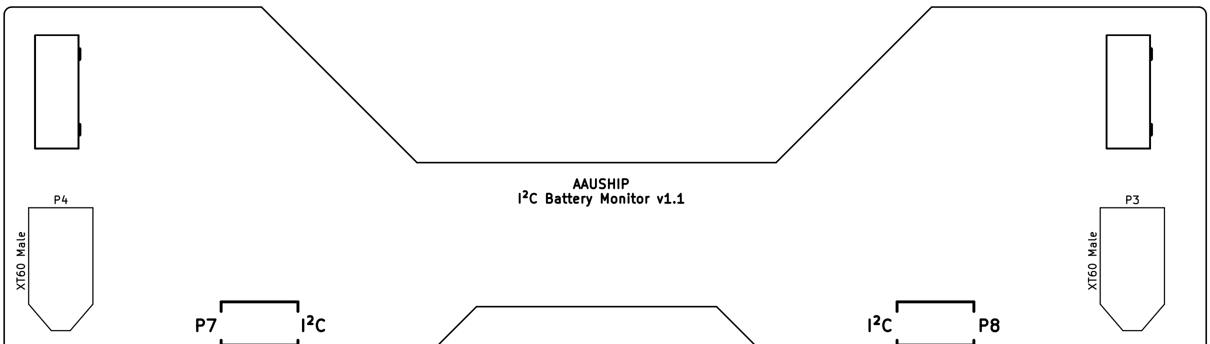

Front Silk

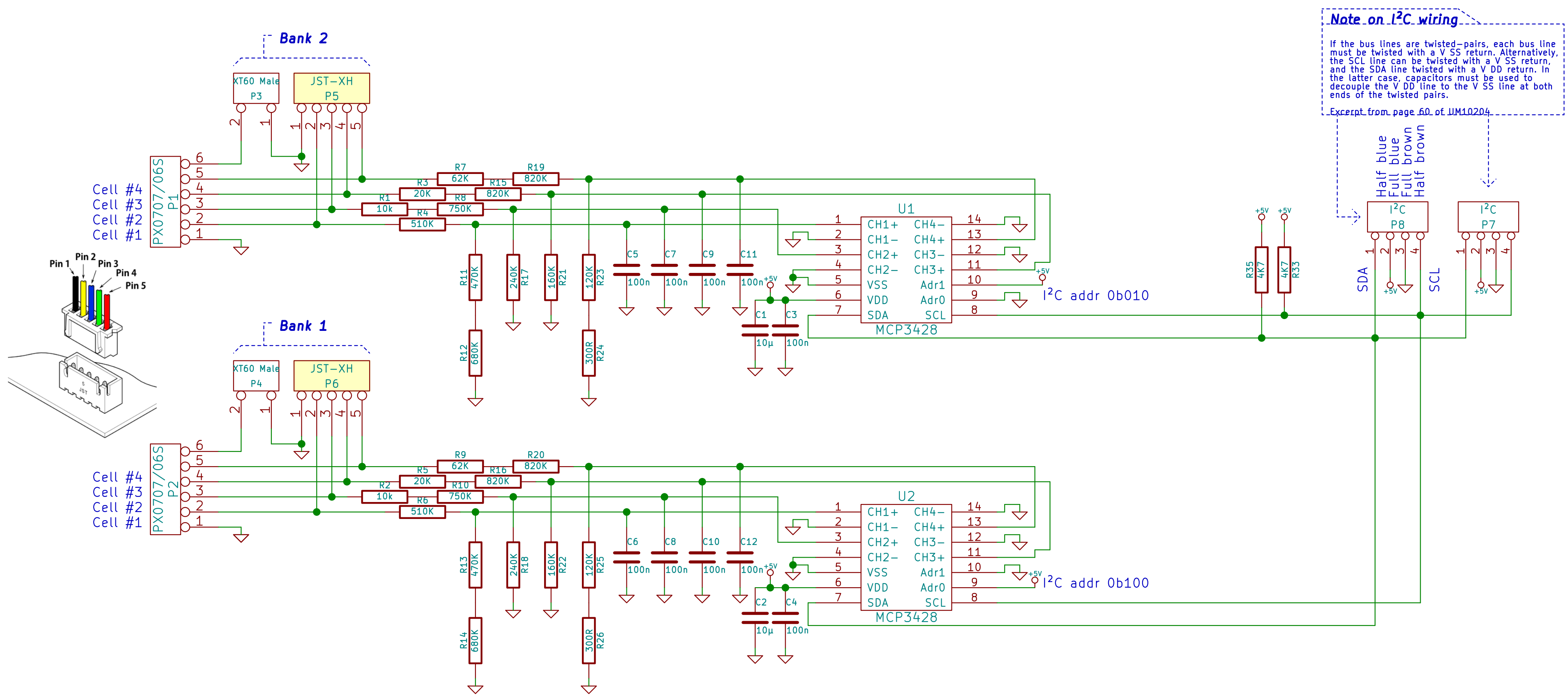

Aalborg University
AAUSHIP

Sheet: /
File: bm.sch

Title: Battery Monitor (BM)

Size: A4 | Date: 10 jul 2013 | **Rev: v1.1**
KiCad E.D.A. kicad (2015-01-01 BZR 5346)-kicad | Id: 1/1

Bibliography

Arrichiello, F., Chiaverini, S., and Fossen, T. I. (2006). Formation control of underactuated surface vessels using the null-space-based behavioral control. In *Intelligent Robots and Systems, 2006 IEEE/RSJ International Conference on*, pages 5942–5947. IEEE.

Augugliaro, F., Lupashin, S., Hamer, M., Male, C., Hehn, M., Mueller, M., Willmann, J., Gramazio, F., Kohler, M., and D'Andrea, R. (2014). The flight assembled architecture installation: Cooperative construction with flying machines. *IEEE Control Systems Magazine*, 34(4):46–64.

Carpin, S. and Parker, L. (2002). Cooperative leader following in a distributed multi-robot system. In *Robotics and Automation, 2002. Proceedings. ICRA '02. IEEE International Conference on*, volume 3, pages 2994–3001.

Egerstedt, M. and Hu, X. (2001). Formation constrained multi-agent control. *Robotics and Automation, IEEE Transactions on*, 17(6):947–951.

Elkaim, G. and Kelbley, R. (2006). A lightweight formation control methodology for a swarm of non-holonomic vehicles. In *Aerospace Conference, 2006 IEEE*, pages 8 pp.–.

Eriksson-Bique, S. D., Kirkpatrick, D. G., and Polishchuk, V. (2012). Discrete dubins paths. *CoRR*, abs/1211.2365.

European Space Agency (ESA) (2014). RTK fundamentals. `http://www.navipedia.net/index.php/RTK_Fundamentals`, [Online accessed, December 2014].

Euston, M., Coote, P., Mahony, R., Kim, J., and Hamel, T. (2008). A complementary filter for attitude estimation of a fixed-wing uav. In *Intelligent Robots and Systems, 2008. IROS 2008. IEEE/RSJ International Conference on*, pages 340–345. IEEE.

Fossen, T. I. (2011). *Handbook of Marine Craft Hydrodynamics and Motion Control*. Wiley.

Goncalves, V., Pimenta, L., Maia, C., Dutra, B., and Pereira, G. (2010). Vector fields for robot navigation along time-varying curves in n-dimensions. *Robotics, IEEE Transactions on*, 26(4):647–659.

I. Fossen, T. and Strand, J. P. (2001). Nonlinear passive weather optimal positioning control (WOPC) system for ships and rigs: experimental results. *Automatica*, 37(5):701–715.

Kwang-Kyo Oh, M.-C. P. and Ahn, H.-S. (17-12-2012). A survey of multi-agent formation control: Position-, displacement-, and distance-based approaches. [Online; accessed 3-June-2014].

Mahony, R., Hamel, T., and Pflimlin, J.-M. (2008a). Nonlinear complementary filters on the special orthogonal group. *Automatic Control, IEEE Transactions on*, 53(5):1203–1218.

Mahony, R., Hamel, T., and Pflimlin, J.-M. (2008b). Nonlinear complementary filters on the special orthogonal group. *Automatic Control, IEEE Transactions on*, 53(5):1203–1218.

National Oceanic and Atmospheric Administration (NOAA) (2014). Magnetic field calculators. [Online database; accessed 1-September-2014]. `http://www.ngdc.noaa.gov/geomag-web/`.

Nielsen, B. B. and Lundgaard, R. (2013). Repetetive control and attitude estimation of marine vessels. Technical report, Aalborg University.

Paul, T., Krogstad, T., and Gravdahl, J. (2008). UAV formation flight using 3D potential field. In *16th Mediterranean Conference on Control and Automation*, pages 1240–1245.

Pereira, G. A. S., Kumar, V., and Campos, M. F. M. (2003). Formation control with configuration space constraints. In *Proc. Int'l Conf. on Intelligent Robots and Systems*, Las Vegas.

Port of Aalborg (28-02-2014). Meeting with Port of Aalborg. [Meeting with Port of Aalborg to see if it was possible to facilitate some of their needs within the maritime subjects of our project. General information of the Limfjord and the Port of Aalborg was given.].

poslarchive.com (2003). Sun on horizon image. [Online; accessed 7-Januray-2014], `http://www.poslarchive.com/math/images/wallpaper/sun-on-horizon.jpg`.

Quigley, M., Conley, K., Gerkey, B. P., Faust, J., Foote, T., Leibs, J., Wheeler, R., and Ng, A. Y. (2009). Ros: an open-source robot operating system. In *ICRA Workshop on Open Source Software*. [Online; accessed 29-September-2014]. `http://www.willowgarage.com/sites/default/files/icraoss09-ROS.pdf`.

SNAME (1950). Nomenclature for Treating the Motion of a Submerged Body Through a Fluid. Technical and Research Bulletin No. 1-5. Technical report, The Society of Naval Architects and Marine Engineers.

Song, P. and Kumar, V. (2002). A potential field based approach to multi-robot manipulation. In *Proc. IEEE Intl. Conf. On Robotics and Automation*, Washington, D.C.

Tanner, H. G., Kumar, V., and Pappas, G. J. (2004). Leader-to-formation stability. *IEEE Transactions on Robotics and Automation*.

Thorvaldsen, C. (2011). Formation control of marine vessels. Master's thesis, Norwegian University of Science and Technology.

TJinGuy (2014a). Lipo basics. [Online; accessed 7-February-2014].

TJinGuy (2014b). Making lipos safe and dealing with failures. [Online; accessed 7-February-2014].

Wondergem, M. (July, 2005). Output feedback tracking of a fully actuated ship. Master's thesis, Technische Universiteit Eindhoven. [Online; accessed 3-June-2014]. DCT 2005.104. `http://alexandria.tue.nl/repository/books/598447.pdf`.

Zhang, Y. and Mehrjerdi, H. (2013). A survey on multiple unmanned vehicles formation control and coordination: Normal and fault situations. In *Unmanned Aircraft Systems (ICUAS), 2013 International Conference on Unmanned Aircraft Systems*, pages 1087–1096.

Østergaard, N., Juul, F., Christensen, R. L., Fodor, A., and Muresan, T. (2012). An autonomous marine environment surveying platform. Technical report, Aalborg University.